UNDERSTANDING POTASSIUM HOMEOSTASIS USING HUMAN AND MOUSE GENETIC MODELS

APPROVED BY SUPERVISORY COMMITTEE

Chou-Long Huang, M.D., Ph.D.

Stephen C. Cannon, M.D., Ph.D.

Makoto Kuro-o, M.D., Ph.D.

Orson W. Moe, M.D.

DEDICATION

To my parents Ching-Hui Cheng and Su-Ying Chen and my wife Jen-Chi Chen.

UNDERSTANDING POTASSIUM HOMEOSTASIS USING HUMAN AND MOUSE GENETIC MODELS

by

CHIH-JEN CHENG

DISSERTATION

Presented to the Faculty of the Graduate School of Biomedical Sciences

The University of Texas Southwestern Medical Center at Dallas

In Partial Fulfillment of the Requirements

For the Degree of

DOCTOR OF PHILOSOPHY

The University of Texas Southwestern Medical Center at Dallas

Dallas, Texas

August, 2012

ACKNOWLEDGEMENT

I first want to thank my mentor, Dr. Chou-Long Huang, for his guidance and support throughout the years. He has led me through every learning step; ranging from forming hypothesis, designing experiments, troubleshooting problems, planning oral presentation and publishing our works. His passion in science, a mindset and confidence that is not afraid of challenging traditional dogma, and self-discipline have been instrumental and critical to my graduate studies. I am also very grateful to Dr. Elizabeth Kuo for all her warm regards and supports to me and my families. My thanks also goes to my present and past colleagues in Dr. Huang's lab: Jian Xie, Aylin Rodan, Sung-Wan An, Joon-Ho Yoon, Matthias Wolf, Seung-Kuy Cha, Hao-Ran Wang, and Thao Truong for their generosity, time and efforts, which have made our lab a great place to work.

I also want to thank Dr. Michel Baum for teaching me the technique of microperfusion and providing unconditional support to my later projects. His thoughtful scientific suggestion, ample knowledge of renal physiology, and experienced editing have guided me through the difficult learning process and extended my vision and ability.

I am indebted to my dissertation committee members: Dr. Stephen C. Cannon, Dr. Makoto Kuro-o and Dr. Orson W. Moe for their invaluable comments on my projects and the understanding of my time limit. I would especially like to thank Dr. Cannon for the exciting brainstorming that came up with an insightful model to explain the disease pathogenesis of hypokalemic paralysis, and members of Dr. Cannon's lab, especially Dr. Fenfen Wu, for technical support and discussion. I also like to express my immense gratitude to Dr. Melanie Cobb and members in her lab,

especially Aileen Klein, for sharing me not only plasmids and reagents but also technical experiences.

My research was greatly benefited from my previous fellowship training in division of nephrology, Tri-Service General Hospital, Taipei, Taiwan where I learned my fundamental understanding of renal physiology from a great mentor, Dr. Shih-Hua Lin. His wisdom and enthusiasm for medical research is contagious and inspiring. Without the foundation he laid for me, I wouldn't have been able to finish the projects in my graduate studies. I am also very grateful to Dr. Yuh-Feng Lin, Dr. Huey-Kang Sytwu, Dr. Pauling Chu and the entire colleagues in Taiwan for all their supports. In addition, I want to express my sincere gratitude to Tri-Service General Hospital, the Ministry of Defense, and my homeland Taiwan for offering me a scholarship grant that allows me to focus fully on the studies.

None of my achievements would have been possible without the support from my loving family. My parents Ching-Hui Cheng and Su-Ying Chen have always been the greatest supporters of my life. They raised me up and taught me the value of family and life. My wife Jen-Chi Chen has devoted herself wholeheartedly to caring and loving me and our children, William and Grace. I can never express enough gratitude for her. With all the help from my family, I can fully commit to my works without distraction and get through every difficult moment. I always remember the message wrapped in the first fortune cookie I ate in United States that said "A new venture will be a success". Now I am starting to believe that.

UNDERSTANDING POTASSIUM HOMEOSTASIS USING HUMAN AND MOUSE GENETIC MODELS

CHIH-JEN CHENG, M.D. Ph.D.

The University of Texas Southwestern Medical Center at Dallas, 2012

CHOU-LONG HUANG, M.D. Ph.D.

Potassium homeostasis is one of the most sophisticated processes involving multiple organs in mammals. Many physiological functions, such as excitability of muscles and neurons, rely on stable extracellular potassium concentration. To maintain potassium homeostasis, endogenous factors including hormones and peptides regulate the activity of potassium transporters in many organs, especially skeletal muscles and kidneys, in response to different conditions.

To study the perplexed regulations of potassium transporters, I choose two genetic models of human potassium disorders, hypokalemic periodic paralysis (hypoPP) and pseudohypoaldosteronism type II (PHA2). Patients with hypoPP are characterized with ictal hypokalemia and muscle paralysis. HypoPP can be divided into familial and non-familial forms. Recent studies have revealed the pathogenesis of familial hypoPP. However, the pathogenesis of non-familial hypoPP, mainly composed of thyrotoxic or sporadic periodic paralysis (TPP/SPP), is mostly unknown. A novel muscle-specific inward-rectifying potassium (Kir) channel, Kir2.6, has been recently suggested to play a role in TPP. Here, I focus on studying the role of Kir channels in non-familial hypoPP and propose the disease mechanisms to explain hypokalemia and muscle paralysis.

PHA2 is a genetic disorder caused by mutations on with-no-lysine kinase 1 or 4 (WNK1/4) and featured with hyperkalemia and hypertension. Studies in PHA2 have revealed that WNK kinases regulate renal sodium transporters and potassium channels. WNK1 enhances the endocytosis of renal outer medullary potassium (ROMK) channel through an intersectin-dependent mechanism, but the upstream regulator is still unknown. Here, I clarified that the phosphoinositol-3-kinase-induced activation of Akt1/SGK can phosphorylate threonin 58 of WNK1 and thus inhibits ROMK current in cultured cells. In addition to full-length WNK1, the kinase-deficient WNK1 isoform, kidney-specific WNK1 (KS-WNK1), also participates in the regulation of renal sodium and potassium handling. Previous studies have shown that high potassium intake enhances KS-WNK1 expression and suppresses renal sodium reabsorption in thick ascending limb (TAL). However, the localization and function of KS-WNK1 in TAL are still debatable. Here, I used KS-WNK1 genetic mouse models to demonstrate that KS-WNK1 is present and function to inhibit sodium reabsorption in cortical TAL. These results contribute to the understanding of potassium homeostasis in skeletal muscle and kidney.

TABLE OF CONTENTS

PRIOR PUBLICATIONS

1. Charles J. Heise, Bing-e Xu, Staci L. Deaton, Seung-Kuy Cha, **Chih-Jen Cheng**, Svetlana Earnest, Samarpita Sengupta, Yu-Chi Juang, Steve Stippec, Yingda Xu, Yingming Zhao, Chou-Long Huang, Melanie H. Cobb. Serum and glucocorticoid-induced kinase (SGK) 1 and the epithelial sodium channel are regulated by multiple with no lysine (WNK) family members. J Biol Chem 2010; 285: 25161-25167.
2. Aylin R. Rodan, **Chih-Jen Cheng**, Chou-Long Huang. Recent advances in distal tubular potassium handling. Am J Physiol Renal Physiol 2011; 300: F821-827.
3. **Chih-Jen Cheng**, Chou-Long Huang. Activation of PI3-kinase stimulates endocytosis of ROMK via Akt1/SGK1-dependent phosphorylation of WNK1. J Am Soc Nephrol 2011; 22: 460-471.
4. **Chih-Jen Cheng**, Shih-Hua Lin, Yi-Fen Lo, Sung-Sen Yang, Yu-Juei Hsu, Stephen C. Cannon, Chou-Long Huang. Identification and functional characterization of Kir2.6 mutations associated with non-familial hypokalemic periodic paralysis. J Biol Chem 2011; 286: 27425-27435.
5. Chih-Chien Sung, **Chih-Jen Cheng**, Yi-Fen Lo, Mei-Shan Lin, Sung-Sen Yang, Yu-Chuan Hsu, Shih-Hua Lin. Genotype and Phenotype Analysis of Patients With Sporadic Periodic Paralysis. Am J Med Sci 2011; 343: 281-285.
6. **Chih-Jen Cheng**, German Lozano, Michel G. Baum. Prenatal Programming of Rat Cortical Collecting Tubule Sodium Transport. Am J Physiol Renal Physiol 2011; 302: F674-678.

7. **Chih-Jen Cheng,** Elizabeth Kuo, Chou-Long Huang. Extracellular potassium homeostasis: Insights from hypokalemic periodic paralysis. Seminar Nephrol. (In print)
8. **Chih-Jen Cheng,** Thao Truong, Michel Baum, Chou-Long Huang. Kidney-specific WNK1 inhibits sodium reabsorption in cortical thick ascending limb. Am J Physiol Renal Physiol. (Revised)

LIST OF FIGURES

LIST OF TABLES

LIST OF DEFINITIONS

ASDN	Aldosterone-sensitive distal nephron
Ba^{2+}	Barium divalent cation
Ca^{2+}	Calcium divalent cation
Cav	Voltage-gated calcium channel
CCD	Cortical collecting duct
Cl^-	Chloride ion
CNT	Connecting tubule
cTAL	Cortical thick ascending limb
DCT	Distal convoluted tubule
Ek	Equilibrium potential for potassium ion
Em	Membrane potential
ENaC	Epithelial sodium channel
Er	Resting membrane potential
FL-WNK1	Full-length WNK1
GAPDH	Glyceraldehyde 3-phosphate dehydrogenase
HEK cell	Human embryonic kidney cell
HypoPP	Hypokalemic periodic paralysis
IGF	Insulin-like growth factor
KCC	Potassium-chloride cotransporter
Kir	Inward-rectifying potassium channel
KS-WNK1	Kidney-specific WNK1
Kv	Voltage-gated potassium channel
MCD	Medullary collecting duct

Mg^{2+}	Magnesium divalent cation
mTAL	Medullary thick ascending limb
mTORC	Mammalian target of rapamycin complex
Na^{+}	Sodium ion
Na^{+}, K^{+}-ATPase	Sodium-potassium adenosine triphosphatase
Nav	Voltage-gated sodium channel
NCC	Sodium-chloride Cotransporter
Nedd4	Neural precursor cell expressed developmentally down-regulated protein 4 (E3 ubiquitin-protein ligase)
NKCC	Sodium-potassium-chloride cotransporter
Maxi-K	Large conductance calcium-activated potassium channel
ROMK	Renal outer medullary potassium channel
OSR1	Oxidative stress-responsive kinase-1
PDK	3-phosphoinositide-dependent protein kinase-1
PD_{TE}	Transepithelial potential difference
PHA2	Pseudohypoaldosteronism type II
PI3K	Phosphatidylinositol 3-kinase
PIP2	Phosphatidylinositol 4,5-bisphosphate
PKA	Protein kinase A
PKB/Akt	Protein kinase B (also known as Akt)
PKC	Protein kinase C
PT	Proximal tubule
PTK	Protein tyrosine kinase
SGK	Serum and glucocorticoid-inducible kinase

SPAK	Ste20-related proline-alanine-rich kinase
SPP	Sporadic periodic paralysis
T_3	Triiodothyronine
T_4	Thyroxin
TAL	Thick ascending limb of Henle's loop
TPP	Thyrotoxic periodic paralysis
TSH	Thyroid-stimulating hormone
TTKG	Transtubular K^+ gradient
T-tubule	Transverse tubule in skeletal muscle
WNK	With-no-lysine kinase

CHAPTER ONE

INTRODUCTION

1.1 Background: Extracellular Potassium Homeostasis

Potassium (K^+) is the major intracellular cation, and only 2% of total body K^+ is present in extracellular space. This small amount of extracellular K^+, however, is the most important determinant of the resting membrane potential (Er) of many excitable cells, including cardiomyocyte, skeletal myocyte and neuron, and is normally under strict regulations to maintain plasma K^+ concentration in a small range of 3.5-5 mM.[1] Skeletal muscles and kidney are the two major organs that master the total body K^+ homeostasis with skeletal muscle serving as the largest single pool of total body K^+ and kidney providing the major access of K^+ excretion.[2] To transport K^+ ions across hydrophobic cell membrane, especially sarcolemma (cell membrane of myocytes), specific K^+ transporters on sarcolemma are required. In general, the K^+ transporters-mediated K^+ movements are defined as influx (net cellular K^+ gain, positive flux) or efflux (net cellular K^+ lost, negative flux).[3] In kidneys, K^+ ions are freely filtered via glomeruli and then undergo avid reabsorption (transtubular K^+ uptake) and relatively small amount of excretion (transtubular K^+ secretion).[4] Under normal K^+ intake, kidney excretes 5-10% of total filtered K^+, which nearly matches the amount of K^+ intake and maintains the net K^+ balance. Various hormones and peptides regulate the activities of the K^+ transporters in skeletal muscle or kidneys and thus affect the total body K^+ homeostasis. Unlike the K^+ secretion in kidneys, the transmembrane K^+ flux only redistributes but does not change the total body K^+, and affects extracellular K^+ much faster than the change of

renal K^+ secretion. This difference makes skeletal muscles and kidneys are prone to be responsible for short-term and long-term regulations of K^+ homeostasis, respectively.

1.2 Total Body Potassium Distribution

Total body K^+ is about 50 mmole per kg of body weight in human.[5] For an average adult male (~ 70 kg), the total body K^+ is ~3500 mmole. About 98% (~3430 mmol) of the total body K^+ is stored in the intracellular space, with muscle containing 80% of the intracellular K^+ with concentration around 150 mM.[6] The remaining 20% is distributed in the bone, liver, and erythrocytes. Only 2% (~70 mmole) of the total body K^+ is circulated in the extracellular space, including interstitial space (75%, 53 mmole) and plasma (25%, 17 mmole).[1] The daily dietary K^+ intake in adult human is about ~80 mmol, in which 90% will be absorbed into extracellular space through intestine. This amount (~72 mmol) of K^+ absorption can imaginably double the plasma K^+ concentration in a situation when there is no acute or chronic regulation of K^+ handling in skeletal muscle and kidney (Figure 1-1).

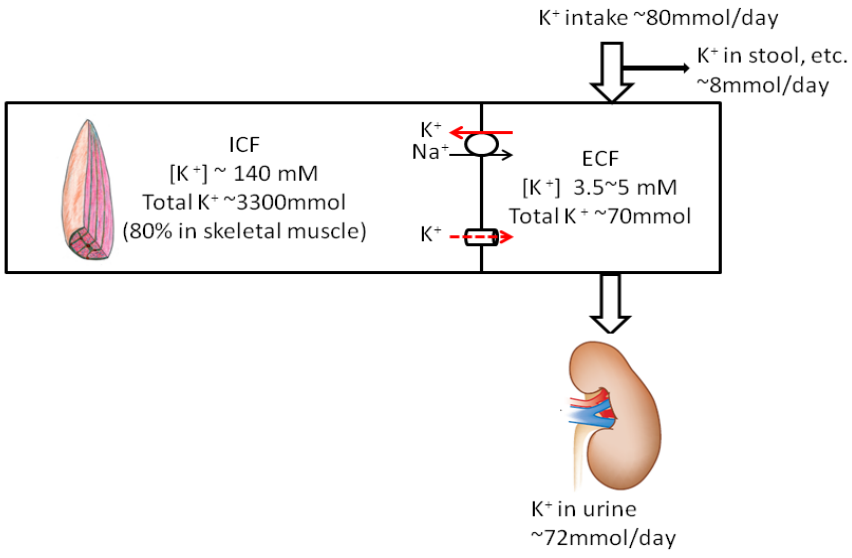

Figure 1-1. Total body potassium distribution and homeostasis.
Red arrow indicates transmemebrane K^+ movements (solid line: uptake, dotted line: release) mediated by K^+ transporters (oval: Na^+, K^+ ATPase; column: K^+ channels). Hallow arrows denote K^+ intake (mainly from oral ingestion) and output (mainly through urination). Black arrow reflects minor accesses of K^+ output including feces and sweat. All the numbers of K^+ are estimated and can be varied among individuals.

1.3 The Role of Skeletal Muscle in Extracellular Potassium Homeostasis

To illustrate the importance of skeletal muscle in K^+ homeostasis, I first explain the role of skeletal muscle in two different scenarios and then introduce the specific K^+ transporters in skeletal muscle.

1.3.1 Skeletal Muscle Buffer the Acute Dietary Potassium Load

One major factor that prevents the acute rising of plasma K^+ concentration after meals is the acute K^+ uptake by skeletal muscles and liver. As I mentioned before, the K^+ in meals can easily induce an upheaval in the levels of plasma K^+ if all the absorbed K^+ ions stay in plasma. In reality, the postprandial plasma K^+ concentration only increases by 0.5 mM at most in fed sheep.[7] Several hypotheses have been put forward to explain this finding of relatively unchanged plasma K^+ concentration following ingestion of a large K^+ load. Among these is a feed forward renal kaliuretic response induced by gut K^+ sensor.[1] Although the gut K^+ sensor hasn't been discovered, plenty of evidences suggest the kidneys enhance K^+ secretion in advance of any small increase of plasma K^+ concentration. Besides, immediate disposal by splanchnic and hepatic uptake followed by redistribution to skeletal muscle mediated by insulin and other hormones has also been proposed.[8, 9]

With respect to the K^+ redistribution to skeletal muscle, it is important to

point out that at the maximal capacity skeletal muscle can turn over the entire extracellular K^+ in half a minute (see discussion in section of Na^+, K^+-ATPase later). Thus, skeletal muscle, with its storage capacity of ~2800 mmole vs. 70 mmole extracellular K^+, can potentially take up K^+ added to plasma without a significant increase in plasma concentration. Thereafter, K^+ stored in muscle may be released slowly and excreted by kidney over many hours without causing significant changes in the plasma concentration. One challenge for this idea is that Km of Na^+, K^+-ATPase for extracellular K^+ is estimated at ~1 mM,[10, 11] suggesting that activity of pump is not sensitive to changes in plasma K^+ concentration at the normal physiological range. This value of Km, however, is determined *in vitro*. The activity of Na^+, K^+-ATPase is stimulated by many factors *in vivo*. It will be interesting to investigate in the future whether the activity of Na^+, K^+-ATPase is more sensitive to extracellular K^+ *in vivo* and K^+ uptake by muscle can adequately defend plasma K^+ from dietary load.

1.3.2 Exercise and Potassium Homeostasis

Opposite to the role of buffering in dietary K^+ load, the K^+ stored in skeletal muscles can be suddenly released and disturbs the extracellular K^+ homeostasis. During exercise, intracellular K^+ is forced to release through K^+ channels to repolarize the membrane potential of skeletal muscle, which is depolarized by the Na^+ influx via voltage-gated Na^+ (Nav) channel opened immediately after the firing of action potentials.[12] Repeated action potential and skeletal muscle contraction thus result in accumulation of considerable amount of K^+ in the extracellular space. If K^+ released by muscle freely enters the systemic circulation, the venous K^+ concentration after 5 minute of cycling exercise can reach a level 7-fold higher than the pre-exercise

level.[13] However, the highest reported plasma K^+ concentration during strenuous exercise is around 8 mM,[14] indicating that some defensive mechanisms prevent the acute rising of plasma K^+ concentration during exercise.

First, people have noticed that most of exercise-induced K^+ release is retained in the extracellular space of muscle, especially in the interstitium of transverse (T)-tubules. Several groups have shown that diffusion of extracellular K^+ of skeletal muscle into systemic circulation is limited; the diffusion coefficient is less than 20% of its value in free solution.[15] The K^+ accumulated in T-tubule causes high local K^+ concentration, which subsequently depolarizes membrane potential of T-tubule, and then leads to inactivation of Nav channel and muscle fatigue. To counter the high K^+ concentration, Na^+, K^+-ATPase in muscle is activated during exercise and in periods following exercise. In addition to the high extracellular K^+ concentration, several exercise-induced changes in muscle, such as intracellular Na^+ and lactic acid accumulation, high β-adrenergic activity, increased muscle temperature, released calcitonin gene-related peptide from nerve endings, contribute to the stimulation of Na^+, K^+-ATPase activity.[16] Exercise may also induce translocation of Na^+, K^+-ATPase from cytoplasm to sarcolemma.[17] Physical activity of muscle causes upregulation of the abundance of Na^+, K^+-ATPase, and explains why athletic training improves exercise endurance. Overall, increased uptake of K^+ by Na^+, K^+-ATPase in the T-tubule of skeletal muscle in conditioned individuals helps avoiding precipitous rise of plasma K^+ concentration and cardiac arrhythmia during exercise.[18, 19] The sustained upregulation of Na^+, K^+-ATPase activity in post-exercise periods also explains why patients with hypokalemic periodic paralysis (HypoPP) may be triggered by strenuous exercise.

1.3.3 Sodium, Potassium-ATPase in Skeletal Muscle

The K^+ uptake by muscle from the extracellular fluid is mediated predominantly by the ubiquitous Na^+, K^+-ATPase. Discovered in 1957, the role of Na^+, K^+-ATPase in skeletal muscle has been extensively studied and reviewed.[5, 13, 20-23] Using the energy expenditure of hydrolysis of one ATP molecule to ADP (so-called Albers-Post cycle), Na^+, K^+-ATPase extrudes three Na^+ ions out and brings two K^+ ions in muscle cell via a ping-pong like mechanism.[24] Thus, Na^+, K^+-ATPase is primarily responsible for maintaining the high extracellular Na^+ and intracellular K^+ concentration relative to the intracellular and extracellular space, respectively. These transmembrane potassium and sodium gradients are essential for normal Er and active transport of substrate that relies on Na^+ gradient, respectively. In the resting state, Na^+, K^+-ATPase consumes 20-30% of the total body ATP production. This huge amount of energy consumption reflects high abundance of Na^+, K^+-ATPase in tissues.

Using [^{3}H] ouabain binding assay, it is estimated that skeletal muscle contains ~0.3 μmole Na^+, K^+-ATPase per kilogram skeletal muscle wet weight, which is only less than brain cortex (11 μmole/kg) and cardiomyocytes (0.7 μmole/kg) but higher than smooth muscle (< 0.1 μmole/kg) and other tissues.[25] The capacity of K^+ uptake through Na^+, K^+-ATPase is a function of the abundance and turnover rate (maximal at ~8000 turnover per minute) of the pump. The estimated maximal capacity of Na^+, K^+-ATPase-mediated K^+ uptake into skeletal muscle is 4.8 mmole · kg^{-1} · min^{-1} (0.3 mole · kg^{-1} x 8000 min^{-1} x 2).[26, 27] In an adult male with skeletal muscle about 42% of the body mass, the maximal K^+ uptake rate in skeletal muscle amounts to ~134 mmole · min^{-1}. Considering the total extracellular K^+ is ~70 mmole,

maximal uptake by Na^+, K^+-ATPase in skeletal muscle can lead to a complete turnover of the extracellular K^+ about every half a minute.

Both the activity and abundance of Na^+, K^+-ATPase are regulated.[25] Acute regulation tends to affect the pump activity, while chronic regulation affects the abundance of pump protein. The activity of Na^+, K^+-ATPase pump is stimulated by its own substrate, i.e. by increased intracellular Na^+ and extracellular K^+ concentrations. Various endogenous and exogenous factors, including thyroid hormone, insulin, catecholamine, aldosterone and exercise, can stimulate the activity of Na^+, K^+-ATPase pump via acute or chronic mechanisms.

1.3.4 Potassium Channels in Skeletal Muscle

The K^+ release from muscle into the extracellular fluid is via K^+ channels including several inwardly rectifier K^+ channels (Kir) and voltage-gated K^+ channels (Kv). Kv channels are closed at hyperpolarized membrane potentials and opened by membrane depolarization. Several types of Kv channels are expressed in skeletal muscle, but none are skeletal muscle-specific. Kir channels allow more inward than outward potassium fluxes when open. The mechanism of asymmetric conductance (i.e., rectification) is due to voltage-dependent block of channel pore by intracellular magnesium cation (Mg^{2+}) and polyamines.[28] When the membrane potential (E_m) is more positive than the equilibrium potential for K^+ (E_k), intracellular Mg^{2+} or polyamines are driven into the channel pore blocking outward K^+ flux.[29] Kir channels are classified into seven subfamilies based on amino acid sequence homologies, rectification properties, and mechanisms of regulation by intracellular factors.[28] Each subfamily has several membranes. Several Kir channel subtypes are present in skeletal muscle and play important roles in the function of muscle and release of K^+

from muscle. These include three members of Kir2 subfamily (Kir2.1, Kir2.2, Kir2.6) and the ATP-sensitive Kir channels (Kir6.1 and 6.2, also known as K_{ATP}). Among these, Kir2.1, Kir2.2 and K_{ATP} are expressed in human skeletal muscle as well as many other tissues. In contrast, Kir2.6 is a skeletal muscle-specific Kir channel. The role of Kir channels in extracellular K^+ homeostasis is best illustrated by the fact that mutations of Kir2.1 and Kir2.6 cause muscle paralysis and hypokalemia, a disease known as hypokalemic periodic paralysis.[30, 31]

1.4 Hypokalemic Periodic Paralysis.

1.4.1 Introduction

Hypokalemic periodic paralysis (HypoPP) is a heterogeneous disease featured by episodic muscle paralysis associated with ictal hypokalemia as a result of shift of K^+ from plasma into muscle cells.[32] The mechanism of cellular K^+ shift is related to the pathogenesis of muscle paralysis, and not caused by any known acid-base disorders or exogenously administrated substances. HypoPP exists in familial and non-familial forms (Figure 1-2). Familial form is inherited in an autosomal-dominant pattern, and is predominantly caused by mutations in genes encoding for skeletal muscle-specific voltage-gated Na^+ channel $Na_v1.4$ or the L-type Ca^{2+} channel $Ca_v1.1$.[33, 34] Non-familial HypoPP can be associated with elevated thyroid hormone function, called thyrotoxic periodic paralysis (TPP) or without, called sporadic periodic paralysis (SPP).[35] The clinical presentation of muscle weakness and acute hypokalemia in patients with non-familial HypoPP is indistinguishable from those with familial HypoPP. Plasma K^+ levels are normal in HypoPP patients at the

baseline, and patients develop profound hypokalemia only during paralytic attacks. The mechanisms of hypokalemia and muscle paralysis in these patients remained mysterious.[31] Recent studies in familial type hypoPP have shown some promising evidences to explain pathogenesis of hypoPP, which might also be applied to non-familial type hypoPP.

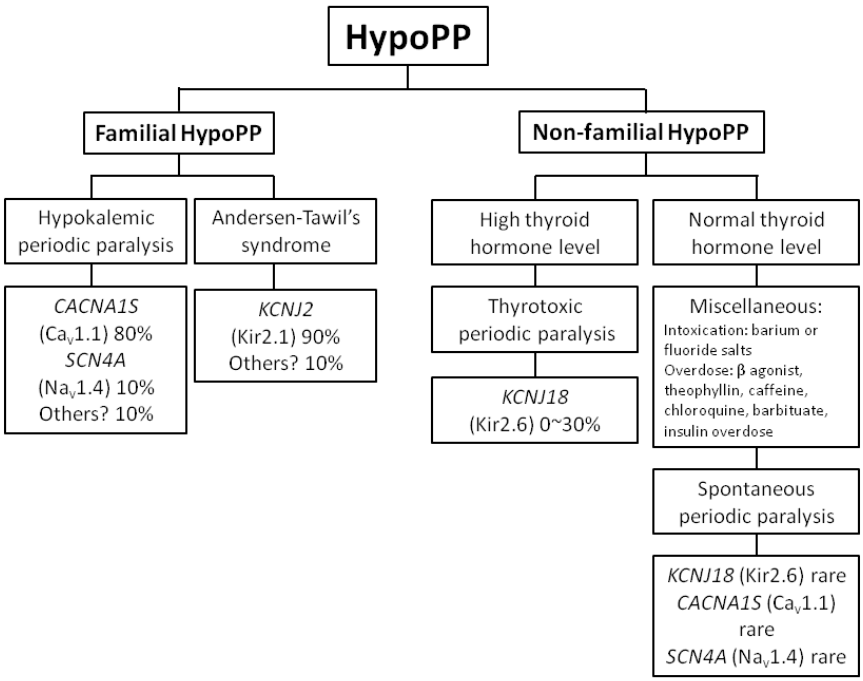

Figure 1-2. Heterogeneous etiologies of hypokalemic periodic paralysis. This diaphragm depicts various causes of hypokalemic periodic paralysis (hypoPP), categorizing into familial and non-familial hypoPP based on the presence or absence of family history of HP. Italic capital letters denote the affected genes and the word in parenthesis represents the transcribed protein (channel). The following number indicates the percentage of diseased population carrying mutations in this specific gene.

1.4.2 Hypokalemia-induced Paradoxical Depolarization

In general, the Er of cells is determined by the balance between outward K^+ currents (I_o) and inward leak currents (I_i) (See Figure 1-3A, where "I" indicates current, and "$_o$" and "$_i$" indicate outward and inward, respectively). In the sarcolemma

of skeletal muscle, the outward K^+ currents are mediated by K^+ efflux through two types of K^+ channels: Kir and Kv channels. This is illustrated in Figure 1-3A using current-voltage (I-V) relationship curve for Kir (I_{Kir}, red curve), for Kv (I_{Kv}, green curve), and for leak current (I_{Leak}, blue line). Note that outward K^+ current through I_{Kir} is hump-shaped because of reduced outward conductance at depolarized membrane potentials (i.e., strong inward rectification) and that outward K^+ current through I_{Kv} becomes significant only at membrane potentials more depolarized than -65 mV (i.e., voltage-gated). As shown in Figure 1-3A, in normal individuals under normal serum K^+ concentration 4 mM, the resting membrane potential is at -93 mV, where outward K^+ current mediated by I_{Kir} and inward cation leak current (I_{Leak}) are equal. Reducing serum K^+ concentration to 2.5 mM has two effects (Figure 1-3B). One is to shift the equilibrium potential for K^+ (E_k) to hyperpolarization (-110 mV) according to Nernst equation (E_k = -58 mV x log $\{[K]_{in}/[K]_{out}\}$). In addition, low extracellular K^+ concentration suppresses the overall conductance of Kir (i.e., bring the I-V curve closer to the zero-current line).[36] As a result, the resting membrane potential is shifted from -93 mV to -98 mV, where a new balance between outward K^+ current and inward leak current can be reached (Figure 1-3B).

The hallmark of HypoPP is depolarization of the sarcolemma induced by hypokalemia during attacks.[37] This hypokalemia-induced depolarization is in contrast to the prediction of Nernst equation and thus termed “paradoxical”. The paradoxical depolarization occurs during hypokalemia is central to the pathogenesis of periodic paralysis because it causes inactivation of Nav channels in skeletal muscle and thus muscle inexcitability and paralysis. The mechanism of hypokalemia-induced paradoxical depolarization in patients with familial HypoPP has been elucidated and

is shown in Figures 1-3C and 1-3D.[38] Mutations of $Ca_v1.1$ or $Na_v1.4$ channels in familial HypoPP create an aberrant conducting pore that allows passage of small cations (Na^+ and H^+) from outside into cells at (and only at) hyperpolarized resting membrane potentials.[39,40] This additional inward cation current through the aberrant conducting pore adds to the existing leak current thus increases the total inward leak current at hyperpolarized resting membrane potentials (shown as dotted blue line for I_{Leak} in Figure 1-3C and 1-3D). In familial HypoPP patients at normal plasma K^+ concentration, the increase in leak current results in slight depolarization in the resting membrane potential (Figure 1-3C; E_r shifts from -93 mV to -84 mV). The increase in the total leak current in familial HypoPP patients, however, poses a problem for the resting membrane during hypokalemia (when E_k is left-shifted and Kir conductance is suppressed). Because of the increase in the total leak current at hyperpolarized membrane potentials, it is now impossible for outward K^+ currents and inward leak currents to reach a new balance during hypokalemia simply by shifting E_r to hyperpolarized membrane potentials (Figure 1-3D; note that outward K^+ currents mediated by I_{Kir} [red curve] is always smaller than inward leak current at hyperpolarized membrane potentials [dotted blue line]). As a result, the balance between inward and outward currents for E_r can only be reached at depolarized E where outward K^+ current is mediated by I_{KDR} (green curve). Thus, hypokalemia causes paradoxical depolarization in patients with familial HypoPP.

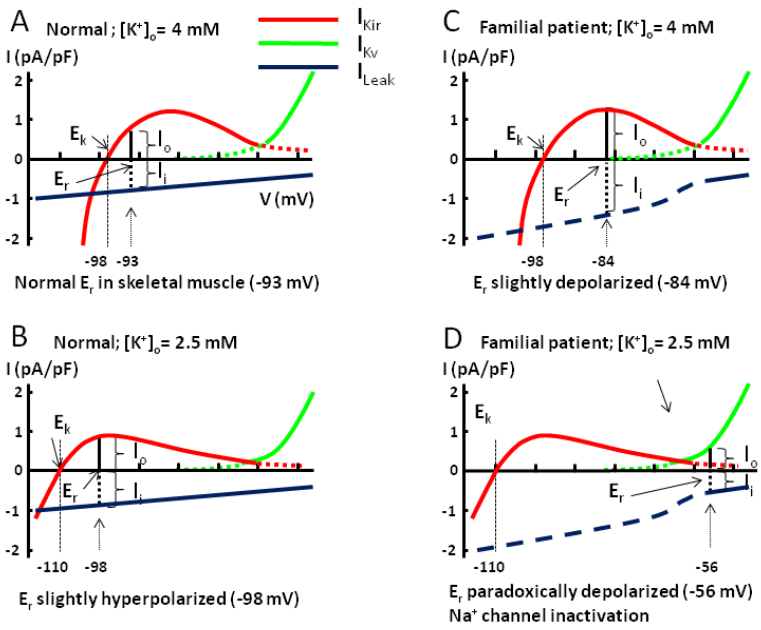

Figure 1-3. Models for paradoxical depolarization in patients carrying voltage-sensor mutations on Cav1.1 or Nav1.4 channels.
Current-voltage (I-V) relationship curves for Kir channel (red curve), Kv channel (green curve), and leak current (blue line). The reversal potential of leak current is 0 mV. Please note that aberrant gating pore current through mutated Ca^{2+} and Na^{+} channels only occur in hyperpolarized potentials (< -60 mV). Thus, the total inward leak current in familial HypoPP patients is increased in hyperpolarized potentials (shown in dotted blue line). The model is intended for conceptual understanding. Numerical value may be slightly different from true *in vivo* value.

1.4.3 The Role of Kir Channel in Hypokalemic Periodic Paralysis

Muscle paralysis and hypokalemia in HypoPP patients are frequently precipitated by strenuous exercise, high carbohydrate food, etc and in the case of TPP is associated with an increase in thyroid function. These precipitating factors stimulate Na^{+}, K^{+}-ATPase-mediated K^{+} uptake into muscles. Because of compensation by increased K^{+} efflux through K^{+} channels, increased uptake of K^{+} by Na^{+}, K^{+}-ATPase alone does not cause significant hypokalemia. Many of these precipitating factors, such as insulin and catecholamines (released during exercise and by high carbohydrate food), not only stimulate Na^{+}, K^{+}-ATPase but also inhibit Kir

channels.[35] Therefore, inhibition of K^+ efflux via Kir channels may be the additional mechanism to develop severe hypokalemia with plasma K^+ concentration < ~2 mM and muscle paralysis. The role of Kir in hypoPP is best illustrated in another familial hypoPP disease, Andersen-Tawil syndrome, an autosomal-dominant multisystem disorder related to mutations on Kir2.1 channel. With the regard to non-familial hypoPP, recent studies identified that mutations on a novel skeletal-muscle specific Kir2.6 channel predispose TPP patients to hypokalemia and paralysis. This report hinted that the similar pathogenesis of Andersen-Tawil syndrome may occur in TPP patients. However, many questions about the role of Kir in non-familial hypoPP remain unanswered. Mutations of Kir in patients with non-familial HypoPP may contribute to hypokalemia, but cannot be solely responsible because their plasma K^+ levels are normal in-between attacks. In my thesis, I plan to further investigate the role of Kir channel in extracellular K^+ homeostasis and pathogenesis of non-familial hypoPP (see detail in Chapter 2). The historic event of barium poisoning presenting hypoPP-like phenotype shares common pathogenesis with hypoPP and gives me idea of modeling the pathogenesis of non-familial hypoPP.

1.4.4 Lessons Learned from Barium Poisoning

It has been known for decades that hypokalemia and muscle paralysis develops in patients with barium intoxication.[41] Barium inhibits many types of K^+ channels, but is most potent for Kir2 subfamily of channels which are present in skeletal muscle and the heart.[28, 42] Struyk et al show that in isolated muscle fibers inhibition of I_{Kir} by barium predisposes sarcolemma to the development of paradoxical depolarization,[43] supporting the hypothesis that the mechanism of hypokalemia in barium poisoning is similar to that in Anderson's syndrome with loss-

of-function mutations of Kir2.1 and TPP/SPP with mutations of Kir2.6. The effect of barium on Kir channels in the heart explains why cardiac arrhythmia develops in patients with barium poisoning. Indeed, mutations of Kir2.1 (which is present in cardiac as well as skeletal muscle) cause Andersen's disease featured by cardiac arrhythmia, skeletal muscle paralysis, and hypokalemia.[30]

It is interesting to consider the role of Na^+, K^+-ATPase in the development of severe hypokalemia and muscle paralysis in barium poisoning. The clinical syndrome of barium poisoning was initially described by Dr. Allen in early 1940's as an endemic illness in rural China where villagers develop symptoms after ingestion of a large amount of food contaminated with barium chloride.[41] In these scenarios after large meals, insulin release and stimulation of Na^+, K^+-ATPase are invariable. On the other hand, a large inhibition of myocyte K^+ efflux by barium may be sufficient to trigger a vicious cycle of hypokalemia and paradoxical depolarization. Of note, mutations of Kir2.1 in Andersen's disease are so far heterozygous. A recent computer modeling study suggests that 50% of total Kir current is required for maintaining normal plasma potassium concentration.[44]

Barium sulfate used for radiographic contrast is not absorbable by the gastrointestinal tract, but soluble salts including barium sulfide, carbonate, and nitrate used in various pest and rodent-killer preparations can cause poisoning.[45, 46] Overdose of other cation blocker of Kir such as cesium (used in the treatment of brain tumor) or drugs that inhibit Kir channels, such as anti-malarial chloroquine or barbiturate (thiopental) can cause hypokalemia by inhibiting potassium efflux.[47-49]

1.5 The Role of Kidneys in Extracellular Potassium Homeostasis

1.5.1 Introduction of Renal Potassium Handling

To maintain the long-term extracellular K^+ homeostasis, the K^+ intake from diet and K^+ release from intracellular space have to be efficiently excreted through kidney or intestine. In normal condition, kidneys excrete approximately 90% of ingested K^+. Only when renal function is severely impaired (e.g. in uremic state of chronic kidney disease), the gastrointestinal K^+ excretion will be enhanced to compensate for the insufficient renal K^+ excretion.[50] In kidneys, K^+ is freely filtered through glomeruli and mostly reabsorbed in proximal tubules and thick ascending limb of Henle's loop (Figure 1-4). The K^+ secretion is mainly occurred in the aldosterone-sensitive distal nephron (ASDN), including late distal convoluted tubule (DCT), connecting tubule (CNT) and cortical collecting duct (CCD).[51] In ASDN, the K^+ conductance of paracellular pathway is low; thus any K^+ movement across the part of renal tubule has to be mediated by the specific K^+ transporters on both luminal and basolateral sides of tubules.[52] The mechanism of K^+ excretion in ASDN is shown in Figure 1-4. The lumen-negative transepithelial potential difference (PD_{TE}) built by the electrogenic epithelial Na^+ channel (ENaC)-mediated Na^+ reabsorption and K^+ channels on luminal surface are essential elements for K^+ excretion.[53] Renal outer medullary K^+ (ROMK) channel and calcium-activated large conductance K^+ (Maxi-K) channel are two major access of K^+ efflux from cells to tubular lumen.[54] ROMK channel is constitutively open, and Maxi-K channel is quiescent in basal state and stimulated by increased luminal (urinary) flow rate.

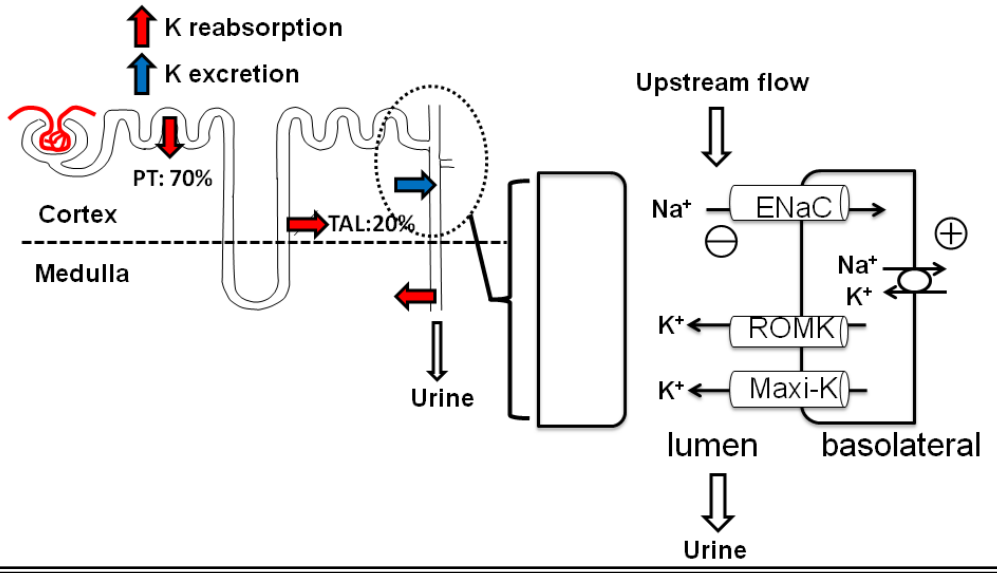

Figure 1-4. Renal K^+ handling and mechanisms of K^+ secretion in CCD.
This figure shows the big picture of K^+ handling in one nephron, functional unit of kidneys. A dotted line roughly separates the cortex (upper part) and medulla (bottom part). Most (~90%) of filtered K^+ ions are reabsorbed in proximal tubule (PT) and thick ascending limb (TAL). The remaining 10% enter the distal nephron, in which K^+ ions in interstitium and plasma can be secreted mainly into aldosterone-sensitive distal nephron (ASDN, dotted circle). The mechanism of K^+ secretion in ASDN is magnified. In medullary collecting duct and intercalated cells of cortical collecting duct, K^+ ions can be reabsorbed.

In medullary collecting duct (MCD) and CCD, K^+ ions can be further reabsorbed through the colonic H^+, K^+ ATPase on the luminal membrane of α-intercalated cells.[55] The K^+ excretion and reabsorption in ASDN and MCD determine the final urine K^+ output and are tightly regulated based on the total body K^+ balance. In the circumstances of K^+ depletion, the surface amount of ROMK and Maxi-K channels are downregulated, and the H^+, K^+ ATPase activity is highly stimulated.[54, 56] In contrast, high dietary K^+ enhances the efficiency of K^+ excretion in ASDN but suppresses the K^+ reabsorption in TAL and MCD. These regulations are controlled by hormones, including aldosterone, tissue kallikrein, and with-no-lysine (WNK) kinases. Here, I focus on the renal adaptive response to high K^+ intake and the role of WNK kinases in the regulation of K^+ secretion via ROMK channel.

1.5.2 Renal Adaptation to Chronic Potassium Load

When dietary K^+ intake is slowly increased, the efficiency of K^+ excretion in distal nephron needs to be correspondingly enhanced, so-called K^+ adaptation, to avoid K^+ accumulation in extracellular space. Early studies have observed a broad extension of the basolateral membrane of principal cells along with the increased quantity and activity of Na^+, K^+ ATPase, which is only found in CNT and CCD but not in PT, TAL and DCT.[57] This site-specific activation of Na^+, K^+ ATPase is co-localized with ENaC, which is stimulated by aldosterone and thus creates negative PD_{TE}.[58, 59] The increased Na^+ entry via ENaC may increase intracellular Na^+ concentration and in turn stimulates Na^+, K^+ ATPase. The activated Na^+, K^+ ATPase then pumps in more extracellular K^+ and increases the intracellular K^+ concentration and results in a more favorable gradient for K^+ secretion. In addition, chronic K^+ adaptation is known to increase the total and membrane abundance of ROMK and Maxi-K channels.[60, 61] They provide the access for passive K^+ efflux under the favorable electrochemical gradients. Some of these adaptive responses have been attributed to the effect of aldosterone, which stimulates ENaC via serum and glucocorticoid-inducible kinase (SGK) mediated signaling and may directly enhance the expression Na^+, K^+ ATPase.[62] However, aldosterone is obviously not the only reason for all K^+ adaptations since full renal adaptation to chronic K^+ loading can be achieved in rodents with adrenalectomy.[63, 64]

Another adaptive mechanism is to increase the Na^+ and flow delivered to distal nephron, so-called K^+-induced natriuresis, and helps maintain the favorable electrochemical gradient for K^+ secretion in distal nephron by enhancing electrogenic Na^+ reabsorption and dilutes the luminal K^+ concentration. This phenomenon was

discovered in the 1930s when people first noticed that high K^+ diet is a natural diuretic.[65-67] Later experiments demonstrated that the natriuretic effect of K^+ can be attributed to the inhibition of Na^+ reabsorption in the PT and Henle's loop.[66, 68-71] Recently, these findings were further supported by the biochemical studies showing reduced protein abundance of Na^+ transporters (Na^+, H^+ exchanger, Na^+, HCO_3^- cotransporter, and NCC) in mice fed a chronic high K^+ diet.[72-74] In contrast with PT and Henle's loop, Na^+ reabsorption via ENaC in distal nephron is stimulated by a high K^+ diet probably through the aldosterone-SGK pathway. As a result of the shift of Na^+ reabsorption from proximal tubule to distal tubule, the negative PD_{TE} is intensified without disturbing the total body Na^+ balance. Meanwhile, the increased flow also helps activate the flow-dependent Maxi-K channel.[75, 76] This adaptive mechanism involves not only K^+ and also Na^+ handling in kidneys. I plan to evaluate the role of WNK kinases, especially kidney-specific WNK1, in the K^+-induced natriuresis (see detail in Chapter 4).

1.6 Pseudohypoaldosteronism Type II

1.6.1 Introduction of WNK Kinases and Pseudohypoaldosteronism Type II

Another human disease, called pseudohypoaldosteronism type II (PHA2), has widely expanded our understanding of K^+ homeostasis and renal K^+ handling. Genetic linkage analysis has linked PHA2 to a newly discovered serine/threonine kinase family, with-no-lysine (WNK) kinase.[77] The funding member of WNK kinase, WNK1, was first identified by Xu et al in 2000.[78] Since then, four members (WNK1-4) have been found expressed in mammals. Difference from other serine/threonin

kinase, WNK kinases have the conserved catalytic lysine upstream the traditional place and therefore are named as with-no-lysine(K) (Figure 1-5A). Four WNK kinases are encoded by different genes but all share highly conserved kinase domain, auto-inhibitory domain, couple coiled-coil domains and proline-rich domains for protein-protein interactions (Figure 1-5B).

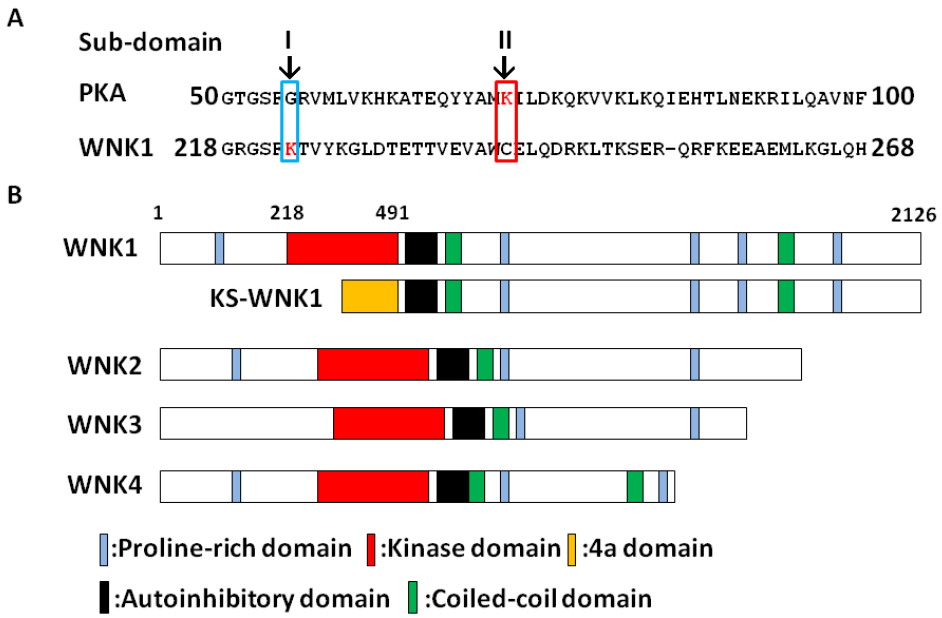

Figure 1-5. With-no-lysine kinases in mammals.
(A)Alignment of partial amino acid sequence of the kinase domain of typical serine/threonin kinase PKA and WNK1. The typical ATP-binding lysine (red color K) is located in sub-domain II (marked by red box) of PKA. WNK1 has its catalytic lysine in sub-domain I (marked by blue box). (B) Domain structure of WNK kinases in mammals.

In kidneys, four WNK kinases, WNK1, WNK3, WNK4 and kidney-specific WNK1 (KS-WNK1), are expressed throughout the nephron. Human mutations of WNK1 or WNK4 lead to PHA2, an autosomal dominant genetic disease.[79] Mutations of WNK1 cause large deletion of intron 1 and thus lead to increased expression of WNK1 mRNA and protein abundance. Mutations of WNK4 are missense mutations

outside the kinase domain. Patients carrying PHA2 mutations are characterized with adolescence-onset hypertension and hyperkalemia secondary to abnormally high Na^+ reabsorption and low K^+ secretion in kidneys, revealing the role of WNK1 and WNK4 in renal Na^+ and K^+ handling. To understand the mechanisms of WNK in the regulation of Na^+ and K^+ transporters/channels, the downstream pathways of WNK have been extensively studied in vitro. The downstream targets of WNK kinases include OSR1 (oxidative stress-responsive kinase-1) and its related kinase SPAK (Ste20-related proline-alanine-rich kinase), and SGK. The WNK-OSR/SPAK pathways regulate cation-chloride cotransporters, including NCC, NKCC and K^+, Cl^- cotransporter (KCC).[80] The WNK-SGK pathway may regulate ENaC activity.[81] The upstream regulator of WNK is mostly unknown. Although osmotic stress is known to stimulate WNK1 autophosphorylation, the underlying signaling pathway remained unclear. In chapter 3, I designed experiments to test whether phosphatidylinositol 3-Kinase (PI3K)-Akt1/SGK1 pathway is the upstream regulator of WNK1-ROMK (see details in chapter 3).

1.6.2 Effect of WNK Kinases on Na^+ Transporters

WNK1 and WNK4 phosphorylate and activate OSR1 (oxidative stress-responsive kinase-1) and its related kinase SPAK (Ste20-related proline-alanine-rich kinase), which in turn phosphorylate and activate the thiazide-sensitive NCC and the bumetanide-sensitive NKCC.[80] On the other hand, WNK4 is also reported to inhibit the membrane trafficking of NCC independent of kinase activity and WNK1 antagonizes this effect.[82] The precise mechanism of NCC regulation by WNK kinases in vivo is still unclear. In regard to ENaC, in vitro study showed that WNK1 enhances membrane trafficking of ENaC by preventing Nedd4-mediated ubiquitination and

endocytosis of the channel. This regulation is dependent on the kinase activity of WNK1 and signals through SGK1 kinase.[83] In contrast, WNK4 inhibits ENaC through kinase-independent mechanism and PHA2 mutations abrogate inhibitions.[84] Overall, these studies in heterogeneous cells make the current hypothesis that the hypertension in PHA2 patients is resulted from enhanced Na^+ reabsorption via NCC and ENaC in distal nephron.

1.6.3 Effect of WNK Kinases on ROMK Channel

ROMK channel, also known as Kir1.1, is first identified by Steven C. Hebert in 1993.[85] Human ROMK1 cDNA encodes a polypeptide of 391 amino acids long with a secondary structure containing two transmembrane (TM) domains, two cytoplasmic termini (C- and N-terminal) and an extracellular loop between TM1 and TM2. Each functional unit of ROMK channel is composed of four identical ROMK polypeptides, which form a homotetramer. On the cytoplasmic termini of ROMK channel subunit, many regulatory spots, including phosphatidylinositol 4,5-bisphosphate (PIP2) binding sites, kinase (PKA, PKC, PTK) phosphorylation sites, and ER retention signal, have been found.[86] In human kidneys, three ROMK isoforms express on the apical membrane of renal tubules spanning from TAL to CCD.[87] In normal condition, ROMK channel is the main access of K^+ secretion. Human mutations on ROMK channel disrupt the K^+ recycling and thereby impair the Na^+ reabsorption through NKCC2 in TAL and consequently lead to a genetic renal Na^+ and K^+ wasting disorder, so-called Bartter syndrome.[88] WNK kinases also regulate ROMK channel through kinase-independent endocytosis mechanism in vitro.[89] The WNK-mediated ROMK endocytosis is appeared to be clathrin and dynamin dependent process. He et al showed that the proline-rich motif of WNK1 and WNK4

bind to the SH3 domains of intersection. Intersection can further recruit dynamin and synaptojanin and eventually form a clathrin-coated vesicle of ROMK channels. PHA2 mutations of WNK1 and WNK4 enhance the endocytosis of ROMK and hypothetically cause the impaired renal K^+ secretion and hyperkalemia in PHA2 patients.

1.6.4 Mouse Models Targeting WNK Kinases or Related Proteins

The function of WNK kinases in vivo is still controversial, albeit the vast array of mechanisms proposed based on in vitro studies. To explore the physiological role of WNK kinases, people have created mouse models using different genetic engineering strategies, including gene trapping, gene knockout, gene knockin, and transgene over-expression.[90-98] Here, I summarize the currently available animal models regarding genetic modification of WNK kinases and its related proteins, and compare their phenotype (Table 1). Although WNK1 was first discovered among four WNK kinases, the development of WNK1 mouse model turns out not smooth presumably mostly due to its huge genomic size. One WNK1-deficient (WNK1+/-) mouse model was created using gene-trapping method and showed lower blood pressure.[90] With the regard to WNK4, three mouse models, including overexpression of WNK4 wild type or WNK4 PHA2 mutant (Q562E) transgene ($TgWNK4^{WT}$, $TgWNK4^{PHA2}$), WNK4 PHA2 mutant (D561A/+) knockin ($WNK4^{D561A/+}$), and hypomorphic WNK4, have been created.[91-93] Both $TgWNK4^{PHA2}$ and $WNK4^{D561A/+}$ displayed hypertension, hyperkalemia and increased abundance and activity of NCC, supporting the pathogenic role of increased NCC-mediated Na^+ reabsorption in PHA2.[91] In $WNK4^{D561A/+}$ mice, the phosphorylation on SPAK/OSR was enhanced, indicating the association of WNK4 and SPAK/OSR in vivo.[92] Some uncertainties,

such as the effect of WNK4 on ENaC, ROMK and Maxi-K, are still controversial. Compared to full-length WNK1 (FL-WNK1) and WNK4, KS-WNK1 lacks kinase activity and has limited distribution at distal nephron.[99] However, the abundance of total KS-WNK1 expression in kidney is approximately 10 times higher than FL-WNK1. In cultured cells, KS-WNK1 antagonizes the effect of FL-WNK1 in vitro.[100] To clarify the effect of KS-WNK1 in vivo, both KS-WNK1 knockout (KS-WNK1 KO) mice and KS-WNK1 transgenic (KS-WNK1 Tg) mice have been created.[94-96] Two KS-WNK1 KO mouse models exhibited similar phenotype with blood pressure intended to be higher and similar biochemical findings of enhanced abundance of total and phosphorylated NCC in DCT.[94, 95] However, the physiological roles of KS-WNK1 in TAL and CCD have not been entirely settled. On the other hand, KS-WNK1 Tg mice basically presented the phenotype mirroring to that in KS-WNK KO mice with hypotension, hypokalemia and decreased NCC and NKCC2 abundance.[95, 96] All these three KS-WNK mouse models strongly approved the role of KS-WNK1 in Na^+ reabsorption in distal nephron, albeit some discrepancies. Recently, mouse models targeting two WNK kinase downstream targets, SPAK/OSR, have also been created and showed the importance of SPAK/OSR in Na^+ reabsorption along the TAL and DCT.[97, 98] Taking the advantage of these animal models, the full understanding of the roles of WNK kinases in kidneys is already on the horizon.

Table 1 Mouse models targeting WNK kinases and related proteins

Mouse model	BP	$[K^+]s$	NKCC2	p-NKCC2	NCC	p-NCC	NCC activity	ENaC	ENaC activity	ROMK	Maxi-K
Human PHA2	↑	↑	?	?	↑	↑	↑	?	?	?	?
WNK1+/- GT, [90]	↓*	↔	ND	ND	↔	↔	↔				
TgWNK4^{WT}, [91]	↓	↔	ND	ND	↓	ND	ND	↔	ND	↑	ND
TgWNK4^{PHA2}, [91]	↑	↑	ND	ND	↑	ND	ND	↔	ND	↔	ND
WNK4$^{D561A/+}$, [92]	↑	↑	ND	ND	↑	↑	↑	↑	↑	↔	↑
WNK4^{hypomorph}, [93]	↓^{ø}	↔	ND	ND	↔	↓	ND	↑	ND	↔	↔
KS-WNK1 KO[94]	↔^{a}	↔	ND	ND	↑	↑	ND	↓	↓	↑^{b}	↑
KS-WNK1 KO[95]	↑†	↔	↑	↑	↑	↑	ND	ND	ND	ND	ND
KS-WNK1 Tg[96]	↓	↓	↓	↓	↓	↓	ND	ND	ND	↑	ND
SPAK KO[97]	↓	↓	↑	↑	↓	↓	↓	ND	ND	ND	ND
Ksp-OSR KO[98]	↓	↓	↔	↓	↑	↑	↔	ND	ND	ND	ND

Abbreviations: BP, blood pressure; $[K^+]s$, serum K^+ concentration; GT, gene-trapping; ND, not determined.

*The result is disputed[101], ^{ø}significant only in the period of high activity, ^{a} only diastolic blood pressure is significantly higher, ^{b}non-quantitative immunofluoresence staining, † under high Na^+ diet. The reference for individual mouse model is marked as a superscript number beside the model name.

CHAPTER TWO

IDENTIFICATION AND FUNCTIONAL CHARACTERIZATION OF KIR2.6 MUTATIONS ASSOCIATED WITH NON-FAMILIAL HYPOKALEMIC PERIODIC PARALYSIS

2.1 Introduction

Hypokalemic periodic paralysis (hypoPP) is a syndrome of ictal hypokalemia and hypokalemia-related skeletal muscular paralysis. A vast array of etiologies can cause hypoPP and can be divided into familial or non-familial form.[102] Most patients with familial hypoPP, inherited in autosomal-dominant pattern, have been linked to mutations in genes encoding for skeletal muscle-specific voltage-gated Na^+ channel $Na_v1.4$ (*SCN4A*)(~30%) or Ca^{2+} channel $Ca_v1.1$ (*CACNA1S*)(~60%).[33, 34] About 10% of cases of familial hypoPP remain genetically undefined.[40] Familial hypoPP is more common among Caucasians.[103]

Among diseases of non-familial hypoPP, thyrotoxic periodic paralysis (TPP) is most common, especially in Asian and Hispanic populations with the incidence of approximately 2% in patients with hyperthyroidism.[35, 104] In Caucasians, the incidence of TPP is estimated at between 0.1 to 0.2%.[105] The clinical presentation of patients with TPP is indistinguishable from those with familial hypoPP. TPP can occur in association with any of causes of hyperthyroidism and may precede other symptoms of hyperthyroidism. Despite no obvious clinical symptoms of hyperthyroidism in some TPP patients, all of them have elevated blood levels of thyroid hormones and depressed thyroid stimulating hormone (TSH) during attacks.[35, 106, 107] The second most common form of non-familial hypoPP, called sporadic periodic paralysis

(SPP), also afflicts predominantly Asians and presents with normal blood levels of thyroid hormones and TSH during attacks.

Despite the improved understanding of the disease mechanism of familial hypoPP with Cav1.1 or Nav1.4 channel mutations, the pathogenesis of non-familial hypoPP remains elusive. Based on the phenotypic similarity between familial hypoPP and TPP/SPP, a disease of channelopathy, malfunction of ion channels, has always been considered in TPP patients and studied through genetic screening of various ion channels. Indeed, a recent study reported that mutations in *KCNJ18* gene encoding a novel member of inward rectifier K^+ channel, Kir2.6, occur in some TPP patients.[31] Of note, the 5' upstream promoter region of *KCNJ18* gene contains a thyroid hormone response element, which allows thyroid hormone to enhance the transcription of *KCNJ18*. Ryan et al has hypothesized that mutations of Kir2.6 may change the membrane excitability of skeletal muscle predisposing patients to muscle paralysis and that the transcriptional upregulation of Kir2.6 by thyroid hormones plays an important role in the pathogenesis of TPP.

In this project, I investigated whether mutations of Kir2.6 occur in other non-familial hypoPP, specifically SPP, and the incidence of Kir2.6 mutations in Chinese TPP patients. In addition, I also tested whether the mutant Kir2.6 channels exert dominant-negative inhibition on wild type Kir2.6 and other Kir2.x channel in skeletal muscle, especially the dominant Kir2.1.

2.2 Materials and Methods

2.2.1 Identification of Patients with TPP or SPP

The study protocol was approved by the Ethics Committee on Human Studies at Tri-Service General Hospital in Taiwan, R.O.C. Written informed consent was

obtained from each patient. I collected DNA and clinical and laboratory data from 100 patients with the diagnosis of TPP and 60 patients with SPP admitted to Tri-Service General Hospital or affiliated hospitals between 2002 and 2009. TPP is defined as acute muscle weakness with inability to ambulate (muscle power less than Medical Research Council [MRC] scale grade 3) accompanied by hypokalemia (plasma K^+ level less than 3.0 mEq/l) at presentation caused by a sudden shift of K^+ into cells (urine transtubular K^+ gradient (TTKG) < 3) and hyperthyroidism, confirmed by suppressed plasma thyroid-stimulating hormone (TSH) and elevated levels of plasma triiodothyronine (T_3) and free thyroxin (fT_4). Renal and intestinal K^+ wasting and medications as causes of hypokalemia were excluded based on TTKG > 3 (suggesting renal K^+ wasting), no medications including diuretics, laxatives, amphetamine, beta-agonist, caffeine, and no history of increased gastrointestinal output. Other identifiable causes of transcellular K^+ shift, such as fluid-electrolyte and acid-base disturbances, are also excluded. SPP is diagnosed based on no family history of episodic paralysis and fulfillment of the above criteria of hypokalemic periodic paralysis except that with normal levels of plasma T_3, fT_4, and TSH. Screening of known genes mutated in familial hypoPP including *CACNA1S, SCN4A, and KCNJ2* were performed. I found no mutations in *CACNA1S, SCN4A, and KCNJ2* in all TPP patients but one mutation (R1239H) in CACNA1S and two (R669H X2, R1135H x1) in SCN4A in four separate SPP patients.[108] Mutations in *KCNJ18* (see below) were found in SPP patients without mutations in *CACNA1S or SCN4A*. Blood and urine biochemical values and electrolytes were determined with the use of automated methods (AU 5000 chemistry analyzer; Olympus, Tokyo, Japan). Thyroid function tests were determined by radioimmunoassay (RIA) method.

2.2.2 Mutational Analysis of KCNJ18 Gene

Genomic DNA was prepared from the peripheral blood of TPP and SPP patients and healthy control subjects using the QIAamp (Qiagen). Sequencing of *KCNJ18* was performed as previously described.[31] PCR primers were designed against the GenBank accession NM_021012 sequence with the forward primer containing two nucleotide mismatches to favor amplification of diverse products. I performed nested PCR of Kir2.6 with 20 ng outer PCR product in 50 μl reaction containing 10 mM Tris-HCl (pH 9 at 25℃), 50 mM KCl, 0.1% Triton X-100, 200 μM each dNTP, 1.5 mM $MgCl_2$, 1 U Taq DNA polymerase, and 25 pmol forward and reverse primers (CGAGGAGGGCGAGTACATC/CAAGATGGTGATGGGCG) under the following conditions: 5 cycles at 66℃ for 30 s and 72℃ for 1 min, plus 30 cycles at 64℃ for 30 s and 72℃ for 1 min, each cycle preceded by a 94℃ step. The resulting products were subcloned into pCR2.1 (Invitrogen, Carlsbad, CA) and sequenced. The products were sequenced with the same primers used for amplification, with BigDye terminator v3.1 mix and subsequent analysis by capillary electrophoresis on an ABI Prism 377 Genetic analysis (Perkin Elmer Applied Biosystems, Foster City, CA, USA).

2.2.3 Plasmid DNA and Transient Expression of Kir Channels in Cultured Cells

Human embryonic kidney (HEK)-293 cells were maintained in Dulbecco's modified Eagle's medium with 10% frozen bovine serum/2 mM L-glutamine/100 units/ml penicillin/streptomycin. Cells were transfected with wild type and/or mutant cDNA of Kir2.6 (pEGFPC2-Kir2.6, a gift from Dr. L.J. Ptacek, University of California, San Francisco) and/or Kir2.1 (in pcDNA3.1 vector) using Fugene HD

(Roche). Point mutations were generated by site-directed mutagenesis (QuickChange kit, Stratagene) and confirmed by sequencing. To avoid saturation of channel protein expression, the maximal amount of cDNA for channels used for transfection was ≤ 0.9 μg. The total amount of plasmid DNA in each experimental group was balanced using empty vector.

2.2.4 Immunoblotting and Surface Biotinylation Assay

Transfected, cultured HEK cells were incubated with lysis buffer (50 mM HEPES (pH 7.6), 150 mM sodium chloride, 0.5% Triton X-100, 10% glycerol, 0.1% SDS) containing protease inhibitor cocktail (Complete Mini, Roche) and phosphatase inhibitor cocktail (PhosSTOP, Roche). After shaking 30 minutes on the rotator at 4℃, extracts were clarified by centrifugation. Protein concentrations of supernatant were measured by the Bradford assay using bovine serum albumin as a standard. Equal amounts of lysates were mixed with Laemmli sample buffer and then separated by SDS-PAGE under reducing conditions. Proteins were transferred to nitrocellulose membranes, blocked by 5% nonfat milk and incubated with the anti-GFP antibody (horseradish peroxidase conjugate; Invitrogen; 1:1000 dilution) to detect protein expression of pEGFP-Kir2.6. Anti-β-actin antibody was used to detect endogenous β-actin as a loading control. Bound antibodies were detected using ECL detection reagent (Pierce).

For biotinylation of cell-surface Kir2.6, transfected HEK cells (per 35 mm well) were washed with 1 ml ice-cold PBS thrice and incubated with 1 ml PBS containing 1.5 mg/ml EZ-link-NHS-SS-biotin (Thermo Scientific) for 2hr at 4^{o}C. After quenching with glycine-containing PBS for 20 minutes, cell were lysed in a RIPA buffer (150 mM NaCl, 50 mM Tris-HCl, 5 mM EDTA, 1% Triton X-100, 0.5

% DOC and 0.1% SDS) containing protease inhibitor cocktail for 30 minutes. Biotinylated proteins were precipitated by streptavidin-agarose beads (Thermo Scientific) for 2 hrs at 4^{o}C. Beads were subsequently washed 3 times with TBS containing 1% Triton X-100. Biotin-labeled proteins were eluted in sample buffer, separated by SDS-PAGE, and transferred to nitrocellulose membranes for Western blotting using anti-GFP antibody. Biotinylation experiment was performed 4 times with similar results.

2.2.5 Electrophysiological Recording

About 36-48 hours after transfection, cells were trypsinized and plated on poly-L-lysine coated cover slips. Whole cell Kir2.x currents were recorded by using an Axopatch 200B amplifier (Axon Instruments, Foster City, CA). The pipette resistance was around 2-4 MΩ. Transfected cells were identified by green fluorescence using epifluorescent microscopy. In whole-cell current recordings, the pipette solution contained (in mM) 110 K-aspartate, 20 KCl, 10 EGTA, 2 Mg-ATP, 5 glucose, 10 HEPES (pH 7.4); the bath solution contained 117 NaCl, 30 KCl, 1 $MgCl_2$, 2 $CaCl_2$, 10 HEPES (pH 7.3), 2 $NaHCO_3$, and 5 glucose. The cell membrane capacitance and series resistance were monitored and compensated (>75%) electronically. The voltage protocol consisted of 0 mV holding potential for 50 ms and 100-ms steps from -60 to 60 mV in 10 mV increments. After initial recording of current, $BaCl_2$ (30 μM) was added to the bath solution to inhibit K^+-specific currents. Residual current in the presence of Ba^{2+} was subtracted from the total current. Data was sampled at 5 kHz with a 2 kHz low-pass filter. ClampX 9.2 software (Axon Instruments) was used for data acquisition. Current density was calculated by dividing current at designated holding potential (pA; measured at 25℃) by

capacitance (pF). Results were shown as means ± S.E.M. (n = 6–10). Each experiment (i.e., set of results shown in each panel of a figure) was repeated two to four times. For cell-attached single-channel recordings, pipette and bath solution each contained (in mM) 150 KCl, 2 $MgCl_2$, 1 EGTA, and 10 HEPES (pH 7.4). Currents were recorded at 50 kHz continuously for 1-10 mins at the test voltage from 120 mV to -120 mV with a 1kHz low-pass filter. Single-channel current were calculated by curve fitting the sum of a number of Gaussian curves to the recorded data. Open probability was calculated from the relative areas of these Gaussian curves. Single channel conductance was calculated from the slope of single-channel current amplitudes between -40 and -100 mV.

2.2.6 Statistical Analysis

Laboratory data of patients were presented as the mean ± S.D. Two-tailed unpaired Student's t-test was used to compare the differences among TPP and SPP. In functional experiments, data analysis and curve fitting were performed with the Prism (v5.03) software (GraphPad Software, San Diego, CA, USA). Data were presented as mean ± S.E.M.. Statistical comparisons between two groups of data were made using two-tailed unpaired Student's t-test. Multiple comparisons were determined using one-way ANOVA (analysis of variance). Statistical significance was defined as *p* values less than 0.05 for single comparison and less than 0.01 for multiple comparisons.

2.3 Results

2.3.1 Clinical and Laboratory Characteristics of TPP and SPP Patients

I studied 120 Taiwanese patients with the diagnosis of TPP and 60 patients with SPP. Identification and the diagnostic criteria for the patients were described in the "EXPERIMETNAL PROCEDURES". As shown in Table 2, the mean age of TPP and SPP patients at diagnosis were similar. The male to female ratio was 116:4 and 60:0 for TPP and SPP, respectively. Thyroid function tests including T_3 and free T_4 (fT_4) were markedly elevated in patients with TPP, but normal in SPP. Consistent with the elevated thyroid hormone function, thyroid stimulating hormone (TSH) was suppressed in patients with TPP. Both groups of patients had ictal hypokalemia. The plasma K^+ concentrations however, were not different between two groups. As reported previously,[35] plasma phosphate concentration during attacks was significantly lower in TPP than SPP, presumably reflecting a transcellular shift of phosphate stimulated by thyroid hormones. The spot urine K^+ concentration and TTKG were very low in the presence of hypokalemia, consistent with the idea that an increased shift of K^+ into cells was responsible for the hypokalemia in these patients. As described in the "EXPERIMETNAL PROCEDURES", other causes of hypokalemia for these patients, including mediations, renal and intestinal K^+ wasting, were excluded.

Table 2. Patient's characteristics in TPP and SPP

	TPP	**SPP**
Number	**120**	**60**
Age	29 ± 6	25 ± 8
M:F	**116:4**	**60:0**
Plasma		
K^+ (3.5-5.1 mEq/l)	2.1± 0.2	2.2 ± 0.2
T_3 (86-187 ng/dl)	334 ± 91*	124 ± 30
fT_4 (0.8-2.0 ng/dl)	4.0 ± 1.1*	1.1 ± 0.4
TSH (0.35-5.0 μU/l)	< 0.03*	2.3 ± 1.0
Na^+ (136-142 mEq/l)	141 ± 2	142 ± 5
Cl^- (98-106 mEq/l)	106 ± 2	103 ± 8
Phosphate (2.6-4.6 mg/dl)	2.0 ± 0.5*	2.6 ± 0.7
Ionized calcium (4.5-5.3 mg/dl)	4.8 ± 0.2	4.7 ± 0.2
Magnesium (1.7-2.4 mg/dl)	1.8 ± 0.3	2.0 ± 0.4
Urea nitrogen (12-20 mg/dl)	12 ± 3	12 ± 6
Creatinine (Cr) (0.7-1.2 mg/dl)	0.7 ± 0.2*	1.0 ± 0.3
Urine		
K^+ (mEq/l)	9 ± 4	11 ± 5
Creatinine (mg/dl)	108 ± 32	112 ± 37
TTKG	2.4 ± 0.9	2.1 ± 0.4

*denotes $p < 0.05$ when TTP vs. SPP.

2.3.2 Identification of Kir2.6 Mutations in Patients with TPP and SPP

In the TPP cohort, two of 100 patients carried the same V168M mutation. A heterozygous guanine to adenosine single-base substitution at nucleotide 502 (G502A, GTG to ATG) in exon 3 resulted in a missense mutation from valine to methionine at codon 168 (V168M) in the second transmembrane domain (Figure 2-1, upper, Figure 2-2A). The thyroid function tests of these two TPP patients are as follows: free T_4 2.92 and 6.21 ng/dl, T_3 235.8 and 334 ng/dl, respectively, TSH both < 0.03 IU/L. In the SPP cohort, two of 60 SPP patients had different mutations in Kir2.6. A heterozygous cytosine to thymine substitution at nucleotide 127 (C127T, CGC to TGC) in exon 1 resulted in a missense mutation from arginine to cysteine at codon 43 (R43C) in the N-terminal cytoplasmic domain (Figure 2-1, lower left, Figure 2-2A). Another heterozygous guanine to cytosine substitution at nucleotide 598 (G598C, GCC to CCC) in exon 3 led to a missense mutation from alanine to proline at codon 200 (A200P) in the C-terminal cytoplasmic domain (Figure 2-1, lower right, Figure 2-2A). The thyroid function tests for these two SPP patients are as follows: free T_4 1.21 and 1.56 ng/dl, T_3 102 and 125 ng/dl, TSH 3.1 and 2.3 IU/L.

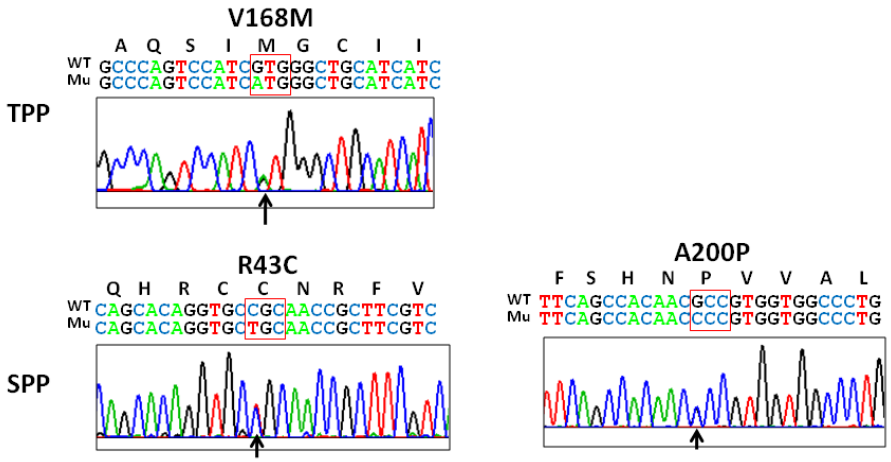

Figure 2-1. *KCNJ18* mutations in TPP and SPP patients.
Chromatograms of partial sequences of *KCNJ18* showing one heterozygous point mutation with guanine 501 mutated to adenosine (GTG→ATG) leading to single amino acid substitution from valine to methionine (V168M) was found in two TPP patient (26- and 32-year-old males); one heterozygous point mutation with cytosine 127 mutated to thymidine (CGC→TGC) leading to the substitution of arginine 43 by cysteine (R43C) was found in a SPP patient (24-year-old male); and one heterozygous point mutation with guanine 598 mutated to cytosine (GCC→CCC) leading to alanine 200 to proline (A200P) mutation was found in another SPP patient (52-year-old male). Bold letters above nucleotide sequence represent corresponding coding amino acids. Mutated nucleotides are pointed by arrows, and mutated codons are surrounded by red box. "WT" and "Mu" designate wild type allele and mutant allele respectively.

R43, V168 and A200 of Kir2.6 are identical or relatively conserved among Kir channel families (Figure 2-2B). None of 100 healthy control subjects had these three mutations in Kir2.6.

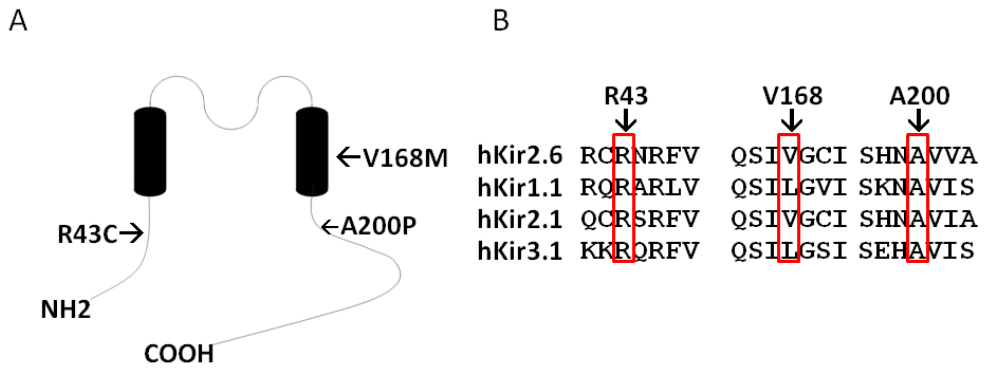

Figure 2-2. R43, V168 and A200 are conserved residues among Kir members.
(A) Membrane topology of Kir2.6 showing relative locations of mutations. (B) Amino acid sequence alignment of three mutation sites from each of the four members of the inward rectifying K^+ channels. Mutations are indicated by red rectangle.

2.3.3 Mutations in Kir2.6 Cause Reduced Currents

To investigate the functional impact of these mutations in Kir2.6 channel, I measured K^+ currents through these mutant channels by ruptured whole-cell patch-

clamp recording (Figure 2-3A). Wild type and three mutant channels expressed similar amount of proteins in transfected HEK cells (Figure 2-3B).

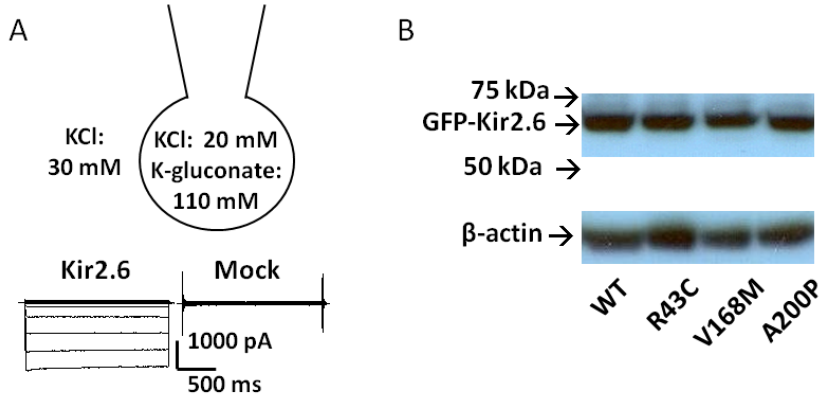

Figure 2-3. Functional evaluation and protein expression of wild type and mutant Kir2.6 channels.
(A) Configuration of ruptured whole-cell recording, voltage-clamp protocol (from -60 mV to 60 mV with 10 mV increment), representative currents from Kir2.6- and mock-transfected cells were shown. (B) Protein expression of wild type (WT) and three mutant (R43C, V168M, A200) GFP-tagged Kir2.6 channels (GFP-Kir2.6) was detected by Western blot. β-actin was used as a loading control.

The current-voltage relationship showed that K^+ currents through Kir2.6 channels were strongly inwardly rectifying with negative slopes for outward currents at highly depolarized membrane potentials (Figure 2-4A, upper). Compared to that for wild type Kir2.6, cells transfected with R43C and V168M mutants displayed reduced currents. Current density in cells expressing A200P mutant were not significantly different from mock-transfected cells (5.3 ± 0.7 pA/pF versus 4.1 ± 0.9 pA/pF at -60 mV for mock-transfection), indicating that A200P mutation in Kir2.6 resulted in a complete loss-of-function. R43C and V168M mutations affected both inward and outward currents. Inward currents through R43C and V168M mutants measured at -60 mV holding potential were ~25% and ~60% of wild type, respectively (Figure 2-4A, lower bar graph). For comparison, outward currents measured at -20 mV holding potential were ~30% and ~40% of wild type, respectively (Figure 2-4B). Thus,

mutations of Kir2.6 in patients with TPP and SPP result in hypofunction or non-function of the channel.

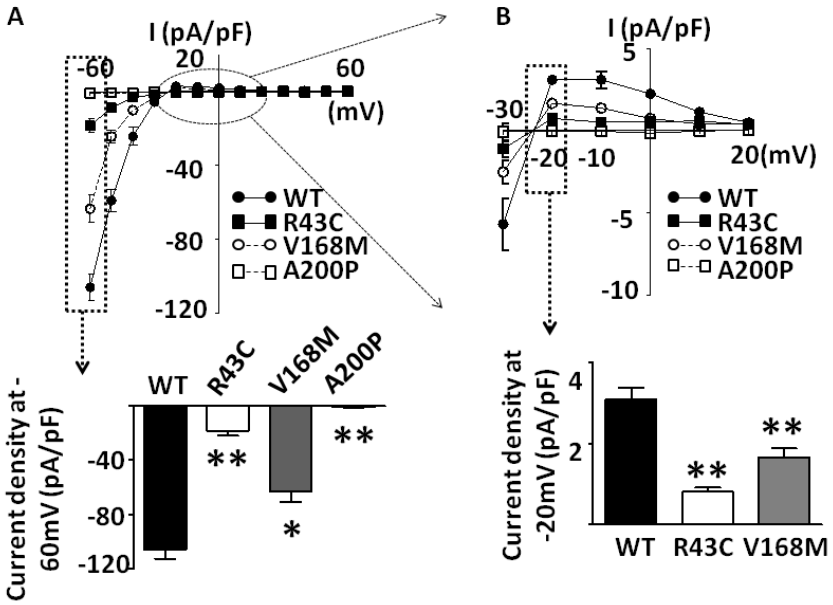

Figure 2-4. Functional characters of R43C, V168M, and A200P *KCNJ18* mutations.
(A) Upper panel, Current-voltage (*I-V*) relationship curve of WT and mutant Kir2.6 channels were shown. Lower panel, representative bar graphs of wild type and three mutant Kir2.6 current density (pA/pF; normalized to the cell surface area) at holding potential -60 mV(inward current, dotted box) (B) The portion of outward hump current in this *I-V* curve was magnified (dotted circle in A, in the range of holding potential from -30 to 20 mV). Representative bar graphs of wild type and three mutant Kir2.6 current density (pA/pF; normalized to the cell surface area) at holding potential -20 mV (outward current, dotted box) (mean ± S.E.M., $n \geq 6$ for each). Single and double asterisk denote $p < 0.05$ and $p < 0.01$ respectively between wild type and each mutation by unpaired two-tailed Student's t test.

2.3.4 Disease Mutations in Kir2.6 Impair Membrane Trafficking

I went on investigate whether these disease mutations alter cell surface abundance of Kir2.6 channels. In preliminary experiments, I found that wild type Kir2.6 protein was barely detectable by cell surface biotinylation, likely due to the fact that no amine group in extracellular loop of Kir2.6 available for biotinylation

reaction. To overcome the problem, I mutagenized histidine-118 of Kir2.6, which is located in the pre-selectivity filter "turret" region of the extracellular loop and not conserved among Kir2.x families, to a lysine. Figure 2-5 showed that H118K mutation did not affect protein expression or whole-cell current density of the "normal" and disease Kir2.6 mutants (i.e., whole-cell current density of H118K mutant was not significantly different from that of wild type; and current density of double mutants carrying H118K and each of the three disease mutations relative to H118K were not significantly different from results in Figure 2-4).

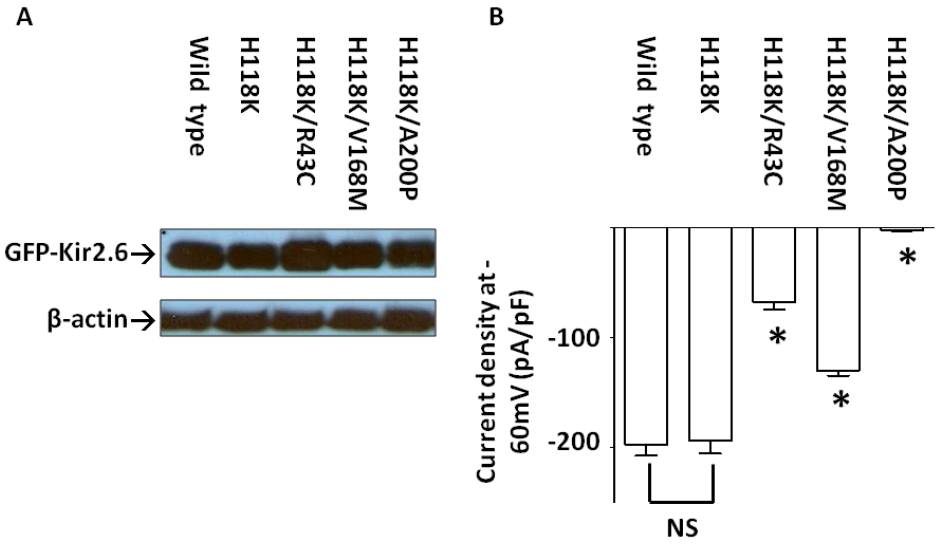

Figure 2-5. Effect of H118K mutation on wild type and three mutant Kir2.6 channels.
(A) The protein expression of wild type and mutant Kir2.6 channels was detected by Western blotting analysis. β-actin was used as a loading control. (B) Kir2.6 inward current density at holding potential -60 mV was measured and presented as a bar graph (mean ± S.E.M., $n \geq 6$ for each). Single asterisk denotes $p < 0.05$ between H118-Kir2.6 and each double mutant channel. NS denotes not statistically significant.

The result of biotinylation experiment using H118K as the backbone showed that R43C and A200P mutants had significantly less surface abundance than wild type (Figure 2-6, lane 3, 5 versus lane 2), but V168M mutant was not different from wild type (lane 4 versus lane 2). To recapitulate patients with heterozygous mutation, we coexpressed equal amounts of wild type and each mutant Kir2.6 cDNA and examined the amount of surface Kir2.6. The results showed that under these heterozygous conditions cell surface abundance of R43C and A200P mutants remained significant lower than wild type (lane 7, 9 versus lane 2). Interestingly, A200P mutant exerted dominant-negative inhibition on the surface abundance of wild type channel (lane 9 versus lane 6). Lane 1 and 10 showed negative control for biotinylation (no biotinylation reagents added) and inefficient biotinylation of wild type channel (lacking H118K mutation), respectively. As protein expression for wild type and disease mutants are similar (Figure 2-3, 2-5), the effects of R43C and A200P mutations on cell surface abundance likely represent defects in the forward membrane trafficking and/or endocytosis of the channel.

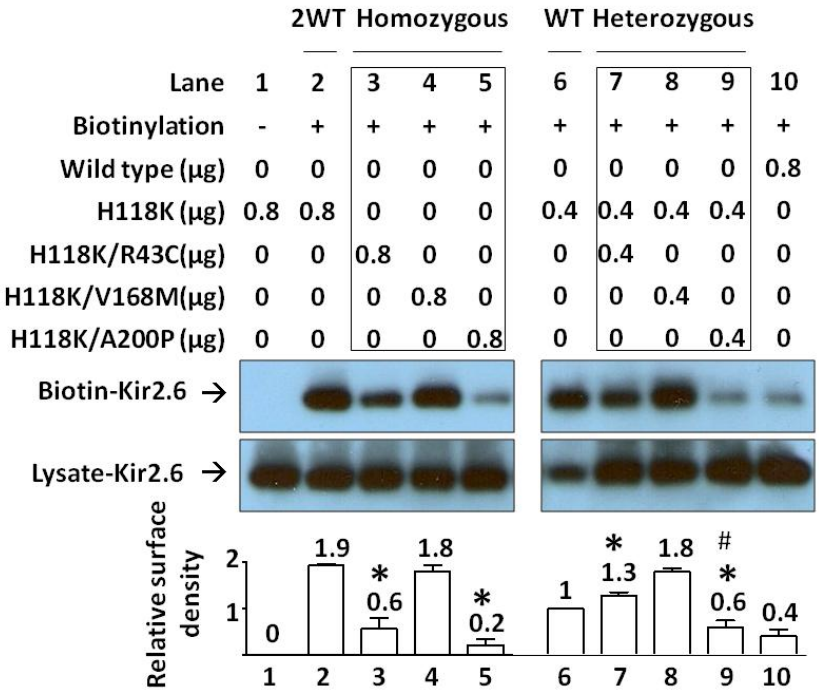

Figure 2-6. Cell surface abundance of mutant Kir2.6 channels.
Effect of three human Kir2.6 mutations on membrane abundance of channel. HEK cells were transfected with wild type and/or mutant Kir2.6 cDNAs (in μg cDNA as indicated). 2WT (lane 2) and WT (lane 6) reflect the ratio of protein expression from two or single allele of *KCNJ18* respectively. Homozygous (lane 3-5) and heterozygous groups (lane 7-9) (marked by box) stand for homozygous mutation with 2 mutant alleles and heterozygous mutation with one mutant allele and one wild type allele respectively. Lane 1 is non-biotinylated group for negative control. Lane 10 shows low efficiency of biotinylation reaction in wild type Kir2.6. Lysate- and Biotin-Kir2.6 represent Kir2.6 channels in HEK cell lysates and in elute from mixture of HEK cell lysates and streptavidin-agarose beads respectively. Bar graph in the bottom is the relative surface density of Kir2.6 channel (normalized to lane 6). Mean ± S.E.M. from four separate experiments is shown on top of each bar. * denotes $p < 0.05$ each group versus lane 2. # denotes $p < 0.05$ lane 9 versus lane 6. Gel shown is representative of four experiments with similar results. The abundance of each band in the gel was measured by densitometry by the Image J program available at the NIH website

2.3.5 R43C and V168M Mutations Affect Single Channel Properties of Kir2.6 Channel

The effects of disease mutations on the conductance and open probability of the channel was examined using cell-attached single channel recording (Figure 2-7A). Figure 2-7B showed representative single channel recordings of wild type, R43C and V168M Kir2.6 channels with 150 mM K^+ in the pipette and bath solution and at -80 mV membrane potential (= -pipette holding potential). As shown, wild type Kir2.6 was constitutively active with a relatively high open probability over the displayed time scale (upper tracing). Compared to wild type, R43C (middle tracing) and V168M mutant (lower tracing) exhibited lower single-channel current amplitude and lower open probability, respectively.

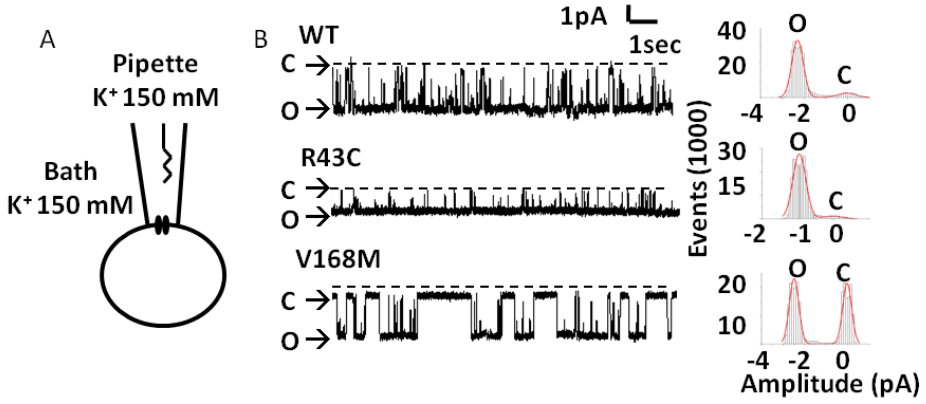

Figure 2-7. Single channel properties of wild type and mutant Kir2.6 channels. (A) Configuration of cell-attached single channel recording of Kir2.6. (B) Left, representative tracings of wild type (WT, upper), R43C (middle) and V168M (lower) Kir2.6 single channel recording at membrane potential -80 mV. Dotted line indicates channel closed. "O" and "C" indicate open and closed state respectively. Right, all-point histogram of the representative tracings. Bin width = 0.1 pA. Curve red lines indicate fits by the sum of two Gaussian distributions.

The single channel slope conductance was measured from current amplitude at between -40 and -120 mV membrane potentials (Figure 2-8A). As shown, R43C mutation reduced the slope conductance by 45% (33.2 ± 2.0 pS for wild type versus

18.4 ± 1.2 pS for R43C, n = 5 for each, $p < 0.01$). V168M mutation has no effect on the slope conductance. We analyzed single channel open probability of wild type and mutant channels between -40 and -120 mV membrane potentials (Figure 2-8B). There was a slight increase in the open probability from -120 mV to -40 mV. Over the voltage range, V168M mutant, but not R43C mutant, showed a lower open probability than wild type (for example, 0.67 ± 0.02 for V168M versus 0.92 ± 0.02 for wild type, at -80 mV, n = 5 each, $p < 0.0001$). In conclusion, R43C and V168M mutation in Kir2.6 reduce single-channel conductance and open probability, respectively.

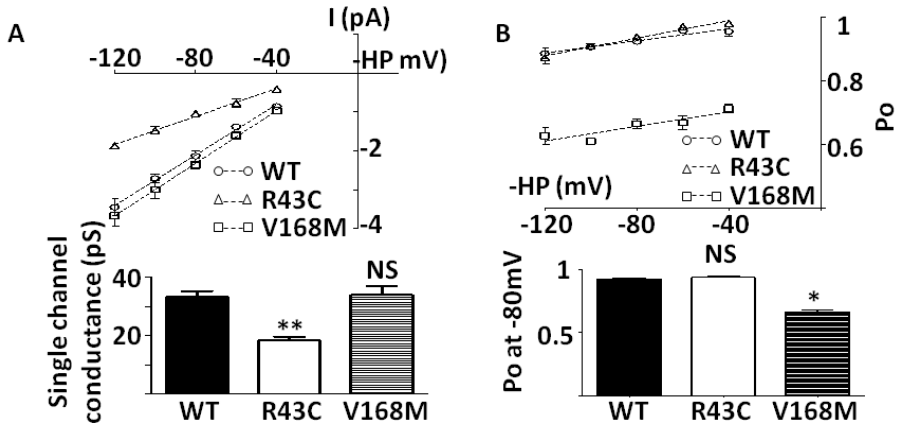

Figure 2-8. R43C and V168M mutant cause reduced conductance and open channel probability, respectively. (A) Upper, single channel current-voltage (*I-V*) relationship. Single channel currents were recorded at membrane holding potentials (HP) ranged from -40 to -120 mV. Slope conductance (dotted line) were calculated by linear regression. Lower, bar graph of single channel conductance. (B) Upper, open channel probability (Po) of WT and mutant single channels were analyzed by amplitude histogram at HP ranged from -40 to -120 mV. Dotted lines were linear regressions of Po. Lower, bar graph of open channel probability of WT and mutants at membrane potential -80 mV. Single and double asterisk denotes $p < 0.05$ and $p < 0.01$ respectively between wild type and each mutation. NS denotes statistically not significant.

2.3.6 Disease Mutants Exert Dominant Negative Inhibition on Wild Type Kir2.6

To better understand the *in vivo* impact of these heterozygous mutations, I further examined potential dominant-negative effects of mutants on wild type channel. In these experiments, I cotransfected HEK cells with wild type and/or mutant Kir2.6 cDNA at indicated concentrations (0-0.9 μg). I have found that surface expression of Kir2.6 channel proteins increased linearly with the amount of transfected DNA within this range (for example, lane 6 versus lane 2, Figure 2-6). Indeed, current density in cells transfected with 0.6 μg wild-type Kir2.6 plasmid was approximately twice as much as in cells transfected with 0.3 μg wild-type plasmid. As shown in Figure 2-9, current density in cells coexpressed R43C mutant and wild type subunit was significantly reduced compared with that with expression of wild type subunits, indicating that R43C mutant exerted dominant negative inhibition on wild type channel.

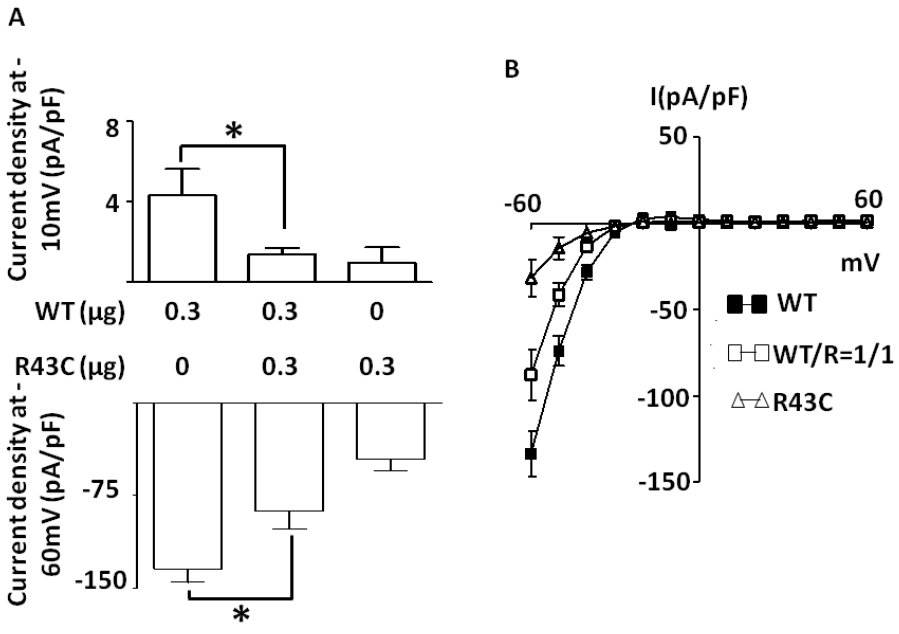

Figure 2-9. R43C exerts dominant negative effect on wild type Kir2.6 channel. (A) Wild type (WT) and mutant pEGFP-Kir2.6 cDNAs (in μg as indicated) were cotransfected into HEK cells to test the dominant negative effect of R43C. Bar graph of whole-cell inward current density at pipette holding potential -60 mV (lower) and -10 mV (upper) for different ratios of wild type Kir2.6 versus mutant Kir2.6 channels (mean ± S.E.M., n ≥ 6 for each). (B) Current-voltage (*I-V*) relationship curves for each group (mean ± S.E.M., n ≥ 6 for each). WT/R denotes the expressed protein ratio of wild type versus R43C mutant. Single asterisk denote s $p < 0.05$ between indicated groups.

Similarly, co-expression of V168M or A200P with wild type channel decreased the wild type current (Figure 2-10, 2-11), indicating dominant-negative inhibition exerted by V168M and A200P, respectively. Interestingly, despite the relatively low cell surface expression (see Figure 2-6 above), A200P mutant exerted a significant dominant-negative inhibition on wild type when transfected at 1:1 ratio (Figure 2-11, 0.3 μg WT + 0.3 μg A200P). One potential explanation for the finding is that incorporation of one A200P subunit is sufficient to render tetrameric channel non-functional.

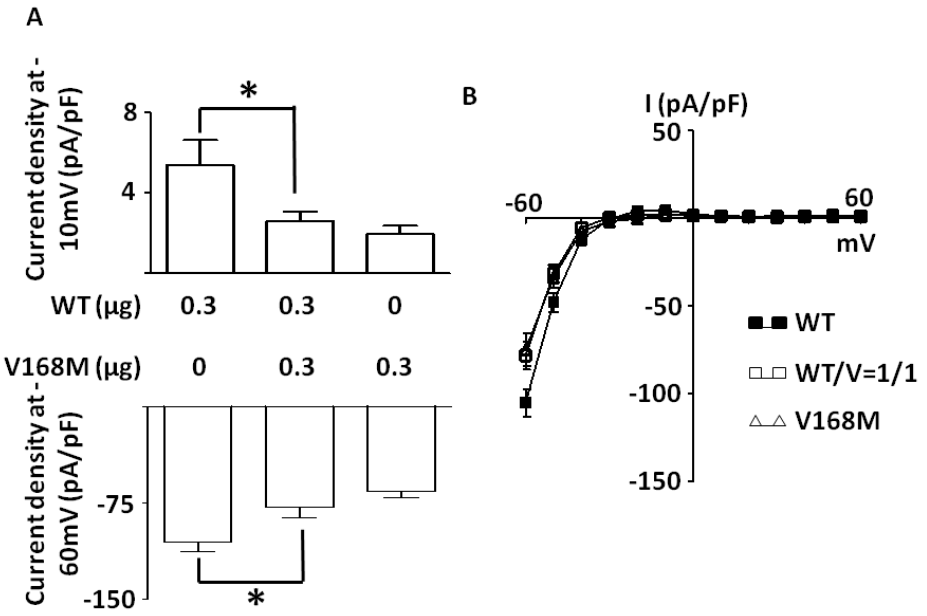

Figure 2-10. V168M exerts dominant negative effect on wild type Kir2.6 channel. (A) Wild type (WT) and mutant pEGFP-Kir2.6 cDNAs (in μg as indicated) were cotransfected into HEK cells to test the dominant negative effect of V168M. Bar graph of whole-cell inward current density at pipette holding potential -60 mV (lower) and -10 mV (upper) for different ratios of wild type Kir2.6 versus mutant Kir2.6 channels (mean ± S.E.M., n ≥ 6 for each). (B) Current-voltage (*I-V*) relationship curves for each group (mean ± S.E.M., n ≥ 6 for each). WT/V denotes the expressed protein ratio of wild type versus V168M mutant. Single asterisk denote s $p < 0.05$ between indicated groups.

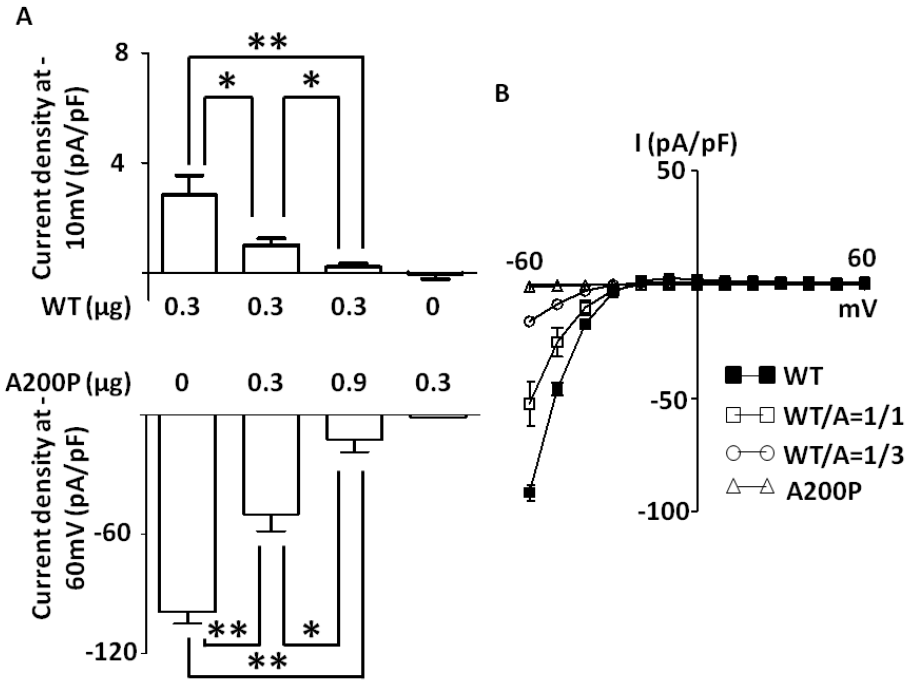

Figure 2-11. A200P exerts dominant negative effect on wild type Kir2.6 channel. (A) Wild type (WT) and mutant pEGFP-Kir2.6 cDNAs (in μg as indicated) were cotransfected into HEK cells to test the dominant negative effect of A200P. Bar graph of whole-cell inward current density at pipette holding potential -60 mV (lower) and -10 mV (upper) for different ratios of wild type Kir2.6 versus mutant Kir2.6 channels (mean ± S.E.M., n ≥ 6 for each). (B) Current-voltage (*I-V*) relationship curves for each group (mean ± S.E.M., n ≥ 6 for each). WT/A denotes the expressed protein ratio of wild type versus A200P mutant. Single and double asterisk denote $p < 0.05$ and $p < 0.01$ respectively between indicated groups

2.3.7 Kir2.6 Forms Heteromultimers with Kir2.1 and Kir2.6 Mutants Exert Dominant Negative Inhibition on Kir2.1

Kir2.1 channel is also expressed in skeletal muscle and reportedly forms heteromultimer with Kir2.6.[109] I thus compared Kir2.1 and Kir2.6 channel properties and explored potential interactions between disease mutant Kir2.6 and wild type Kir2.1. Cells expressed more Kir2.1 than Kir2.6 currents when transfected with the same amount of cDNA for each (Figure 2-12A). Moreover, the characteristics of currents through Kir2.1 and Kir2.6 were different. As shown in bar graph (Figure 2-12A) and *I-V* relationship curves (Figure 2-12C), Kir2.1 passed relatively more outward currents than Kir2.6 at membrane potentials above the equilibrium, giving a more prominent outward "hump-shaped" current relative to Kir2.6. This difference in the *I-V* relationship is better illustrated in Figure 2-12B, where Kir2.6 currents are normalized to Kir2.1. Thus, the rectification ratio, defined herein as inward current at -60 mV over outward current at -10 mV was 6.7 for Kir2.1 and 33 for Kir2.6, respectively. I next examined K^+ currents in cells co-expressing Kir2.1 and Kir2.6. I found cotransfection with cDNA for Kir2.1 and Kir2.6 (0.2 μg each) produced currents much less than currents from transfected with Kir2.1 alone (Figure 2-12A; inward and outward current density were -126 and 6.8 pA/pF, respectively, for cotransfection versus -237 and 38.4 pA/pF, respectively for Kir2.1 alone). The rectification ratio for cotransfection was 18.5, a value between that for Kir2.1 alone (i.e., 6.7) and for Kir2.6 alone (i.e., 33). Cotransfecting an increased amount of Kir2.6 DNA (0.6 μg) further increased the rectification ratio to 31.5, a value similar to that for transfection of Kir2.6 alone (i.e., 33). These results support the idea that Kir2.1 and Kir2.6 can form functional heteromultimers at the cell surface.

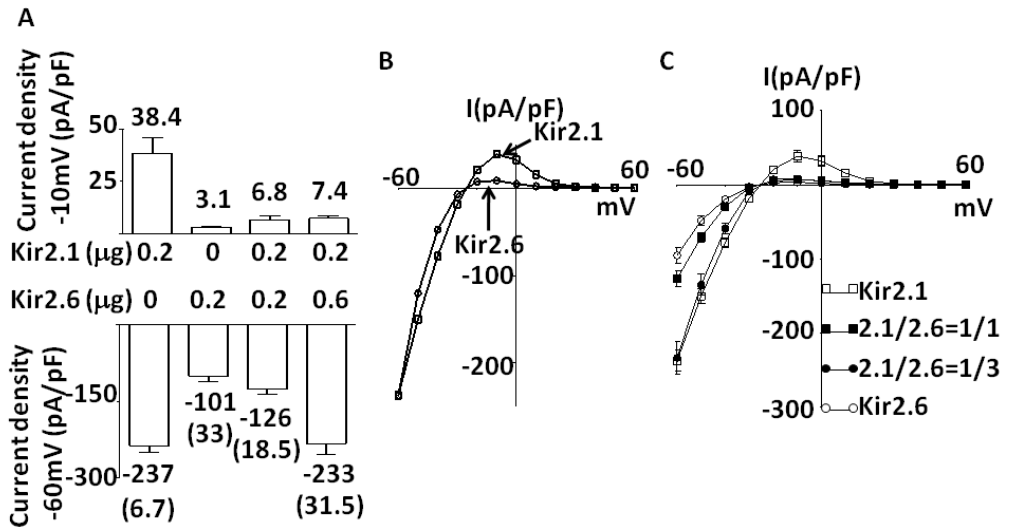

Figure 2-12. Currents and I-V relationships of homomeric and heteromeric Kir2.1 and Kir2.6 channels. (A) Kir2.1 and wild type Kir 2.6 (in μg cDNA as indicated) were cotransfected in HEK cells. Bar graph of whole-cell inward current density at pipette holding potential -60 mV (lower) and -10 mV (upper) for different ratios of wild type Kir2.1 versus wild type Kir2.6 channels (mean ± S.E.M., n ≥ 6 for each). Number above or below each bar represents the mean current for each group. Number enclosed in the parentheses in indicates the absolute value of the ratio between inward current at -60 mV and outward current at -10 mV for each group. (B) The overlap of normalized current voltage (*I-V*) relationships curves of Kir 2.1 and wild type Kir2.6. (C) Current-voltage (*I-V*) relationship curves for each group in figure A (mean ± S.E.M., n ≥ 6 for each). 2.1/2.6 denotes the expressed protein ratio of wild type Kir2.1 versus wild type Kir2.6.

I examined potential effects of dominant negative inhibition on Kir2.1 by disease Kir2.6 mutants. Cotransfection of A200P mutant with Kir2.1 at 1:1 and 1:3 cDNA ratios caused a dose-dependent inhibition of Kir2.1 current (Figure 2-13; for example, inward current density was -277, -100, and -20 pA/pF for 0, 0.2, and 0.6 μg A200P cDNA, respectively). For comparison, co-expression of a non-functional Kir2.6 mutant carrying a glycine to alanine mutation within the GYG selective filter caused a similar degree of inhibition on Kir2.1 currents (Figure 2-13A, last bar highlighted by the box labeled "GA"). Figure 2-13B shows *I-V* relationships for experiments in Figure 2-13A.

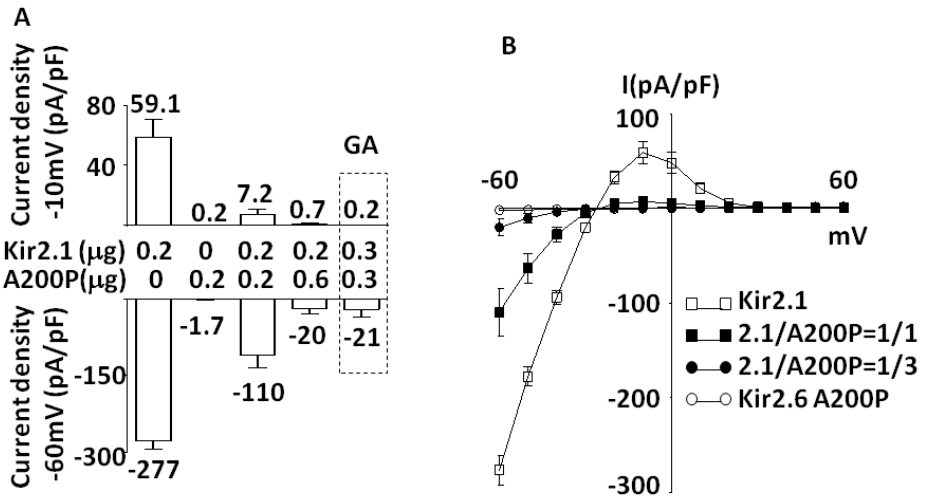

Figure 2-13. Kir2.6 A200P mutant exerts dominant negative inhibition on Kir2.1 (A) Kir2.1 and Kir 2.6 mutants (including A200P and G145A) (in μg cDNA as indicated) were cotransfected in HEK cells to test the dominant negative effect of A200P. Bar graph of whole-cell inward current density at pipette holding potential -60 mV (lower) and -10 mV (upper) for different ratios of wild type Kir2.1 versus wild type Kir2.6 channels (mean ± S.E.M., n ≥ 6 for each). Number above or below each bar represents the mean current for each group. (B) Current-voltage (*I-V*) relationship curves for each group in figure A (mean ± S.E.M., n ≥ 6 for each). 2.1/A200P denotes the expressed protein ratio of wild type Kir2.1 versus Kir2.6 A200P mutant.

I next examined effects of R43C and V168M Kir2.6 mutants on wild type Kir2.1. Cells co-expressing R43C or V168M mutant and Kir2.1 at 3:1 cDNA ratio (Figure 2-14, 3rd and 4th bar from left, respectively) had currents smaller than cells expressing Kir2.1 alone (1st bar from left) or cells co-expressing wild type Kir2.6 and Kir2.1 (2nd bar from left), indicating that R43C and V168M mutants also exert dominant-negative inhibition on Kir2.1. Figure 2-14B shows *I-V* relationships for experiments in Figure 2-14A.

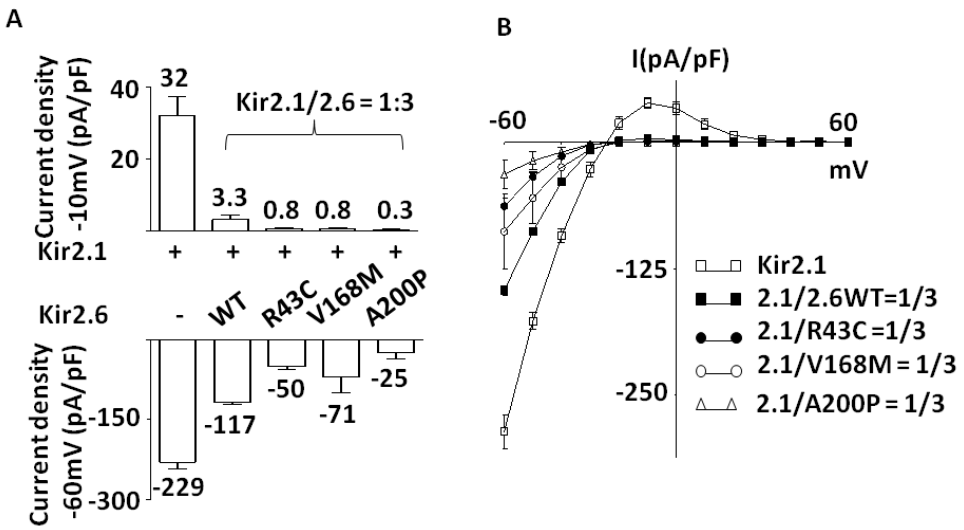

Figure 2-14. Disease mutant Kir2.6 exerts dominant negative inhibition on Kir2.1 (A) Kir2.1 and Kir 2.6 (in μg cDNA as indicated) were cotransfected in HEK cells to test the dominant negative effect of disease mutant Kir2.6. cDNA ratio of Kir2.1 versus either wild type (WT) or disease mutant (R43C, V168M, A200P) Kir2.6 are all 1/3 (Kir2.1 0.15 μg, Kir2.6 0.45 μg). Bar graph of whole-cell inward current density at pipette holding potential -60 mV (lower) and -10 mV (upper) for different ratios of wild type Kir2.1 versus wild type Kir2.6 channels (mean ± S.E.M., n ≥ 6 for each). Number above or below each bar represents the mean current for each group. (B) Current-voltage (*I-V*) relationship curves for each group in figure A (mean ± S.E.M., n ≥ 6 for each). 2.1/2.6 and 2.1/A200P, R43C, or V168M denotes the cDNA ratio respectively

2.4 Discussion

In this project, I found three novel mutations in *KCNJ18* encoding the newly identified skeletal muscle-specific Kir2.6 channel in patients with SPP as well as patients with TPP. Ryan et al. recently reported that mutations of Kir2.6 in patients with TPP.[31] Based on that *KCNJ18* contains a thyroid-responsive element and thyroid hormone up-regulates the transcription of Kir2.6, Ryan et al suggested that upregulation of Kir2.6 is important for mutations of the channel to contribute to the pathogenesis of hypokalemic periodic paralysis. My finding that mutations of Kir2.6 occur in patients with SPP with normal levels of thyroid hormone does not support this hypothesis. The mutations I identified in patients with TPP and SPP are heterozygous, missense substitutions of amino acids that result in partial or complete loss-of-function of Kir2.6 by decreasing single channel conductance, open probability and/or cell surface expression. These disease mutations exert dominant-negative mutations on wild type Kir2.6 and Kir2.1, both of which play an important role in regulating resting membrane potentials of skeletal muscle. These results provide important insights into the mechanism of pathogenesis of hypoPP.

It has been known for long that mutations of skeletal muscle voltage-gated Ca^{2+} channel $Ca_v1.1$ or Na^+ channel $Na_v1.4$ cause familial hypoPP. The majority of mutations in $Ca_v1.1$ or $Na_v1.4$ occur in the S4 voltage sensors, changing positively charged amino acids to uncharged.[40] One hallmark of hypoPP is paradoxical depolarization of sarcolemma induced by hypokalemia during attacks, which is believed to be a central mechanism of Na^+ channel inactivation thus inexcitability of muscle. How mutations of cationic amino acids in the voltage sensor cause the paradoxical depolarization of sarcolemma during hypokalemia, however, had been an enigma. Recent studies showing that mutations in the voltage sensor create an

aberrant conducting pore ("gating pore") that allows passage of small cations (Na^+ and H^+) at hyperpolarized resting membrane potentials provide a mechanistic explanation for paradoxical depolarization of sarcolemma during hypokalemic attacks.[39, 110]

The resting membrane potential (E_r) of cells is determined by the balance between outward (I_o) and inward (I_i) current (Figure 2-15A). In the sarcolemma of skeletal muscle under most conditions, this balance occurs between the outward hump current of Kir (I_{Kir}) and inward cation leak current (I_{Leak}). Under some conditions, this balance can only be achieved by outward current mediated by the delayed rectifying K^+ channel (I_{KDR}), which are activated when membrane potentials depolarized to > -65 mV. These features give rise to the bi-stable distribution of resting membrane potentials of skeletal muscle sarcolemma. When extracellular K^+ concentration ($[K^+]_o$) decreases, the shift in the equilibrium potential for K^+ (Ek) toward hyperpolarized membrane potentials decreases the outward K^+ current through Kir relative to the leak current. In addition, decreased $[K^+]_o$ has a direct effect on Kir to reduce K^+ conductance.[36, 111] As a result, the balance between inward and outward currents for E_r is reset to a hyperpolarized membrane potential (Figure 2-15B; E_r -98 mV versus -93 mV in Figure 2-15A). In normal individuals, unless the $[K^+]_o$ is extremely low (< 1 mM), I_{Kir} is able to maintain the balance with I_{Leak} at hyperpolarized E_r. The ability to balance inward leak currents and I_{Kir} during hypokalemia by hyperpolarization of E_r is disrupted in familial hypoPP. As shown, increases in the leak current in familial hypoPP cause a slight depolarization at normal $[K^+]_o$ (Figure 2-15C). The hyperpolarizing shift in E_k in hypokalemia, however, renders imbalance between outward current mediated by Kir and the large inward leak current. As a result, E_r is reset to a more depolarized membrane potential

where outward K^+ current is mediated by delayed rectifier K^+ channel in order to reach a new balance between outward and inward current (Figure 2-15D).

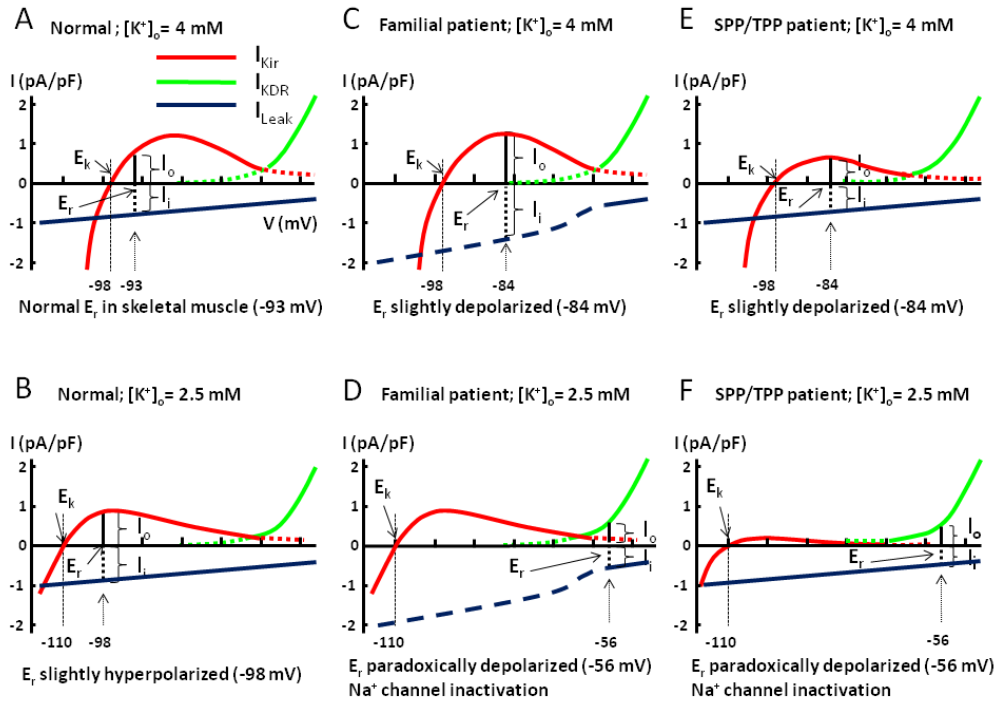

Figure 2-15. Schematic models illustrating reduced outward current of Kir induces paradoxical depolarization in patients with Kir2.6 mutation.
The steady-state current-voltage (I-V) relationship curve for mammalian skeletal muscle is a combination of I-V curves of inward rectifying K^+ channel (Kir, red line) and delayed rectifying K^+ channel (KDR, green line). Leakage current (blue line) has a reversal potential of 0 mV. Because gating pore currents from mutations of the voltage sensor only occur in hyperpolarized potentials, the inward leak current in familial hypoPP patients is not linear (blue dotted line). The model is intended for conceptual understanding. The numerical value may be slightly different from true in vivo value. See text and ref. 110 for details. Abbreviations: E_k: equilibrium potential of Kir channel; E_r: resting membrane potential; I_o: outward cation current; I_i: inward cation current; I_{Kir}: current of inward rectifying potassium channel; I_{KDR}: current of delayed rectifying potassium channel; I_{Leak}: inward cation leak current; $[K]_o$: extracellular potassium concentration.

The above model for hypokalemia-induced paradoxical depolarization predicts that reduced K^+ current through I_{Kir} could lead to same effect as enhanced I_{Leak} (Figure 2-15E, F). This notion is supported by a recent study by Struyk et al showing that partial blockage of I_{Kir} by barium predisposes sarcolemma to the development of paradoxical depolarization under relatively normal $[K^+]_o$.[43] Moreover, studies have shown that patients with non-familial hypoPP and experimental models of TPP develop paradoxical depolarization under moderate hypokalemia despite no evidence of aberrant inward cation leak. Recordings from external intercostals muscle biopsied from TPP patients[112, 113] and hindlimb muscle fibers of rat with hyperthyroidism[114] displayed persistently depolarized E_r. In the study of intercostals muscle of TPP patients, outward Kir currents were reduced along with diminished voltage-activated inward Na^+ currents.[113] My findings that mutations of Kir2.6 cause decreased outward K^+ currents through Kir2.6 and/or through Kir2.1 and Kir2.6 heteromultimeric channels supports this model of hypokalemia-induced paradoxical depolarization and muscle inexcitability as a central mechanism of pathogenesis for paralysis in hypoPP (Figure 2-15E, F). These findings may also explain why hypoPP patients develop severe hypokalemia. Due to heterogeneity, muscle fibers develop paradoxical depolarization at different extracellular K^+ concentrations; the percentage of muscle fibers that develop paradoxical depolarization increases proportionally with decreasing $[K^+]_o$.[115] K^+ efflux at the paradoxically depolarized membrane potential is much lower than that in the normal resting membrane potential (compare Figure 2-15D &F with Figure 2-15A). Thus, an increase in the number of muscle fibers with paradoxical depolarization from the initial mild hypokalemia may set in motion a vicious cycle of worsening hypokalemia and paradoxical depolarization. The

observation that hypokalemia and muscle paralysis develops in patients with barium intoxication supports this notion.[110, 116]

Many members of Kir2.x family including Kir2.1, Kir2.2, and Kir2.6 are present in skeletal muscle.[28] The subcellular distribution in the muscle and relative contribution of each member remain largely unknown. Some insights can be gained from human mutations and animal models. Mutations of Kir2.1 cause a multisystem disease featured by prolonged QT syndrome, facial and skeletal dysmorphism, and hypokalemic periodic paralysis known as Andersen-Tawil syndrome.[30] The multi-organ involvement is consistent with the broad distribution of Kir2.1 in these and other organs.[28] Mice homozygous for inactivation of Kir2.1 gene die at young age due to palatal defects and difficulties in feeding.[117] These findings indicate that Kir2.1 is essential for maintaining a normal E_r in cardiac and skeletal muscle as well as other tissues. Mice with knockout of Kir2.2 have no obvious phenotype.[117] The report by Ryan et al and ours indicate an important role of Kir2.6 in the regulation of skeletal muscle membrane potentials.[31] During the course of my present study, Dassau et al reported that Kir2.6 co-assembles with Kir2.1 and Kir2.2.[109] Based on immunofluorescent staining of recombinant Kir2.6 in transfected rodent tissues, the authors concluded that Kir2.6 is predominantly distributed to the endoplasmic reticulum and functions as a dominant negative regulator of cell membrane abundance of Kir2.1 and other Kir2.x channels. In this study, I find that Kir2.6 expresses on the cell surface of a human cell line (HEK cells) and is functional. Ryan et al also observed functional expression in HEK cells.[31] As acknowledged by Dassau et al, different cell types may account for the apparent discrepancy. I also find that Kir2.6 interacts with Kir2.1 to form functional channels with mixed properties on the cell surface. Moreover, disease Kir2.6 mutants exert dominant-negative inhibition on

Kir2.1. Future study will investigate subcellular distribution of Kir2.1 and Kir2.6, physiological significance of differential distribution and potential impact of disease mutants on homomeric and/or heteromeric subunits.

Ryan et al reported mutations of Kir2.6 in ranging from zero to 33% TPP patients from several different populations.[31] In Taiwanese population, I found four mutations in 160 SPP and TPP patients. Mutations in $Ca_v1.1$, $Na_v1.4$, and Kir2.1 have not been reported in TPP (28-31).[118-121] Mutations in $Ca_v1.1$ and $Na_v1.4$, however, have been reported in some SPP patients.[108, 122] These patients may be variants of familial hypoPP due to an incomplete penetration of female carriers or may be afflicted by *de novo* gene mutations. Whether decreased protein expression and/or function of Kir2.6, promoter polymorphism and/or deep intron mutations of *KCNJ18* may account for disease phenotypes in some of TPP and SPP patients not mapped to mutations of the coding region of Na^+, Ca^{2+}, and Kir2.6 channels awaits further investigation. Of note, insulin, of which an increased blood level is a predisposing factor for hypoPP, was reported to inhibit Kir currents.[123]

In conclusion, my present report provides the first evidence that mutations in Kir2.6 occur in SPP as well as TPP, supporting the notion that decreased K^+ currents predispose sarcolemma to paradoxical depolarization in hypokalemia leading to muscle paralysis.

CHAPTER THREE

PHOSPHATIDYLINOSITOL 3-KINASE (PI3K)-AKT1/SGK1-DEPENDENT PHOSPHORYLATION OF WNK1 STIMULATES ENDOCYTOSIS OF ROMK

3.1 Introduction

Extracellular K^+ concentration is tightly regulated with a small range between 3.5-5 mM and is a major determinant of resting membrane potential (Er) of many excitable cells. Disruption of K^+ homeostasis can lead can life-threatening consequences, such as cardiac arrhythmia and muscle paralysis. To maintain the steady content of total body K^+, ~90% of dietary K^+ intake is excreted through the kidney with processes including glomerular filtration, tubular reabsorption and secretion. The transepithelial K^+ secretion in the kidney occurs mainly in the aldosterone-sensitive distal nephron (ASDN), where K^+ uptake into cells by the basolateral Na^+, K^+ ATPase and exit into lumen through two major apical K^+ channels, maxi-K and ROMK (Kir1.1) channels.[85,124]

With constitutively high open probability of channel, the density of ROMK channel at the lumen surface is the major determinate of renal K^+ secretion.[125] The clathrin-dependent endocytosis regulates membrane abundance of ROMK channel. WNK (with-no-lysine [K]) kinases have been identified as important regulators of renal handling of K^+. WNKs are serine-threonine protein kinases with an unusual position of the catalytic lysine in sub-domain I instead of sub-domain II.[78] Mammalian WNK family comprises of four members, WNK1-4, which share 85-

90% sequence identity in their kinase domain.[78, 79, 126] Mutations in WNK1 and WNK4 in humans cause a syndrome of genetic hypertension and hyperkalemia, so-called autosomal-dominant disease pseudohypoaldosteronism type 2 (PHA2).[79] Studies have shed light on the mechanisms of WNK1 and WNK4 in regulating renal Na^+ and K^+ transporters and dysfunction of WNK kinases cause enhanced Na^+ reabsorption for hypertension and impaired K^+ excretion for hyperkalemia in PHA2.

WNK kinases regulate renal Na^+ transporters through both catalytic and non-catalytic mechanisms. Sharing 90% similarity in amino acid sequence of kinase domain, both WNK1 and 4 phosphorylate and activate two Ste20-type kinases, OSR1 and SPAK, which in turn phosphorylate and activate the thiazide-sensitive Na^+-Cl^- cotransporter (NCC) and the bumetanide-sensitive Na^+-K^+-$2Cl^-$ cotransporter (NKCC).[127, 128] Besides their catalytic activity, WNK1 and 4 also regulate ENaC and NCC via non-catalytic mechanisms that involve protein-protein interaction with serum- and glucocorticoid-induced kinase-1 (SGK1) for the regulation of ENaC and with transporter directly for the regulation of NCC.[82, 83] With respect to K^+ transport, WNK1 and 4 stimulate endocytosis of ROMK via a kinase-independent mechanism that involves a direct interaction with an endocytic scaffold protein, intersectin.[89]

Compared to the downstream effects of WNKs, the physiological upstream regulators of WNKs are less understood. Vitari et al showed that insulin-like growth factor (IGF1) induces phosphorylation of endogenous WNK1 in cultured human embryonic kidney (HEK) cells at threonine-60 (equivalent to threonine-58 of rat WNK1).[129] The effect of IGF1 is through activation of phosphatidylinositol 3-kinase (PI3K) leading to activation of the 3-phosphoinositide-dependent protein kinase-1 (PDK1) and protein kinase B (PKB)/Akt1. Phosphorylation of WNK1 by Akt1 does not affect its kinase activity or subcellular distribution.[129] Jiang et al reported that

insulin induces a similar phosphorylation of WNK1, which underscores the inhibition of cell proliferation of 3T3-L1 preadipocytes by insulin.[130] Xu et al reported that WNK1 activates SGK1 through direct protein-protein interactions independently of WNK1 kinase activity.[81] Xu et al further showed that phosphorylation of rat WNK1 at threonine-58 by IGF1-Akt1 pathway enhances the ability of WNK1 to stimulates SGK1 kinase activity leading to activation of ENaC.[83] Others have also showed that insulin stimulates ENaC via Akt1, although the role of WNK1 was not investigated.[131] The mechanism for WNK1 regulation of ROMK and ENaC are fundamentally distinct, raising an interesting question as to whether phosphorylation of WNK1 by PI3K-activating hormones, such as insulin and IGF1, affects its regulation of ROMK. I investigated this question in this project.

3.2 Materials and Methods

3.2.1 DNA Constructs and Reagents

pEGFP-ROMK1, pCMV5-Myc-WNK1, pIRES-Flag-KS-WNK1, and dominant-negative intersectin and dynamin have been created and used in Dr. Chou-Long Huang's lab.[100] The plasmids encoding N-terminal 60 amino acids truncated and Flag-tagged wild type, S422D mutant and kinase-dead mutant SGK1 (pCMV7-3xFlag-ΔSGK1), HA-tagged wild-type, myristoylated and kinase-dead mutant Akt1 (pCMV-HA-Akt1), and myc-tagged PDK1 (pcDNA3-Myc-PDK1) were generous gifts from M. Cobb (University of Texas Southwestern Medical Center). Point mutations were generated by site-directed mutagenesis (QuickChange kit; Stratagene) and confirmed by sequencing. Sense and antisense oligonucleotides (Dharmacon RNA Technology) for human WNK1 siRNA were 5'-UGUCUAACGAUGGCCGCUUdTdT-3' and 5'-

AAGCGGCCAUCGUUAGACAdTdT-3'. Sense and antisense oligonucleotides for human SGK1 were 5'-GUCCUUCUCAGCAAAUCAAUU-3' and 5'-UUGAUUUGCUGAGAAGGACUU-3'. Sense and antisense oligonucleotides for human Akt1 were 5'-GACCGCCUCUGCUUUGUCAdTdT-3' and 5'-UGACAAAGCAGAGGCGGUCdTdT-3'. Insulin from bovine pancreas and IGF1 was purchased from Sigma. The following antibodies were used: anti-WNK1 antibody (Q256)(1:5000 dilution; gift from M. Cobb),[100] anti-Flag antibody (M2)(1:5000 dilution; Sigma) and anti-c-Myc (1:5000 dilution; Sigma), anti-HA antibody (12CA5)(1:5000 dilution; Berkeley Antibody Co), anti-WNK1 phospho-Thr-58 (1:1000 dilution; Abcam), anti-Akt1 (AW24; 1:1000 dilution; Millipore), anti-Akt1 phospho-Thr-308 (C31E5E; 1:1000 dilution; Cell Signaling), anti-Akt1 phospho-Ser-473 (D9E; 1:1000 dilution; Cell Signaling), anti-SGK1 phospho-Thr-256 (1:1000 dilution; Santa Cruz) and anti-GFP HRP conjugate (1:1000 dilution; Invitrogen).

3.2.2 Cell Culture, Transfection, Preparation of Cell Lysates, Immunoblotting, and Kinase Assays

HEK-293 cells were co-transfected with cDNA (0.3 μg per 6-well) for GFP-ROMK1 plus other indicated cDNAs using transfection reagent, Fugene HD (Roche). In each experiment, the total amount of DNA for transfection was balanced by using empty vectors. Transfected cells were identified by green fluorescence. Approximately 36-48 hr after transfection, cells were dissociated and placed in a chamber for ruptured whole-cell recordings. For knockdown by siRNA, oligonucleotides (200 nM each) were mixed with cDNAs for ROMK1 and other indicated constructs for cotransfection by PolyFect (Quagen). For serum deprivation

studies, cells were washed by PBS for 2 times and cultured in serum-free DMEM medium for different time periods as indicated.

Cultured cells were incubated with lysis buffer (50 mM HEPES, pH 7.6, 150 mM NaCl, 0.5% Triton X-100, 10% glycerol, protease inhibitor cocktail [Mini EDTA-free, Roche], and phosphatase inhibitor cocktail [PhosSTOP, Roche]). After shaking 30 minutes on a rotator at 4℃, extracts were cleared by centrifugation. Protein concentrations of supernatant were measured by the Bradford assay using bovine serum albumin as a standard. Equal amounts of lysates were boiled in Laemmli sample buffer and then separated by SDS-PAGE under reducing conditions. For western blotting, proteins were transferred to nitrocellulose membranes, blocked using 5% nonfat milk, incubated with the appropriate antibodies, and detected using ECL detection reagent (Pierce).

For kinase assays, epitope-tagged PDK1, Akt1 and/or SGK1 were cotransfected in HEK cells as indicated. Lysates (500 μg) were incubated with respective antibodies (anti-rabbit anti-Myc for PDK1, anti-mouse anti-HA for Akt1 and anti-mouse anti-Flag for SGK1 each at 1:300 dilution) and 30 μl of 50% slurry of protein A (for immunoprecipitating PDK1) or protein G (for immunoprecipitating Akt1 and SGK1) at 4 ℃ overnight. Then beads were washed 3 times by 1ml wash buffer (0.25 M Tris, pH 7.4, 1 M NaCl, 0.1% Triton X-100, proteinase and phosphatase inhibitor cocktails) for 10 minutes and followed by one wash with 1ml kinase wash buffer (10 mM HEPES, pH 7.6 and 10 mM $MgCl_2$). After removing kinase wash buffer, beads were incubated with 2 μg WNK1(1-119) wild type or T58A mutant proteins purified from E coli, in 30 μl of kinase buffer (20 mM HEPES, pH 7.6, 5 μM ATP [5 μCi of γ-32P ATP], 10 mM $MgCl_2$, and 10 mM β-glycerol phosphate) at 30 ℃ for 45 minutes. The samples were then boiled with 7.5 μl 5-fold

sampling buffer in 90℃ for 5 minutes. Supernatants were separated by SDS-PAGE for western blot and phosphoimager analysis. The radioisotope intensity of the bands was determined by phosphoImager, Storm 860 (GE Healthcare, Piscataway, NJ) and ImageQuant 5.2 software (GE Healthcare, Little Chalfont, Buckinghamshire, UK).

3.2.3 Whole-Cell Patch-Clamp Recording of ROMK1 Channels

After 48-hour transfection, cells were trypsinized and plated on poly-L-lysine coated cover slips. Whole-cell ROMK currents were recorded by using an Axopatch 200B amplifier (Axon Instruments, Foster City, CA). The pipette resistance was around 1.5-3 MΩ. Green fluorescence of GFP-ROMK in transfected cells were identified by epifluorescent microscopy. The pipette solution contained 140 mM KCl and 10 mM HEPES (pH 7.2); the bath solution contained 140 mM KCl, 1 mM $MgCl_2$, 1 mM $CaCl_2$, and 10 mM HEPES (pH 7.4). The cell membrane capacitance and series resistance were monitored and compensated (>75%) electronically. The voltage protocol consisted of 0 mV holding potential and 500-ms steps from -100 to 100 mV in 25-mV increments. ClampX 9.2 software (Axon Instruments) was used for data acquisition. Current density was calculated by dividing current at -100 mV (pA; measured at 25℃) by capacitance (pF). Results were shown as mean ± S.E.M. (n = 6–10). Each experiment (i.e., set of results shown in each panel of a figure) was repeated two to four times.

3.2.4 Surface Biotinylation Assay

For biotinylation of cell-surface ROMK, cells were washed with ice-cold PBS and incubated with 0.75 mL PBS containing 1.5 mg/mL EZ-link-NHS-SS-biotin (Thermo Scientific) for 1hr at 4^oC. After quenching with glycine (100 mM), cell were

lysed in a RIPA buffer (150 mM NaCl, 50 mM Tris-HCl, 5 mM EDTA, 1% Triton X-100, 0.5 % DOC and 0.1% SDS) containing protease inhibitor cocktail. Biotinylated proteins were precipitated by streptavidin-agarose beads (Thermo Scientific). Beads were subsequently washed 4 times with PBS containing 1% Triton X-100. Biotin-labeled proteins were eluted in sample buffer, separated by SDS-PAGE, and transferred to nitrocellulose membranes for Western blotting. ROMK proteins on the membrane were detected using anti-GFP HRP conjugate antibody. Biotinylation experiment was performed 3 times with similar results.

3.2.5 Data Analysis

Data analysis and curve fitting were performed with the Prism (v5.03) software (GraphPad Software, San Diego, CA, USA). Data were presented as mean ± S.E.M. Statistical comparisons between two groups of data were made using two-tailed unpaired Student's *t*-test. Multiple comparisons were determined using one-way ANOVA (analysis of variance). Time-course and dose-response curve were fitted by non-linear regression analysis. Statistical significance was defined as p values less than 0.05 for single comparison and less than 0.01 for multiple comparisons.

3.3 Results

3.3.1 Effects of Serum Deprivation, Insulin and IGF1 on ROMK

Whole cell recording of barium-sensitive K^+ current were performed on HEK cells transfected with ROMK. All the recordings were done under the condition of symmetrical 140 mM [K^+], proved by reverse potential of barium-sensitive K^+ current at 0 mV. The barium-sensitive K^+ current was defined as ROMK-mediated K^+

currents and displayed the characteristic weak inward-rectification (left panel, Figure 3-1). No currents were observed in mock-transfected cells. To allow for testing the effect of insulin and IGF1 on ROMK, I first examined the effect of serum deprivation. After culturing in the serum-containing media for 48 hours to allow maximal expression of the channel, ROMK-transfected cells were deprived of serum for 3 to 25 hour before ruptured whole-cell recording. As shown, ROMK current density (normalized to capacitance, pA/pF) increased progressively with increasing duration of serum deprivation (right panel, Figure 3-1). Six hours after serum deprivation, current density was significantly higher than that before deprivation. ROMK currents continued to increase and reached a plateau at 16-20 hours (Figure 3-1).

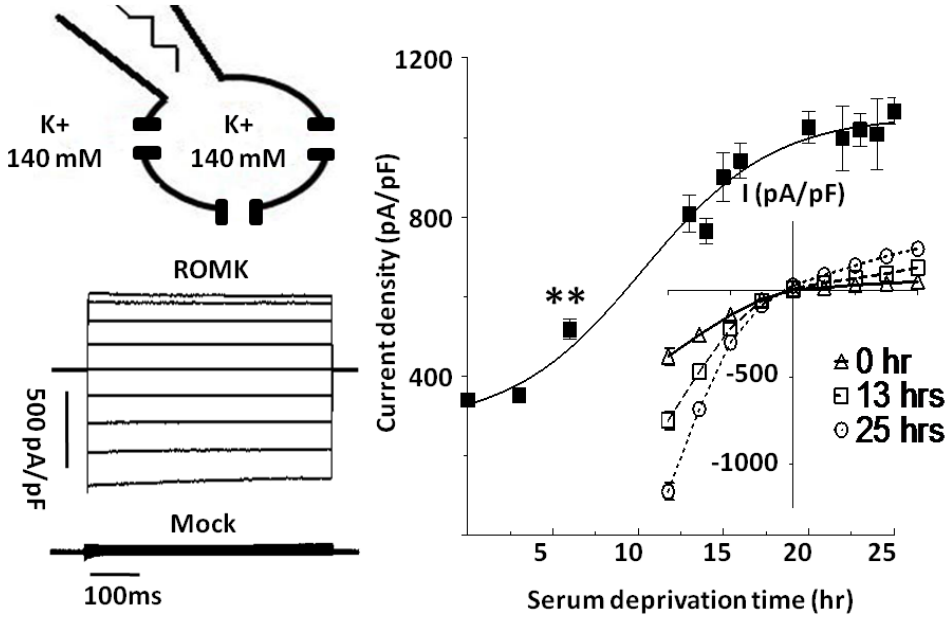

Figure 3-1. Serum deprivation increases ROMK current.
Left, configuration of whole-cell recording, voltage-clamp protocol (from -100 mV to 100 mV), representative currents from ROMK- and mock-transfected cells are shown. Right, ROMK current density (pA/pF at -100 mV; normalized to the cell surface area) at different time of serum deprivation were shown (mean ± S.E.M., n ≥ 6 for each) and analyzed by nonlinear regression curve. Inset shows current-voltage (I-V) relationship curve of ROMK with serum deprivation for 0, 13, and 25 hours. Data in each time point was compared to serum-containing group (0-hr serum deprivation). Double asterisk denotes $p < 0.01$. All time points beyond 6-hr are significant compared to serum-containing group (not indicated by asterisk). All time points between 16 hrs and 25 hrs are not significantly different (not indicated).

Addition of insulin thereafter caused a significant inhibition of ROMK currents in 30 minutes (Figure 3-2, left). ROMK currents reached the nadir at ~2-hour incubation with insulin (Figure 3-2, right).

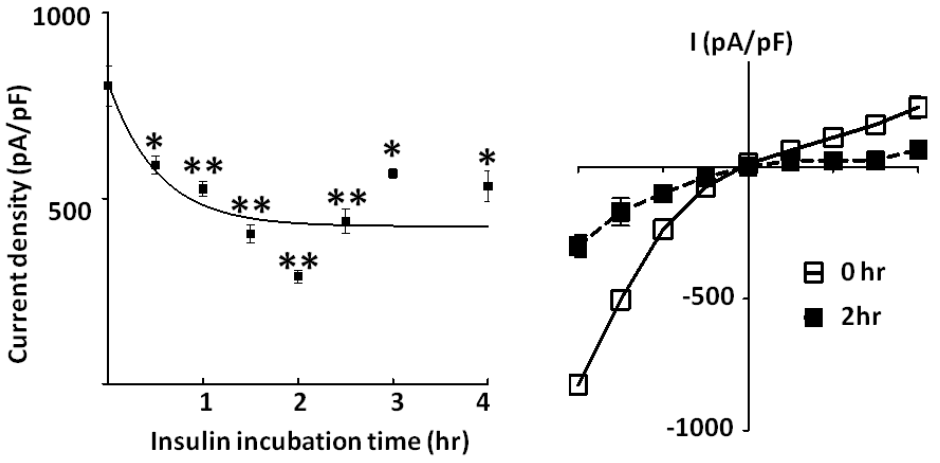

Figure 3-2. **Time course of effect of insulin on serum-deprived ROMK current.** Cells were cultured in serum-free medium at least 16 hours before addition of insulin (100 nM) for different time periods. Data points are mean ± S.E.M. ($n \geq 6$ for each) and compared to serum-deprived (0-hour insulin incubation) and analyzed by nonlinear regression curve (left panel). Right panel shows I-V curve of ROMK current before and after 2 hour insulin.

The dose-response relationship for inhibition of ROMK was examined by incubating insulin ranging from 1 nM to 100 nM for 2 hour. Insulin significantly inhibited ROMK at the concentration as low as 1 nM (Figure 3-3A, left). The concentration for half-maximal inhibition (IC_{50}) of ROMK for insulin was estimated at 3.2 nM (Figure 3-3A, right). For the reference, the plasma concentration of insulin in normal individuals is 10-150 pM at fasting but may reach 300-800 pM after carbohydrate meals.[132] IGF and insulin act on similar membrane receptors and elicit overlapping cellular responses.[133] Accordingly, I found a similar inhibition of ROMK by IGF1, with IC_{50} for IGF1 estimated at 18.5 ng/ml (= 2.4 nM) (Figure 3-3B). The plasma concentration of IGF1 ranges from 50-1,000 ng/ml.[134]

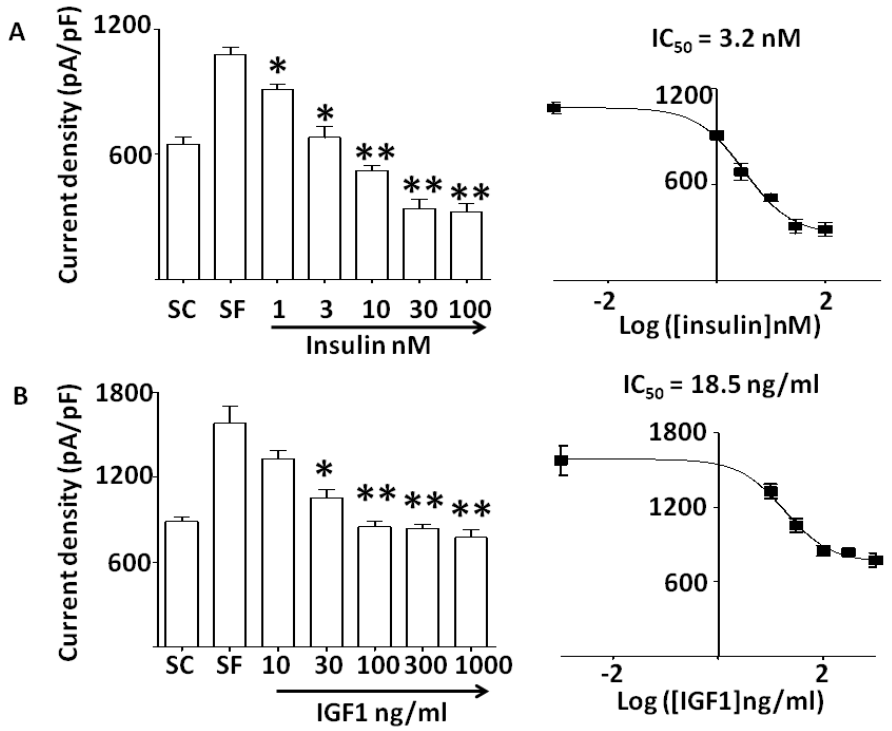

Figure 3-3. Dose-response curve of insulin and IGF1 on serum-deprived ROMK.

ROMK current density (mean ± S.E, n ≥ 6) at -100 mV were measured in cells cultured in serum-containing medium (SC), serum-free medium (SF) and 2-hour incubation of different concentration of insulin (A) or IGF1 (B). Data of each insulin or IGF1 treatment group were compared to SF group. Dose response curve and IC_{50} of insulin or IGF1 on ROMK were resulted from nonlinear regression analysis. One asterisk denotes $p < 0.05$ versus designated group by unpaired two-

3.3.2 Effect of Insulin and IGF1 Is Dependent on PI3K and WNK1-T58 Phosphorylation

To investigate whether the insulin/IGF1-mediated inhibition of ROMK is PI3K-dependent, ROMK-transfected cells were incubated with insulin or IGF1 with or without a specific PI3K inhibitor, wortmannin. In these experiments, I also compared the effects of insulin and IGF1 on ROMK with or without serum. I found that 100 nM of insulin caused a significant inhibition of ROMK even in the presence of serum (Figure 3-4, left), indicating that the receptors are not maximally occupied by insulin present in the serum. For comparison, IGF1 at 100 ng/ml did not cause further inhibition of ROMK in the presence of serum (Figure 3-4, right). As before, serum deprivation increased ROMK currents and application of insulin or IGF1 thereafter inhibited the currents. Co-application of wortmannin ("WM", 100 nM) completely abolished the effect of insulin and IGF1 on ROMK, indicating that the effect of insulin and IGF1 depends on PI3K.

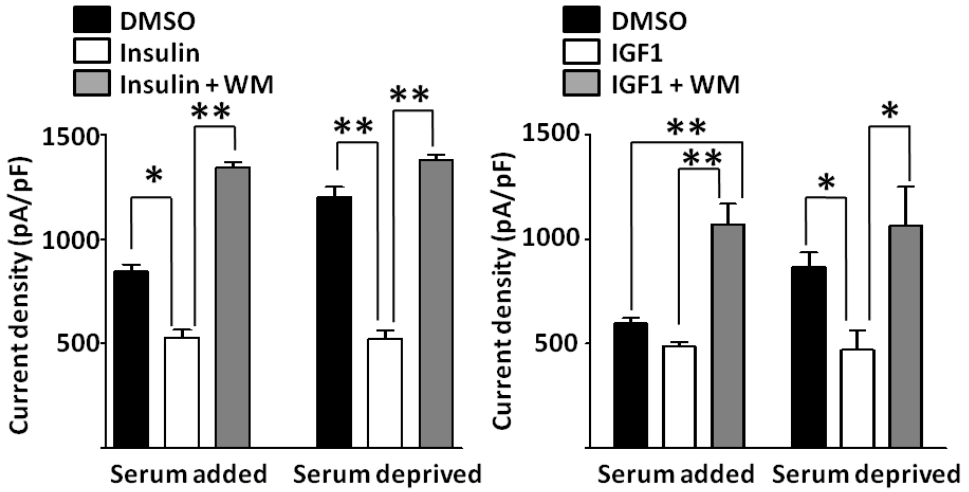

Figure 3-4. Effect of insulin and IGF1 on ROMK is blocked by wortmannin. Cells cultured with or without serum were treated by DMSO, insulin 100 nM or insulin 100 nM plus wortmannin ("WM", 100 nM) respectively for 2 hours (Mean ± S.E.M., n ≥ 6). One and two asterisk denotes $p < 0.05$ and $p < 0.01$, respectively between indicated groups by unpaired two-tailed Student's t test.

Stimulation of PI3K by hormones or growth factors produces 3-phosphoinositides in the plasma membrane and leads to activation of downstream Akt1 and SGK1 via multiple concerted actions. First, it stimulates the mammalian target of rapamycin complex-2 (mTORC2) complexes to phosphorylate Akt1 or SGK1 at the hydrophobic motif. Phosphorylation of Akt1 or SGK1 by mTOR enhances its binding with PDK1, which then phosphorylates Akt1 or SGK1 at the T-loop to activate its catalytic activity. Finally, the recruitment and binding of PDK1 to Akt1 is also facilitated by the production of 3-phosphoinositides in the plasma membrane. To understand the role of PI3K in WNK1 regulation of ROMK, I examined the phosphorylation status of endogenous Akt1 and WNK1 in HEK cells using respective residue-specific phospho-antibodies. In the absence of serum, there was a basal level of phosphorylation of Akt1 at threonine-308 (T308) of the T-loop and serine-473 (S473) of the hydrophobic motif, respectively (Figure 3-5, lane 4). Serum and/or insulin increased phosphorylation of Akt1 at both residues (lanes 1, 2, 5). Wortmannin abrogated basal and serum or insulin-stimulated phosphorylation of Akt1 (lanes 3, 6). I demonstrated the same pattern of phosphorylation also occurred on overexpressed SGK1 T256 because endogenous SGK1 in HEK cells is undetectable by the anti-SGK antibody I used and similar results has been shown in previous study by using other cell lines. Phosphorylation of WNK1 at threonine-60 (T60 = T58 of rat WNK1) was not detectable in the absence of serum (lane 4) but was enhanced by serum and/or insulin in a wortmannin-sensitive manner (lanes 1, 2, 5). Serum and insulin also stimulated wortmannin-sensitive phosphorylation of overexpressed SGK1 at the T-loop (threonine-256) (Figure 3-5, bottom two gels). Overexpressed SGK1 was used because endogenous SGK1 was below detection by our antibody.

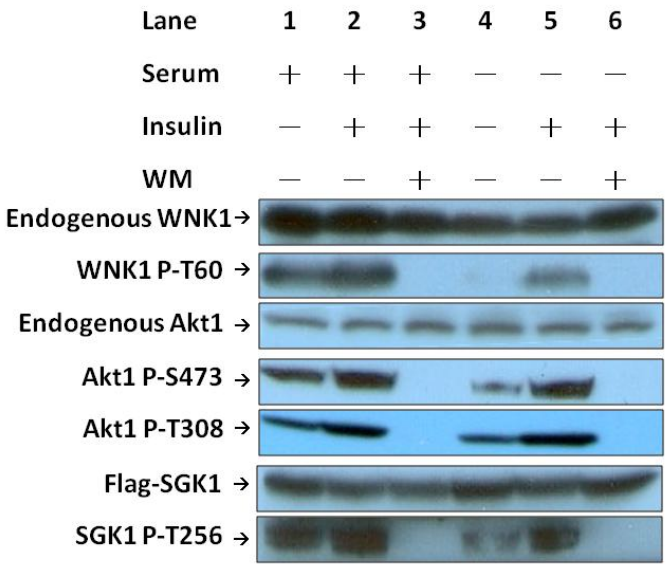

Figure 3-5. Effect of serum, insulin and wortmannin on phosphorylation of endogenous WNK1 & Akt1 and overexpressed SGK1.
Phosphorylation on specific residues was determined by specific anti-phosphoantibodies. Shown is representative of 3 separate experiments of similar results.

To understand if insulin/IGF1 inhibits ROMK through reducing membrane abundance of ROMK, I quantified the membrane ROMK by biotinylation. ROMK without biotinylation served as a negative control (Figure 3-6, lane 1). Serum deprivation increased membrane abundance of ROMK (lane 2, 3), which can be brought back into cells by insulin and IGF1 in a wortmannin-sensitive way (lane 4-6). These results indicate insulin/IGF inhibits ROMK possibly through enhancing endocytosis pathway, where WNK1 plays an important role.

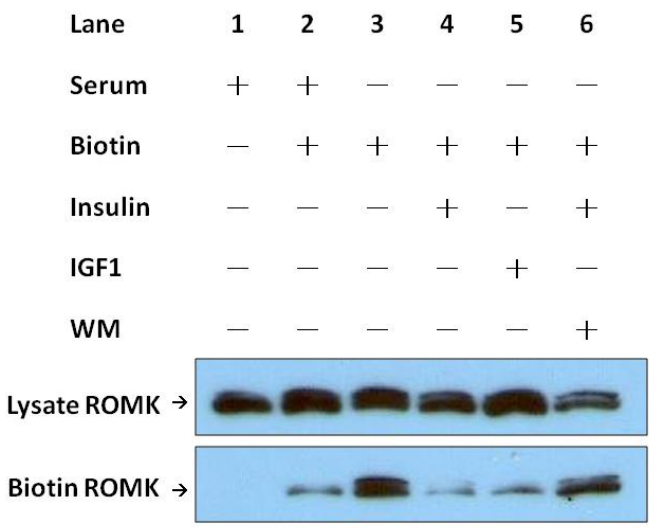

Figure 3-6. Effect of Insulin/IGF1 on surface abundance of ROMK.
Insulin (100 nM), IGF1 (100 ng/ml) and WM (100 nM) were treated in designated serum-deprived HEK cells for 2 hours before biotinylation (Biotin). ROMK in total cell lysates (Lysate ROMK) and elute from avidin beads (Biotin ROMK) were detected by western blot.

To confirm the role of WNK1 in the PI3K-mediated regulation of ROMK, I knocked down endogenous WNK1 using small interference RNA (siRNA). Efficacy of WNK1 siRNA was validated by blotting endogenous WNK1 in HEK cells (Figure 3-7A). Cells transfected with WNK1 siRNA ("WNK1 siRNA"; white bar) or control oligonucleotides ("Control oligo", black bar) had similar ROMK current in the absence of serum ("serum-free"). Addition of insulin inhibited ROMK currents in cells transfected with control oligonucleotides, but not in cells whose endogenous WNK1 was knocked down by siRNA.

Next, I used phospho-deficient T58A mutant to examine the role of T58 phosphorylation on WNK1 (Figure 3-7B). Insulin inhibited ROMK in cells expressing endogenous ("vector") or exogenous WNK1 ("WNK1(1-491)/WT"), but not in cells expressing exogenous T58A mutant of WNK1 ("WNK1(1-491)/T58A"), which exerted dominant negative effect on endogenous WNK1. These results

strongly support the notion that phosphorylation on T58 of WNK1 is important for inhibition of ROMK by hormones or growth factors that activate PI3K.

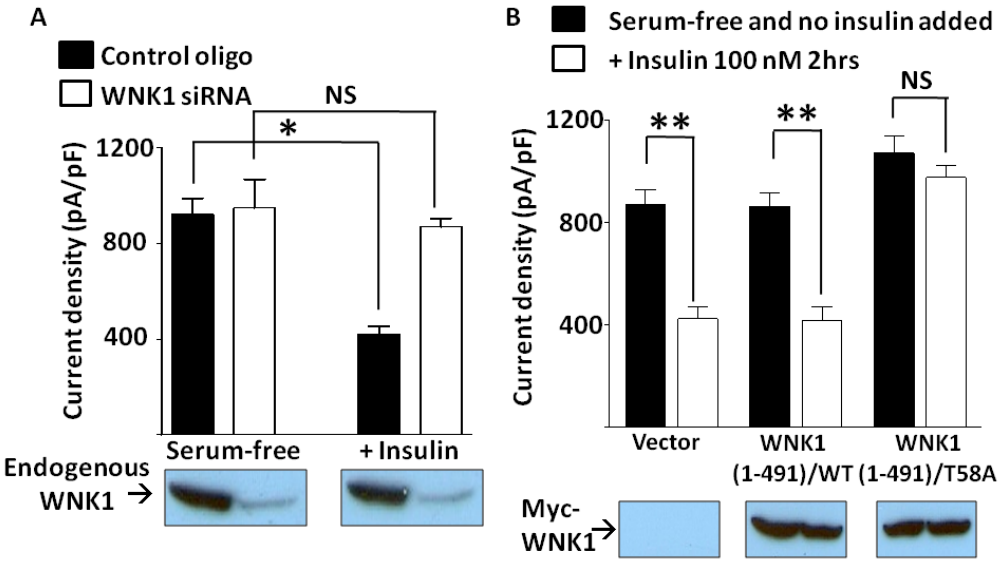

Figure 3-7. Insulin inhibits ROMK through WNK1 T58 phosphorylation. (A) Cells transfected with control oligonucleotide or WNK1 siRNA (200 nM each) were deprived of serum for 16 hours (serum-free group). Insulin (100 nM) was added for 2 hours (+Insulin group). Successful knockdown of endogenous WNK1 by siRNA is evident by western blot analysis. (B) Cells transfected with empty vector, wild type (WT) or T58A mutant WNK1(1-491) were cultured in serum-free medium for 16 hours and received insulin (100 nM) or not for 2 hours. Equal amount of WT or T58A WNK1(1-491) expression is evident by western blot analysis. Mean ± S.E.M. ($n \geq 6$ each). One asterisk denotes $p < 0.05$ between indicated groups by unpaired two-tailed Student's t test. Double asterisk denotes $p < 0.01$. NS denotes statistically not significant.

3.3.3 Akt1 and SGK1 Phosphorylate WNK1 at Threonine-58 *In Vitro* and *In Vivo*

It is known that WNK1 is a substrate for both Akt1 and SGK1. However, the kinase activities of different status of Akt and SGK1 on WNK1 phosphorylation have not been clearly clarified yet. In this project, I designed experiments to examine kinase activity of Akt1 and SGK1 systematically with the goal to guide our physiological studies. I first examined the ability of exogenously expressed Akt1 and

SGK1 to phosphorylate WNK1 *in vitro* with or without coexpressed PDK1. Expressed epitope-tagged Myc-PDK1, HA-Akt1 or Flag-SGK1 was immunoprecipitated from HEK cell lysates by respective antibodies. Purified bacterial His-tagged fragment of WNK1 consisting of amino acids 1-119 was used as the substrate. T58A mutant WNK1 was used as the control for specific phosphorylation at T58. As shown, PDK1 by itself did not phosphorylate WNK1 (Figure 3-8, lane 1). For Akt1, both wild type Akt1 and myristoylated Akt1, but not their kinase dead mutant, phosphorylated WNK1 (lane 2-4). Though myristoylated Akt1 is reported catalytically more active than wild type toward certain substrates, I did not find so using WNK1 as a substrate. Coexpression of PDK1 did not further enhance the *in vitro* kinase activity of Akt1 (lane 8-10). For SGK1, only S422D (not wild type or kinase-dead mutant) phosphorylated WNK1 in the absence of PDK1 (lane 5-7). The SGK1-S422D mutant with serine-422 in the hydrophobic motif substituted by aspartate is constitutively active because it does not require phosphorylation by mTOR for activation by PDK1.[135] Co-expression of PDK1 enhanced the kinase activity of WT and SGK1-S422D (lanes 11-13). The increase in the kinase activity on S422D mutant was so much that phosphorylation on WNK1 also occurred at residue(s) other than T58 (see lane 11, on WNK1(1-119)/T58A mutant). The averaged relative kinase activity of Akt1 and SGK1 (normalized to "Akt1-Myr" in lane 2, which is given as 1) representing specific phosphorylation on WNK1-T58 phosphorylation (i.e., after subtracting the phosphorylation signal on T58A mutant from the signal on wild type of WNK1(1-119) from multiple experiments is shown in bar graph in the bottom.

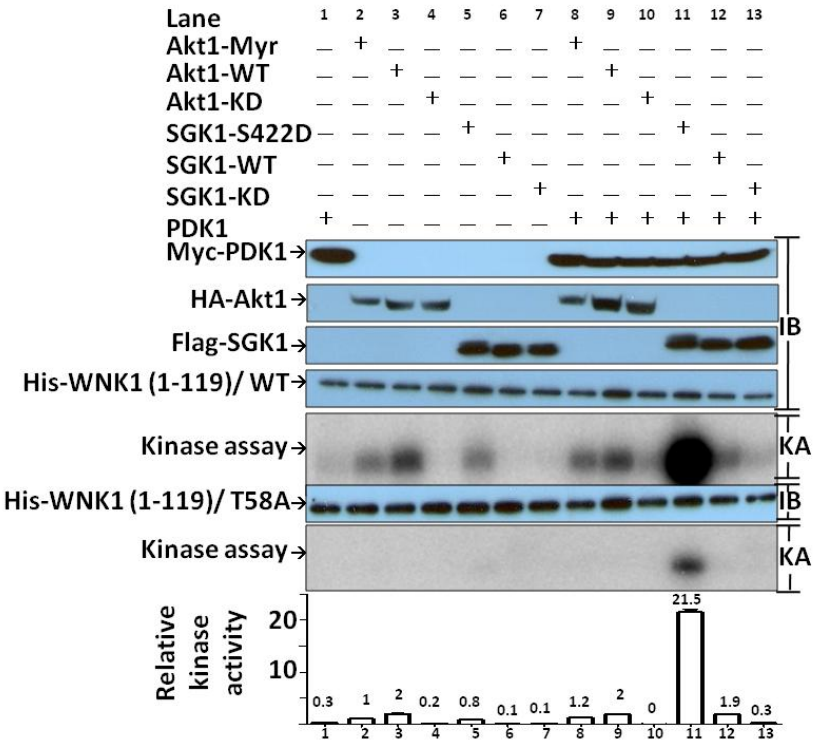

Figure 3-8. *In vitro* kinase assay of PDK1, Akt1 and SGK1.
Epitope-tagged (Myc-, HA- or Flag-) wild type SGK1 (SGK1-WT), kinase-dead SGK1 (SGK1-KD), constitutively active mutant SGK1 (SGK1-S422D), WT Akt1 (Akt1-WT), myristoylated-Akt1 (Akt1-Myr), and kinase-dead Akt1 (Akt1-KD) were expressed in HEK cells with or without wild type PDK1. Kinase activity of immunoprecipitated PDK1, Akt1 and SGK1 were assayed using wild type or T58A WNK1 (1-119) as a substrate. Immunoblots of precipitated proteins by respective epitope antibody (labeled "IB" on the right) and autoradiograph of kinase assay analyzed by phosphoimager (labeled "KA" on the right) are shown. Bar graph in the bottom is the relative kinase activity (normalized to lane 2, "Akt1-Myr") specific for phosphorylation at T58 (i.e., subtracting non-T58 phosphorylation signal on WNK1 (1-119)/T58A mutant from signal on wild type WNK1(1-119)). Mean ± S.E.M. from 3 separate experiments is shown on top of each bar.

I further examined the activity of these kinases acting *in vivo* (i.e., in intact cells). WNK1(1-220) (which lacks kinase domain thus avoiding autophosphorylation) was coexpressed with epitope-tagged Akt1, SGK1 and/or PDK1 as indicated. Phosphorylation at T58 was probed by anti-WNK1-T58 phospho-antibody. T58A mutant of WNK1(1-220) was used as a negative control (Figure 3-9, lane 14, labeled as "M" for mutant). As shown, there was a low basal level of phosphorylation on WNK1(1-220) (lane 1), presumably from the endogenous Akt1. Myristoylated and wild-type Akt1, but not kinase-dead mutant, caused phosphorylation of WNK1 above the basal level (lanes 2-4). Coexpression with PDK1 slightly enhanced kinase activity of myristoylated Akt1 but not wild type Akt1 (lanes 8-10). The increase in the kinase activity of myristoylated Akt1 by PDK1 *in vivo*, but not *in vitro*, may be due to preferential targeting of the myristoylated Akt1 to the cell membrane, thus increased colocalization with PDK1. As *in vitro* studies, S422D and wild type SGK1 phosphorylated WNK1 *in vivo* (lanes 5, 6). PDK1 slightly enhanced SGK1 kinase activity but not as much as the effect found in the *in vitro* experiments (lanes 11, 12). Differences in the ratio of substrate relative to kinase and/or the efficiency of kinase may account for the discrepancy. To our surprise, expression of kinase-dead SGK1 caused some phosphorylation of WNK1 above the basal level, though the activity is less compared to wild type or S422D mutant (lanes 7, 13). At the moment, I don't have a good explanation for the finding, only to speculate that it may be due to altered activity of endogenous Akt1. Overall, these results from *in vitro* and *in vivo* kinase assays support the idea that Akt1 and SGK1 can phosphorylate WNK1 at T58.

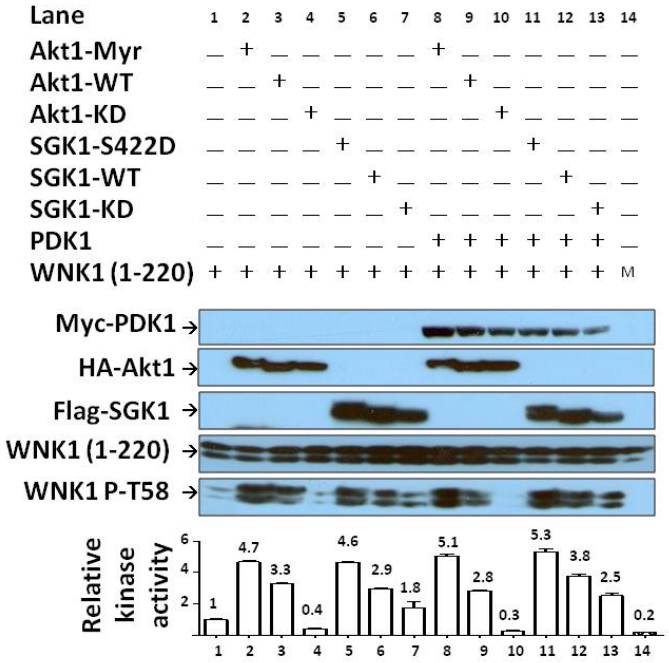

Figure 3-9. *In vivo* phosphorylation on T58 of WNK1 by Akt1 and SGK1.
Cells were transfected with epitope-tagged Akt1, SGK1 or PDK1 with wild type WNK1(1-220) (lanes 1-13) or with WNK1(1-220)/T58A mutant (lane 14 labeled "M"). Protein expressions were blotted by specific antibodies. Phosphorylation on T58 of WNK1(1-220) was detected by anti-phospho-T58 WNK1 antibody. Doublet bands detected by anti-WNK1 and anti-phospho-T58 WNK1 antibodies were always found in WNK1(1-119), WNK1(1-220) but not in WNK1(1-491). The doublets probably represent different conformational forms of eukaryotic WNK1 proteins as they are not observed for purified His-tagged WNK1(1-119) proteins produced in the bacteria (see Figure 3-8). The abundance of each band in the gel reflecting kinase activity of Akt1 or SGK1 was measured by densitometry by the Image J program available at the NIH website. Basal level of T58 phosphorylation on WNK1(1-220) without exogenous Akt1or SGK1 (lane 1) was defined as one for relative kinase activity measurement. Mean ± S.E.M. from 3 separate experiments is shown on top of each bar.

3.3.4 Akt1 Inhibits ROMK through WNK1

In previous experiments (Figure 3-4), I found that supraphysiological concentration of insulin can further inhibit ROMK in the presence of serum. This result suggests that normally the endogenous Akt1 and WNK1 are not maximally activated. In line with the idea, exogenous WNK1 inhibits ROMK (Figure 3-7B and ref. 100).[100] I thus asked whether overexpression of Akt1 may inhibit ROMK by enhancing WNK1-T58 phosphorylation. Myristoylated Akt1 was chosen because it can be enhanced by PDK1 in intact cells. Myristoylated Akt1 ("Akt1-Myr") inhibited ROMK but did not cause additional effect when WNK1(1-491) was cotransfected (Figure 3-10A). Kinase dead mutant of Akt1 (Akt1-KD) did not cause inhibition of ROMK, but reversed WNK1(1-491)-mediated inhibition. Thus, Akt1 and WNK1 act on the same pathway. To confirm the role of Akt1 is from phosphorylation on T58 of WNK1, I showed that WNK1(1-481)/T58A had no effect on ROMK, but reversed myristoylated Akt1-mediated inhibition of ROMK (Figure 3-10B).

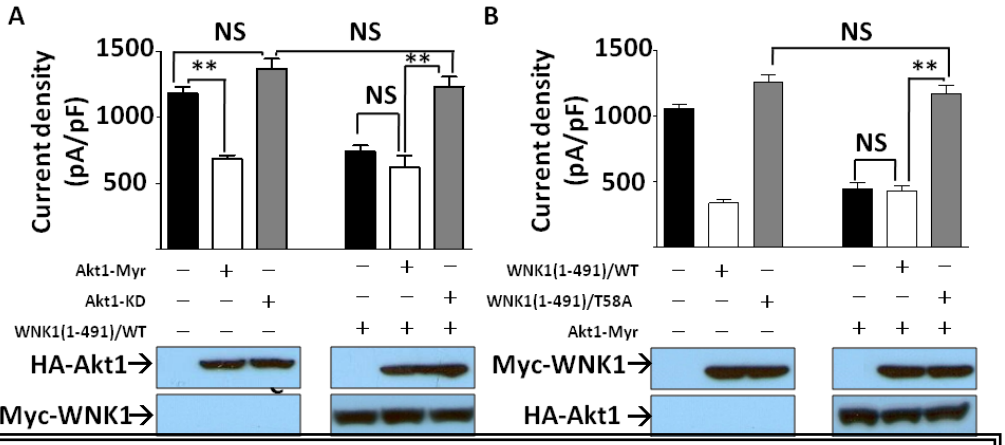

Figure 3-10. Akt1 inhibits ROMK in a WNK1-T58 phosphorylation-dependent manner.
(A) Effect of Akt1 on ROMK. Cells were transfected with ROMK and with myristoylated Akt1 (Akt1-Myr), kinase-dead Akt1 (Akt1-KD) and/or WNK1(1-491) as indicated. (B) Effect of myristoylated Akt1 (Akt1-Myr) on ROMK in the presence of wild type (WT) or T58A mutant of WNK1(1-491). ROMK current densities (pA/pF at -100 mV) were represented as mean ± S.E.M. ($n \geq 6$). Double asterisk denotes $p < 0.01$. NS denotes statistically not significant.

Then, I knocked down endogenous WNK1 by siRNA and demonstrated that myristoylated Akt failed to inhibit of ROMK without endogenous WNK1 (Figure 3-11A). Finally, I tested the effect of insulin on membrane abundance of ROMK in the absence of Akt1. Insulin failed to decrease membrane abundance of ROMK when endogenous Akt1 was knocked down by siRNA (Figure 3-11B).

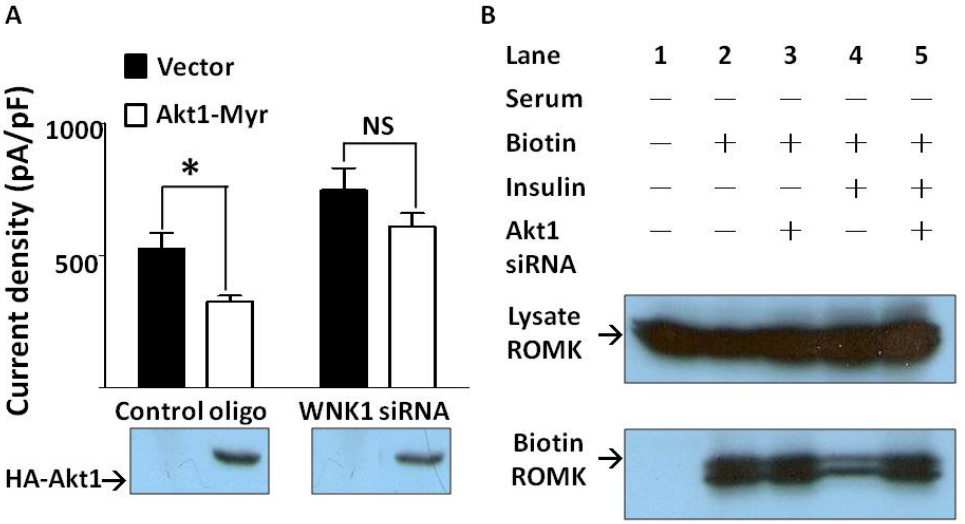

Figure 3-11. Effect of Akt1 on ROMK endocytosis.
(A) Cells were transfected with ROMK and with control oligonucleotide or WNK1 siRNA (200 nM each) and with empty vector or myristoylated Akt1 (Akt1-Myr). ROMK current densities (pA/pF at -100 mV) were represented as mean ± S.E.M. ($n \geq 6$). One asterisk denotes $p < 0.05$ between indicated groups by unpaired two-tailed Student's t test. NS denotes statistically not significant. (B) Effect of insulin on membrane abundance of ROMK in the absence of endogenous Akt1. Cells were transfected with ROMK and control oligonucleotide or Akt1 siRNA (200 nM each) and deprived of serum for 16 hours. Insulin (100 nM) was treated in designated group for 2 hours before biotinylation (Biotin). ROMK in total cell lysates (Lysate ROMK) and elute from avidin beads (Biotin ROMK) were detected by western blot.

3.3.5 SGK1 Inhibits ROMK through WNK1 and Works Together with Akt1

I next examined the potential role of SGK1, another member of the AGC kinase family that can also mediate downstream effect of PI3K, in regulating WNK1 inhibition of ROMK. Similar to Akt1, constitutively active SGK1 mutant, S422D,

inhibited ROMK but did not cause additional effect when WNK1(1-491) was coexpressed. Kinase-dead SGK1 did not inhibit ROMK, but reversed the inhibition caused by WNK1 (Figure 3-12A). In the presence of T58A mutant of WNK1(1-491), even constitutively active form of SGK1 cannot inhibit ROMK (Figure 3-12B). Knocking down endogenous WNK1 by siRNA also abrogated the effect of SGK1 on ROMK (Figure 3-12C). Thus, exogenous Akt1 and SGK1 displayed similar inhibitory effect on ROMK and both effects depend on WNK1-T58 phosphorylation.

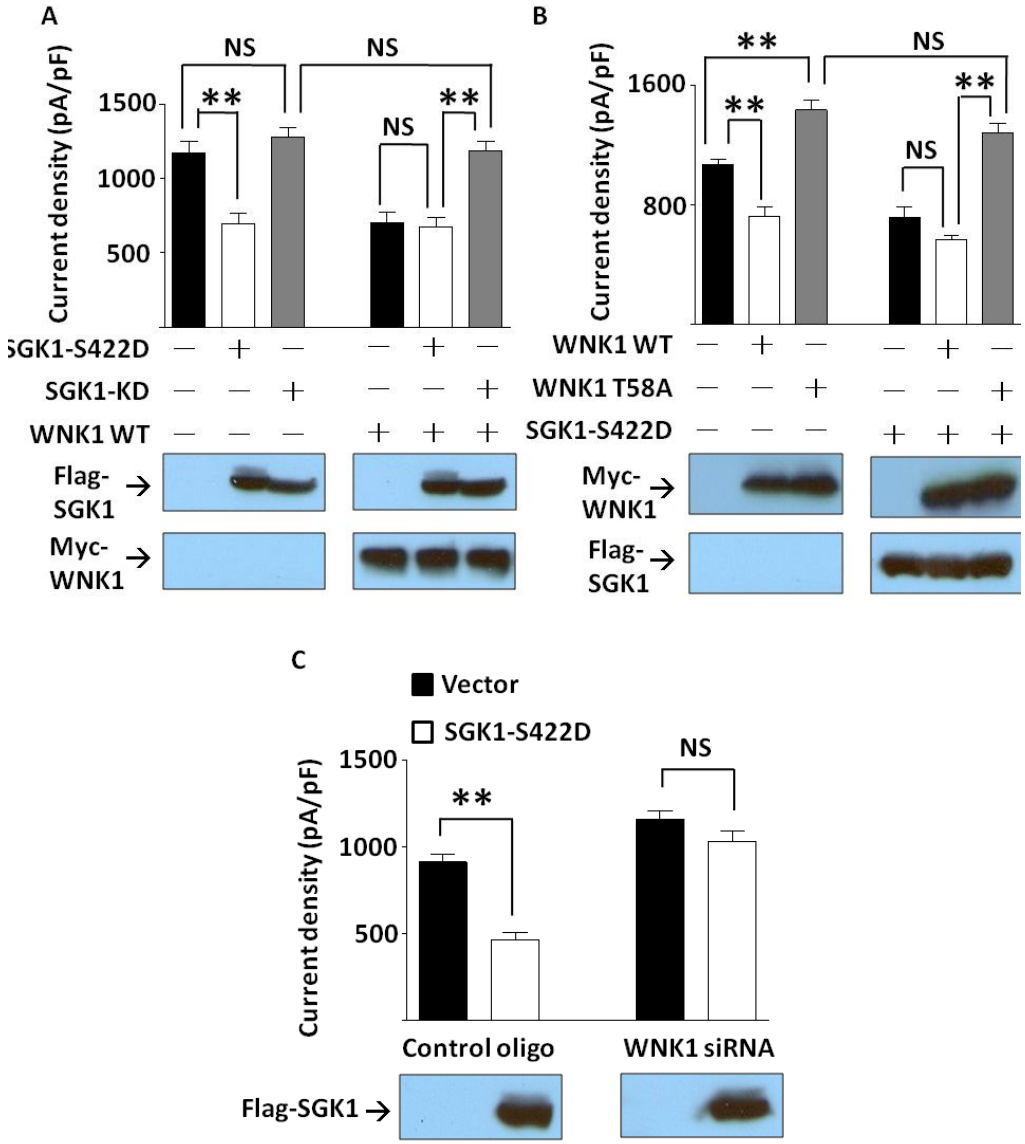

Figure 3-12. SGK1 inhibits ROMK in a WNK1-T58 phosphorylation-dependent manner.
(A) Cells were co-transfected with ROMK and constitutively active SGK1 (SGK1-S422D) or kinase-dead SGK1 (SGK1-KD) with or without WNK1(1-491). (B) Cells were co-transfected with ROMK, wild type (WT) or T58A mutant WNK1(1-491) and SGK1- S422D as designated. (C) Cells were transfected with ROMK, with control oligonucleotide or WNK1 siRNA (200 nM each) and with empty vector or SGK1-S422D. ROMK current density was measured and presented as mean ± S.E.M. ($n \geq 6$ for each group). Double asterisk denotes $p < 0.01$ between indicated groups by unpaired two-tailed Student's *t* test. NS denotes statistically not significant. Equal expression of protein was confirmed by western blot.

Next, I examined potential synergistic effects of Akt1 and SGK1 on ROMK by silencing endogenous Akt1 and/or SGK1 using siRNA in the absence ("vector") or presence of exogenous WNK1 ("WNK1(1-491)"). Knocking down Akt1 or SGK1 individually increased ROMK current significantly with or without exogenous WNK1 (Figure 3-13). The effect of knocking down of both Akt1 and SGK1 is greater than knocking down each individually in the "WNK1(1-491)"-transfected, but not in the "vector"-transfected group. Differences in the abundance of WNK1 substrate likely account for the different results. In summary, both Akt1 and SGK1 phosphorylate WNK1 and contribute to its regulation of ROMK. The importance of Akt1 versus SGK1 *in vivo* will depend on the relative abundance of each respective kinase and WNK1 in the setting.

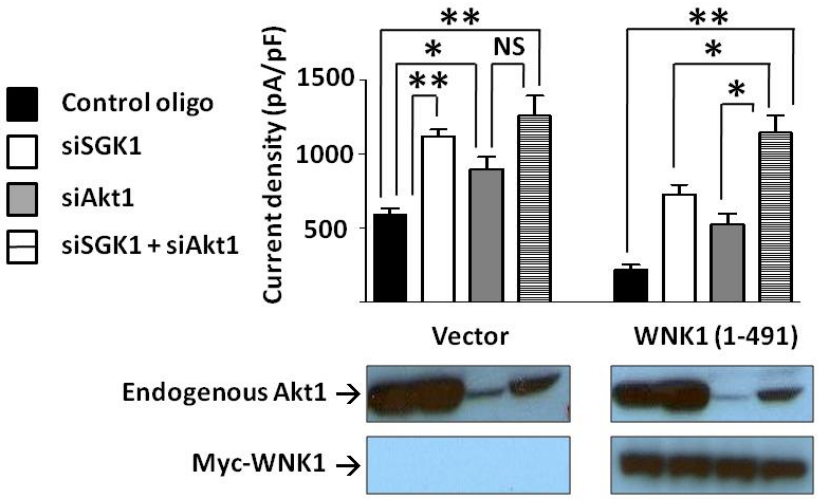

Figure 3-13. Effect of siRNA of Akt1 and/or SGK1 on ROMK.
Cells were transfected with ROMK, with siRNA for Akt1 (siAkt1) and/or SGK1 (siSGK1, 200 nM each) and with vector or WNK1(1-491). ROMK current density was measured and presented as mean ± S.E.M. ($n \geq 6$ for each group). One asterisk denotes $p < 0.05$ between indicated groups by unpaired two-tailed Student's *t* test. Double asterisk denotes $p < 0.01$. NS denotes statistically not significant. Efficacy of Akt1 siRNA and equal expression of protein were confirmed by western blot.

3.3.6 Inhibition of ROMK by SGK1 via Enhanced Endocytosis and Not by Phosphorylation of ROMK

WNK1 inhibits ROMK by enhancing endocytosis through a dynamin-dependent, clathrin-mediated pathway.[100, 125] This effect of WNK1 requires an interaction with intersectin.[89] Previous studies reported that SGK1 can directly phosphorylate on ROMK1 at serine-44, though this effect is believed to result in an increase of the cell-surface abundance of ROMK.[136] I found that co-expression of a dominant-negative ("DN") intersectin or dynamin prevented inhibition of ROMK by SGK1-S422D (Figure 3-14).

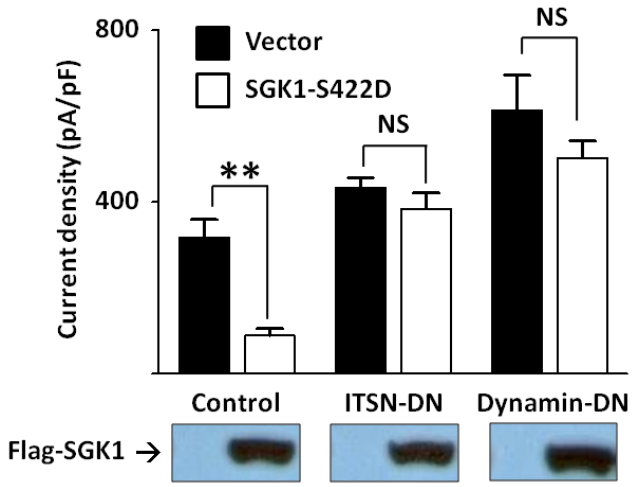

Figure 3-14. Effect of SGK1 on ROMK is dynamin and intersectin-dependent. Cells were transfected with ROMK, with SGK1-S422D and with empty vector, ITSN(intersectin)-DN or dynamin-DN. ROMK current density was measured and presented as mean ± S.E.M. ($n \geq 6$ for each group). Double asterisk denotes $p < 0.01$ between indicated groups by unpaired two-tailed Student's *t* test. NS denotes statistically not significant. Equal protein expression was confirmed by western blot.

These results, together with previous reports that these experimental maneuvers abolish inhibition of ROMK by WNK1, support that phosphorylation of WNK1-T58 by SGK1 leads to inhibition of ROMK by increasing endocytosis of

ROMK. In further support of this idea, I found that SGK1-S422D inhibited ROMK bearing a mutation of serine-44 (S44D) as well as wild type ROMK (Figure 3-15).

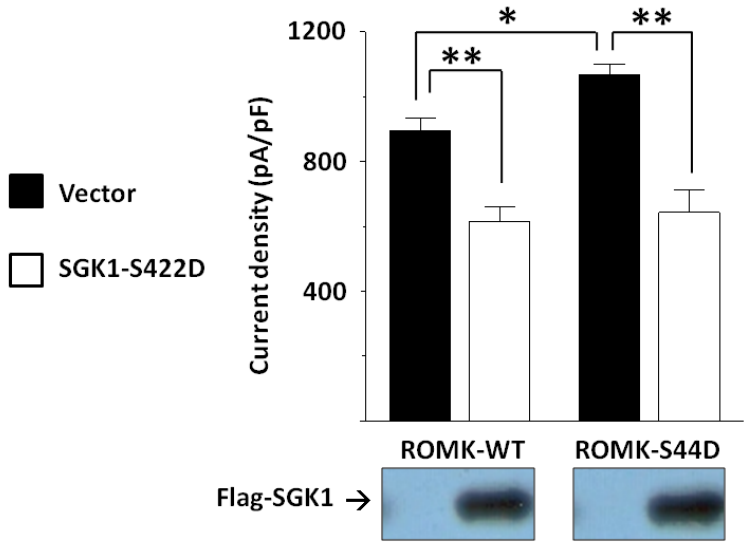

Figure 3-15. Effect of SGK1 on ROMK is not dependent on phosphorylation of ROMK at S44.
Cells were cotransfected with ROMK, with SGK1-S422D and with wild type ROMK (ROMK-WT) or S44D mutant of ROMK (ROMK-S44D). ROMK current density was measured and presented as mean ± S.E.M. ($n \geq 6$ for each group). One asterisk denotes $p < 0.05$ between indicated groups by unpaired two-tailed Student's *t* test. Double asterisk denotes $p < 0.01$. Equal protein expression was confirmed by western blot.

3.3.7 Kidney-Specific WNK1 Blocks SGK1 Effect on ROMK without Interfering with Phosphorylation on WNK1

WNK1 has multiple isoforms among tissues, including the full-length WNK1 (also known as long WNK1) and a kidney-specific WNK1 (KS-WNK1) that lacks most of the kinase domain and preceding amino acids in the N-terminus.[137] Long WNK1 contains T58, the target of Akt1/SGK1. In contrast, KS-WNK1 lacks T58. It has been reported that KS-WNK1 binds and antagonizes long WNK1-induced ROMK inhibition.[100] Here, I asked whether KS-WNK1 antagonizes the effect of long

WNK1 in the presence of Akt1/SGK1. As reported previously, KS-WNK1 reversed WNK1(1-491)-induced inhibition of ROMK (Figure 3-16, left 3 bars). The ability of KS-WNK1 to antagonize WNK1(1-491)-induced inhibition of ROMK was unaltered in the presence of exogenous constitutively active SGK1 (SGK1-S422D) (Figure 3-16, the last bar on the right).

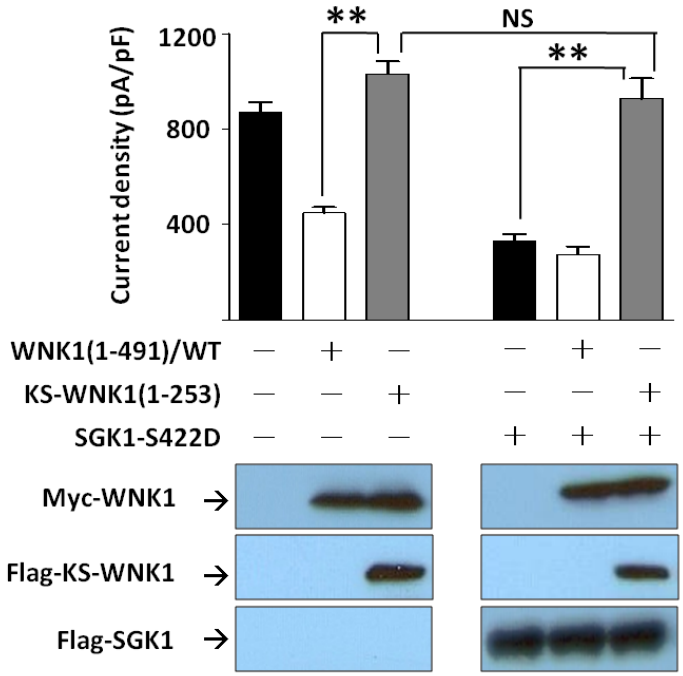

Figure 3-16. Effect of SGK1 on ROMK is reversed by KS-WNK1.
Cells were transfected with SGK1-S422D, WNK1(1-491) and/or KS-WNK1(1-253) as indicated. KS-WNK1(1-253) consists of amino acids 1-253 of KS-WNK1. ROMK current density was measured and presented as mean ± S.E.M. ($n \geq 6$ for each group). Double asterisk denotes $p < 0.01$ between indicated groups by unpaired two-tailed Student's *t* test. Equal protein expression was confirmed by western blot.

KS-WNK1 may antagonize long WNK1 inhibition of ROMK by interfering with its phosphorylation by Akt1/SGK1 (Figure 3-17A, pathway "1") or interfering with its interaction with downstream effectors of endocytosis, such as intersectin (pathway "2"). To distinguish between these two possibilities, I examined the effect

of KS-WNK1 on serum-induced phosphorylation of WNK1(1-491) in HEK cells coexpressed with SGK1-S422D. Serum deprivation decreased T58 phosphorylation on WNK1, which was enhanced by SGK1-S422D (lane 1-3) (Figure 3-17B). Coexpression of KS-WNK1 did not affect phosphorylation of WNK1 at T58 (lanes 4-6). KS-WNK1 alone had no effect on WNK1 phosphorylation (lane 7). Thus, KS-WNK1 likely affects WNK1 interaction with downstream effectors.

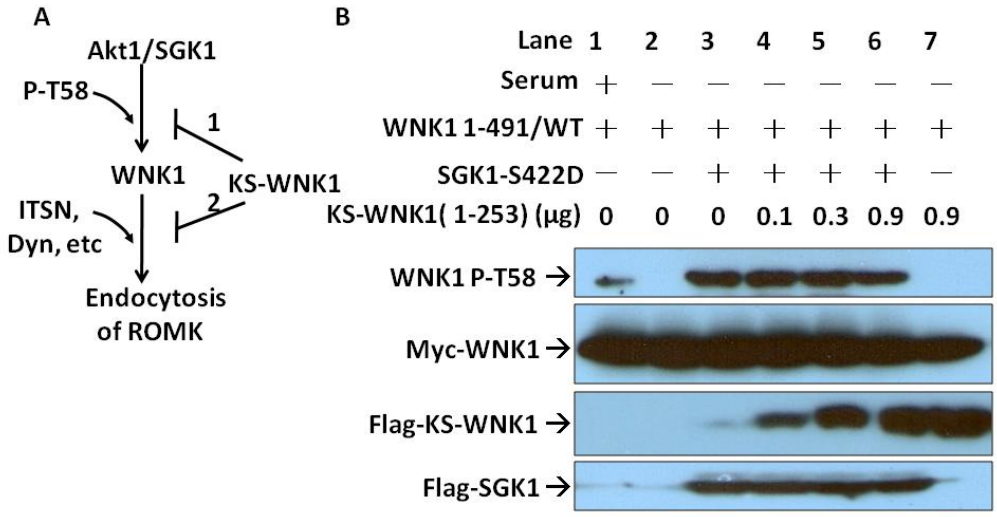

Figure 3-17. KS-WNK1 did not affect T58 phosphorylation of WNK1.
(A) Possible mechanisms for KS-WNK1 to block SGK1 effect on ROMK. Mechanism 1: Interfering with WNK1 phosphorylation by SGK1. Mechanism 2: Interring with WNK1 interaction with downstream effectors (intersectin, dynamin, etc.). (B) Effect of KS-WNK1 on WNK1-T58 phosphorylation by SGK1. Cells were all transfected with WNK1(1-491), KS-WNK1(1-253) (at DNA amount from 0-0.9 μg) and/or SGK1-S422D and incubated with or without serum as indicated. Basal level of WNK1(1-491) phosphorylation was shown in lane 1. For experiments shown in lanes 2-7, cells were incubated in serum-free media for 16 hours. Protein expression was detected by specific antibodies. Phosphorylation on WNK1-T58 was determined using anti-phospho-T58 WNK1 antibody.

3.4 Discussion

Constitutive endocytosis is the main way to control ROMK abundance and mediated by clathrin-dependent mechanism.[125] By increasing ROMK endocytosis, WNK kinases including WNK1 and WNK4 inhibit ROMK current.[100] WNK1 and 4 interact with intersectin, an endocytic scaffold protein that binds dynamin and other endocytic accessory proteins, to enhance the recruitment and assembly of endocytic machinery.[89] Therefore, the interaction with intersectin promotes the formation of ROMK-containing clathrin-coated vesicles and stimulate endocytosis of ROMK. In this project, I show that the insulin/IGF-induced activation of PI3K (probably also induced by other serum growth factors) enhances endocytosis of ROMK through phosphorylation of T58 on WNK1. This effect on ROMK via WNK1 depends on ACG kinases, Akt1 and/or SGK1. Figure 3-18 summarizes this signaling process, starting from the activation of PI3K stimulates mTOR complex-2 (mTORC2) to phosphorylate Akt1 and SGK1 at S473 and S422 in the hydrophobic motif, respectively. The serine phosphorylated Akt1 and SGK1 allow binding of PDK1, which phosphorylates Akt1 and SGK1 at T308 and T256 in the T-loop, respectively, to fully activate their catalytic activity. The serine and threonine double-phosphorylated Akt1 and SGK1 phosphorylate T58 of WNK1 much more efficiently than non-phosphorylated or single phosphorylated forms and result in increased endocytosis of ROMK via an intersectin-dependent mechanism.

This PI3K-Akt/SGK-WNK1 signaling mechanism for ROMK regulation has several potential physiological or pathophysiological relevancies. One of these is the maintenance of K^+ homeostasis during chronic (about 1 week) K^+ deficiency. IGF1 is produced in the kidney and the production is upregulated by dietary K^+ restriction.[138] It is believed that upregulation of IGF1 plays a role in the K^+-deficiency-induced

renal hypertrophy. Through increased IGF1, the activated PI3K-Akt/SGK pathway can reduce renal K^+ secretion via ROMK and helps to conserve K^+ during K^+ deficiency. Indeed, intravenous injection of IGF1 in humans decreased renal K^+ excretion without significant changes in glomerular filtration rate and the filtered load of K^+.[139] In contrast, mice with liver-specific deletion of IGF1 have ~80% reduction in the circulating IGF1 and increased renal K^+ excretion despite a normal filtered load of K^+.[140] In humans, the normal range of plasma IGF1 is 50-1000 ng/ml, far exceeding the IC_{50} for inhibition of ROMK by IGF1 in cultured cells measured in this study (18.5 ng/ml). Inhibition of PI3K in CCD cells from mice on a low-K diet increased ROMK-like small conductance K^+ channel through enhancing membrane amount of channel.[141]

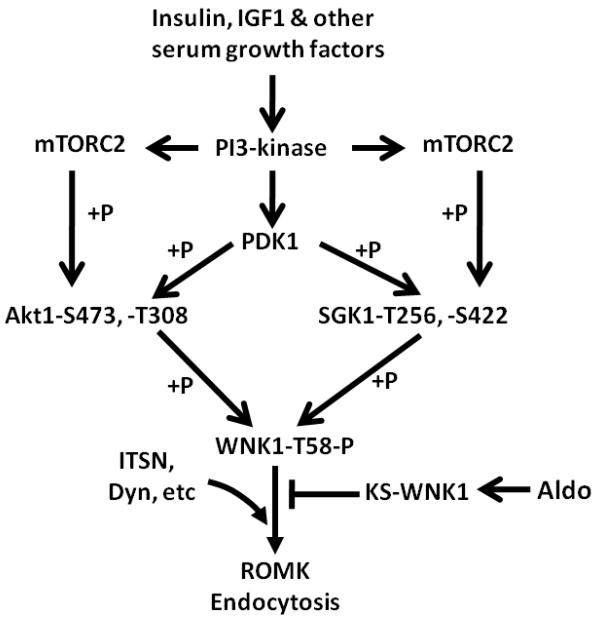

Figure 3-18. A working model for regulation of ROMK by PI3K-activating hormones via Akt1/SGK1 and WNK1 and by aldosterone.
See texts for details.

Insulin functions similarly to IGF1 in the stimulation of PI3K and thus theoretically also inhibits renal K^+ excretion via the Akt1/SGK1-WNK1 pathway. This inhibitory role of insulin on renal K^+ excretion *in vivo*, however, is not universally accepted. While it is known that insulin decreases urinary K^+ excretion, some suggested that the effect is entirely from the decrease in the plasma K^+ due to the intracellular shift.[142] Conversely, other studies did intravenous infusion of insulin in humans and showed that the insulin-induced reduction of urinary K^+ excretion is more than the decrease in the total filtered K^+ load secondary to the decreased plasma K^+ concentration, supporting that insulin inhibits renal K^+ excretion *in vivo*.[143, 144] Furthermore, adding of insulin to the bath of isolated perfused rabbit CCD exerts effect on the basolateral side of tubule through insulin receptor and turns out to inhibit the net transepithelial K^+ secretion.[145] In that microperfusion study, the reported IC_{50} for inhibition of K^+ secretion in the CCD is 500 pM, which is higher than the normal fasting level of insulin (10-150 pM) but within the normal postprandial level (300-800 pM).[132] In this study, the minimal concentration of insulin to effectively inhibit ROMK is 1 nM. This value is higher but not far from the effective concentration of insulin in the microperfused CCD and the peak level of insulin during the postprandial period *in vivo*. The difference could be resulted from the different experimental systems. If insulin indeed inhibits ROMK-mediated renal K^+ secretion in vivo, this K^+ conserving mechanism will help to maintain the extracellular K^+ homeostasis during the postprandial state, in which a very active intracellular shift of K^+ occurs.

The finding that SGK1 inhibits ROMK in this study is different from other reports that SGK1 stimulates ROMK.[136, 146] Several animal studies supported that the results in this study have *in vivo* importance and implication. First, mice homozygous

for *Sgk1* deletion have higher abundance of ROMK in the apical membrane of distal nephron than their wild type littermates.[62] It was hypothesized that the increased abundance of ROMK in *Sgk1* knockout mice was due to a compensatory response to hyperkalemia mainly caused by reduced ENaC-mediated Na^+ reabsorption in CCD and thus reduced the PD_{TE} for K^+ secretion. Second, in mice with double knockout of *Sgk1* and *Sgk3* (in which Na^+ wasting is evident in normal Na^+ diets), the fractional urinary K^+ excretion is higher than that in wild type littermates despite a normal blood K^+ level and an impairment in Na^+ reabsorption in the double knockout mice.[147] These results underpin the notion that SGK1 (perhaps also SGK3 or isoforms) inhibit(s) ROMK *in vivo*. This finding does not exclude the possibility that SGK1 can exert a stimulatory effect on ROMK under different physiological contexts or presence of certain co-regulators. The present study, nonetheless, provides compelling evidence to support the inhibitory effect on ROMK and renal K^+ secretion from PI3K-activating hormones induced Akt1/SGK1-mediated phosphorylation of WNK1.

Aldosterone, another upstream regulator of SGK1, appears to enhance K^+ secretion. The finding in this study that SGK1 inhibits ROMK seems to be counterintuitive to the kaliuretic effect of aldosterone. However, SGK1 is not the only downstream target of aldosterone. It is known that aldosterone also stimulates the transcription of KS-WNK1,[148] which antagonizes the effect of full-length WNK1 on ROMK (see Figure 3-18 and ref. 100). Accordingly, insulin and IGF1 activate Akt1/SGK1 to enhance WNK1 inhibition of ROMK. Aldosterone, in contrast, activates two opposing pathways on WNK1 regulation of ROMK (SGK1 and KS-WNK1) and therefore has no net effect on ROMK. The increase in the electrical driving force (PD_{TE}) for K^+ secretion secondary to enhanced ENaC-mediated Na^+

reabsorption is likely the predominant cause of stimulation of K^+ secretion by aldosterone. Although this study is based on cell culture system, it still provides a novel model for ROMK regulation. To better understand the effect on ROMK from these SGK-activating factors, deletion of specific genes that critically involve in this pathway in mice, such as SGK1- and WNK1-null mice, may serve as a good model for future experiments.

CHAPTER FOUR

KIDNEY-SPECIFIC WNK1 INHIBITS SODIUM REABSORPTION IN CORTICAL THICK ASCENDING LIMB

4.1 Introduction

With-no-lysine (WNK) kinases belong to serine/threonine kinase superfamily and are comprised of four members (WNK1-4) in mammals. WNK1, first identified by Xu et al in 2000, is the founding member of WNK family and ubiquitously expressed in different tissues.[78] The main function of WNK kinases is to regulate renal handling of Na^+ and K^+ as is evident by findings that mutations in WNK1 and WNK4 genes cause a syndrome of hereditary hypertension and hyperkalemia, called pseudohypoaldosteronism type II.[79] Many studies, mostly in vitro, have suggested that WNK1 and 4 modulate the activities of various Na^+ transporters and K^+ channels in the distal nephron via catalytic and non-catalytic mechanisms leading to increased Na^+ absorption and impaired K^+ secretion.[80, 82, 89, 128] Kidney-specific WNK1 (KS-WNK1) is a shorter splice variant of full-length WNK1 predominantly expressed in distal nephron segments.[137] The transcription of KS-WNK1 is initiated by an alternative promoter in exon 4A, which resides in intron 4 between exons 4 and 5. Thus, the transcript of KS-WNK1 is shorter, containing exon 4a and the remaining exon 5~28 of full-length WNK1 and the encoded protein lacks the kinase domain encoded by exon 3 and 4.[99] Results of studies based on heterologous cells have suggested that KS-WNK1 functions as an antagonist of full-length WNK1 with respect to regulation of renal Na^+ and K^+ transporters.[100, 149]

To explore the function of KS-WNK1 in vivo, KS-WNK1 knockout mice and transgenic mice that overexpress KS-WNK1 in the kidney have been created.[95, 96] In KS-WNK1 transgenic mice, the total and phosphorylated forms of NCC and NKCC2 in renal cortex are reduced. These mice display renal Na^+ wasting and lower blood pressure under normal Na^+ diet.[95] Conversely, KS-WNK1 knockout mice have increased expression of NCC and NKCC in renal cortex and hypertension when fed a high Na^+ diet.[95] Another group has also generated KS-WNK1 knockout mice and reported similar findings of increased NCC abundance and mild expansion of volume status in the mice.[94] These two studies are consistent with KS-WNK1 being an inhibitor of NCC in the DCT. The role of KS-WNK1 on NKCC2, however, remains unsettled despite our studies on KS-WNK1-KO and transgenic mice. This is in large part due to previous reports based on *in situ* hybridization that KS-WNK1 was not detected in thick ascending limb (TAL)[99, 150] and that there have not been direct functional studies of Na^+ transport in this nephron segment.

Dietary K^+ is an important modulator of Na^+ reabsorption in the kidney. It has been reported that dietary K^+ loading causes natriuresis in part from suppression of Na^+ reabsorption in TAL.[70] The underlying mechanism of this K^+ adaptive response in TAL is unknown. Previous study has demonstrated that a high K^+ diet increases the expression of KS-WNK1 in whole kidney and transgenic mice that overexpress KS-WNK1 in the kidney have decreased NKCC2 expression.[95, 100] In this project, I study the effect of KS-WNK1 on Na^+ transport in TAL and its role in the regulation of sodium transport by dietary K^+ using in vitro microperfusion.

4.2 Materials and Methods

4.2.1 Animals

KS-WNK1 knockout (KS-WNK1 KO) by deleting exon 4A in 129/sv strain and transgenic mice over-expressing amino acid 1-253 of KS-WNK1 (KS-WNK1 Tg) in C57BL/6 strain have been created by Chou-Long Huang's lab.[95, 100] All of the experimental procedures involving these animals were performed in accordance with relevant laws and institutional guidelines approved by the University of Texas Southwestern Medical Center at Dallas Institutional Animal Care and Use Committee.

4.2.2 Balance Studies

For plasma biochemical data in control and high K^+ diet, ten KS-WNK1 KO mice and control littermates (129/sv wild type) (4 female, 6 male, ~4-month old) were fed a control K^+ (1% KCl, 1 g per 100 g diet) or a high K^+ (10% KCl) diet (Harlan Teklad, Madison, WI, USA) with free access to water for two weeks before the collection of blood samples. Mice were anesthetized with isoflurane and whole blood was drawn by retro-orbital bleeding into Na^+-heparin-coated glass capillary tubes. Plasma was recovered immediately by centrifugation. Plasma electrolytes were analyzed using STAT-CCC Analyzer (Nova Biomedical, Waltham, MA, USA). Plasma creatinine level was measured by capillary electrophoresis (P/ACE MDQ) (Beckman Coulter, Brea, CA, USA).[95] For balance studies, ten KS-WNK1 KO mice and control littermates (129/sv wild type) (4 female, 6 male, ~4-month old) were fed the indicated diet and water *ad libitum* and placed in metabolic cages (Hatteras Instruments, Cary, NC, USA) for collection of urine. The concentrations of Na^+ and K^+ in urine were measured using a microflame-emission photometer (Jenway, Essex, UK). The osmolality of plasma and urine were measured using an osmometer

(Advanced Instruments, Model 3D3, Norwood, MA, USA). The osmole-free water clearance (CH_2O) was calculated by the equation:

$$CH2O = \frac{\text{Daily urine volume } (\mu L)}{1440 \text{ min}} \times \frac{\text{Plasma osmolality} - \text{Urine osmolality}}{\text{Plasma osmolality}}$$

A positive value implies that the kidneys excrete solute-free water and dilute urine. In contrast, a negative value implies that the kidneys retrieve water and concentrate urine.

4.2.3 Mice Prepared for Microperfusion and Microdissection Studies

These experiments were performed on KS-WNK1 KO and KS-WNK1 Tg mice at 8-10 weeks of age, and age- and gender-matched wild-type littermates (129/sv strain for KS-WNK1 KO and C57BL/6 strain for KS-WNK1 Tg). The mice were raised in a 12-hour day and night cycle and fed a control (1% KCl) K^+ or a high (10% KCl) K^+ diet and plain drinking water *ad libitum* for two weeks before sacrifice.

4.2.4 In Vitro Microperfusion, Sodium Flux and Transepithelial Potential Difference.

After the mouse was sacrificed, the kidney was removed quickly, sliced in thin coronal sections and placed in Hanks' solution containing (in mM) 137 NaCl, 5 KCl, 0.8 $MgSO_4$, 0.33 Na_2HPO_4, 0.44 KH_2PO_4, 1 $MgCl_2$ 10 tris (hydroxymethyl) amino methane hydrochloride, 0.25 $CaCl_2$, 2 glutamine, and 2 L-lactate at 4^oC. The cortical thick ascending limb of Henle's loop was then dissected free hand without collagenase and transferred to a 1 ml temperature-controlled bathing chamber. Tubules were perfused *in vitro*.[151]

Isolated cTALs were perfused at a rate of ~5 nl/min. The perfusate contained (in mM) 115 NaCl, 25 $NaHCO_3$, 2.3 Na_2HPO_4, 10 Na acetate, 1.8 $CaCl_2$, 1 $MgSO_4$, 5 KCl, 8.3 glucose and 5 alanine and had an osmolality equal to that of the bathing solution which contained 6 gm/dl of albumin. There were at least 3 measurements of the perfusion and the collected tubular fluid in each experiment. Na^+ transport (J_{Na}) was calculated using the equation:

$$J_{Na}\ (pmol.min^{-1}.mm^{-1}) = ([Na]_{perfusate} - [Na]_{collected})(\dot{V}_L)/\ L$$

where $\dot{V}_L$ is collection rate (~5 nl/min) and L is the tubular length (0.4-0.8 mm). The transepithelial potential difference was determined using the perfusion pipette as a bridge into the tubular lumen and referenced to the bathing solution using a Keithley 6517A programmable electrometer (Cleveland, OH, USA). Furosemide used to inhibit NKCC2 was purchased from Sigma-Aldrich (St. Louis, MO, USA). Na^+ concentrations of perfusate and collected drops were measured using a Na^+-selective electrode (Sodium Ionophore II-Cocktail A, Fluka).[152, 153]

4.2.5 Microdissection and Reverse Transcription-PCR.

Slices of kidney were placed into pre-warmed collagenase type I (Worthington, Lakewood, NJ, USA) (1.5 mg/ml dissolved in DMEM/F12) solution in 15 ml test tube, which was then shaken vigorously on a titer plate shaker at 37℃ for 10-15 minutes. After digestion, the individual nephron segments were dissected in 4°C Hank's solution and transferred by adhering the tubules to small glass beads (0.5-mm diameter, Thomas Scientific, Swedesboro, NJ, USA) and then transferring the beads to 1.5 ml tubes containing 0.6 ml RNase inhibitor-containing lysis buffer. Total RNA was immediately extracted using Quick-RNA™ MicroPrep kit (Zymo

Research, Irvine, CA, USA). Reverse transcription was performed using TaqMan® Reverse Transcription Reagents (Applied Biosystems, Carlsbad, CA, USA). Quantitative real-time PCR was carried out on MyiQ single color RT-PCR detection system (Bio-rad, Hercules, CA, USA). I verified that no amplification was produced when reverse transcription was omitted in each sample. Sequences of primers for RT-PCR analysis were provided in Table 3.

Table 3. Primer sequences for RT-PCR of WNK isoforms and specific tubular markers

Target	Sequence (5'-3')	Orientation
FL-WNK1	GTCTGGACACCGAAACCACT	Sense
	CGAACAATGTTGGGATGTTG	Antisense
KS-WNK1	AGAAACTACTAGTAGCAAAATCCCTGTC	Sense
	GCTTCACTCCCTCATTTATACAATCC	Antisense
NKCC2	CCAGAGCGTTGTCTAAAGCA	Sense
	TGGGCAGCTGTCATCACTTA	Antisense
NCC	GGGTTTGTGTCATGAGGATG	Sense
	CTCGTCCGATCGTGGTAGA	Antisense
AQP2	CTGGCTGTCAATGCTCTCCAC	Sense
	TTGTCACTGCGGCGCTCATC	Antisense
GAPDH	CGTCCCGTAGACAAAATGGT	Sense
	TCAATGAAGGGGTCGTTGAT	Antisense

Relative mRNA levels of target proteins were standardized with an internal control (glyceraldehyde 3-phosphate dehydrogenase, GAPDH). For comparison

between KS-WNK1 and FL-WNK1, the efficiencies of KS-WNK1 and FL-WNK1 primers in RT-PCR assay were calculated from the results of three serial (4-, 16-, 64-fold) dilutions of cDNA, which encompass our working dilution (~10-fold dilution).[154] The slope of threshold cycles obtained from KS-WNK1 or FL-WNK1 PCR reactions of serially diluted sample tubular cDNA was used to calculate the corresponding efficiencies (E) according to the equation: $E = 10^{(\frac{-1}{slope})}$. Each sample was assayed in triplicate.

4.2.6 Statistical Analysis

All results are expressed as mean ± standard error mean (SEM). Difference between groups was assessed using Student's *t* test. A p value less than 0.05 (*) was considered to be statistically significant.

4.3 Results

4.3.1 Characterization of WNK1 Isoforms mRNA Expression in Renal Tubules in Control and High Potassium Diet.

The relative expression of WNK1 isoforms including FL-WNK1 and KS-WNK1 in individual renal tubules has not been studied. I measured relative mRNA abundance of KS-WNK1 and FL-WNK1 in renal tubules including the medullary and cortical thick ascending limb (mTAL, cTAL), distal convoluted tubule (DCT), connecting tubule (CNT), and cortical collecting duct (CCD) using quantitative RT-PCR. The purity of these samples was confirmed by measuring the mRNA abundance of nephron segment-specific markers (NKCC2 for TAL, NCC for DCT, aquaporin-2 for CNT and CCD) (Figure 4-1).

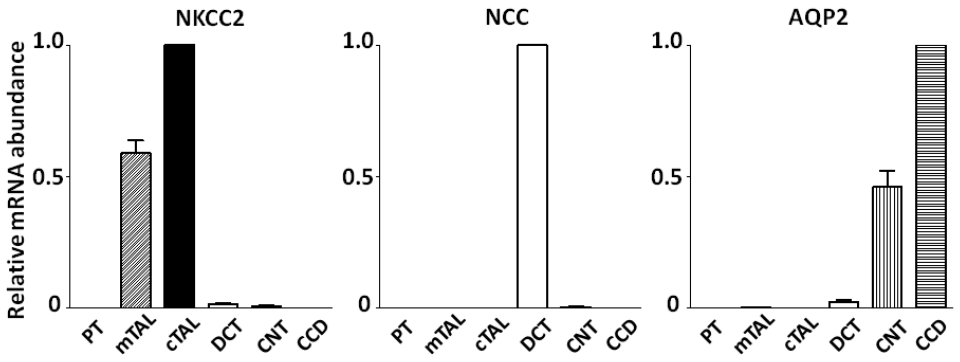

Figure 4-1. Purity of dissected tubules confirmed by measuring mRNA level of tubule specific marker.
(*A*) NKCC2 expression relative to cTAL (*B*) NCC expression relative to DCT (*C*) AQP2 expression relative to CCD in different nephron segments. (n = 10 for each segments) Abbreviations: AQP2: aquaporin 2, CCD: cortical collecting duct, cTAL: cortical thick ascending limb of Henle's loop, CNT: connecting tubule, DCT: distal convoluted tubule, mTAL: medullary thick ascending limb of Henle's loop, NCC: sodium chloride cotransporter, NKCC2: sodium, potassium, and chloride cotransporter, PT: proximal tubule. Data are presented as means ± S.E.M.

To allow comparison of abundance of KS-WNK1 and FL-WNK1, I first determined efficiencies of PCR primers used in KS-WNK1 and FL-WNK1 RT-PCR assays (Figure 4-2A). The calculated efficiencies of KS-WNK1 and FL-WNK1 RT-PCR assays were 1.94 and 1.92, respectively (Figure 4-2B), supporting the legitimacy of direct comparison between two RT-PCR assays.[154]

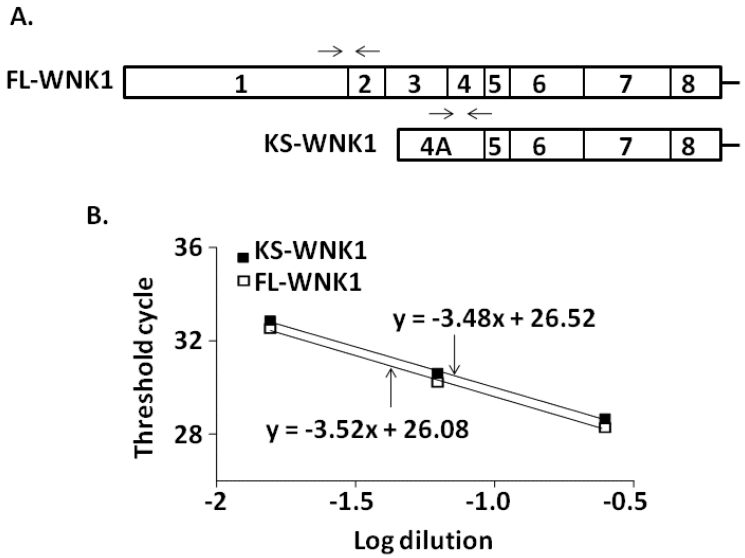

Figure 4-2. Comparable efficiencies of KS-WNK1 and FL-WNK1 RT-PCR assays legitimate direct comparison between two PCR reactions.
(A) Schematic representation of WNK1 exons showing the positions of primers (arrows) used for RT-PCR analysis of full-length WNK1 (FL-WNK1) and kidney-specific WNK1 (KS-WNK1) in this study. (B) Similar efficiencies of KS-WNK1 and FL-WNK1 RT-PCR assays. Wild type cTAL cDNA was serially diluted ¼ (4-, 16-, 64-fold dilution), and 3 μl of each dilution was used in the KS-WNK1 and FL-WNK1 PCR assays. The threshold cycle was measured and plotted against the log of the dilution.

Under control (1%) K^+ diet, the expression of KS-WNK1 was most abundant in the DCT, but also present in the cTAL, CNT, and CCD (Fig 4-3, left panel). The KS-WNK1 transcript was almost undetectable in mTAL and proximal tubule (not shown for proximal tubule). As for FL-WNK1, its mRNA expression was more evenly distributed along the nephron in lower abundance compared to KS-WNK1 (Fig 4-3, right panel). The ratio of KS-WNK1 to FL-WNK1 mRNA is ~18 fold in the DCT, but closer to 1 in other segments (0.85, 2, and 0.5 for cTAL, CNT, and CCD, respectively).

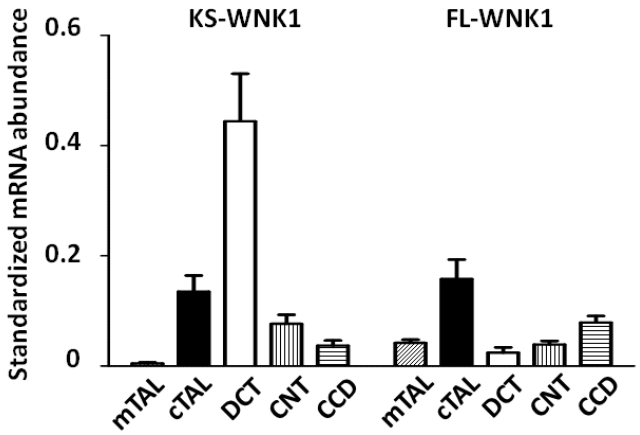

Figure 4-3. Quantitative comparison of WNK1 isoform expression under normal potassium diet in distal nephron.
The standardized mRNA expression levels of KS-WNK1 and FL-WNK1 in each individual tubular segments (mTAL: medullary thick ascending limb, cTAL: cortical thick ascending limb, DCT: distal convoluted tubule, CNT: connecting tubule, CCD: cortical collecting duct) under control (1%) K^+ diet. WNK1 isoforms in each sample were standardized to the mRNA level of its own housekeeping GAPDH gene. n=10

To test the effect of a high K^+ diet on KS-WNK1 and FL-WNK1 mRNA expression, mice were fed either a 1% K^+ or 10% K^+ diet for two weeks before isolation of renal tubules. A high K^+ diet increased KS-WNK1 mRNA expression in cTAL and DCT (90% and 60% increase, respectively), but not in other segments (Figure 4-4A). In contrast, a high K^+ diet had no effect on FL-WNK1 mRNA (Figure 4-4B).

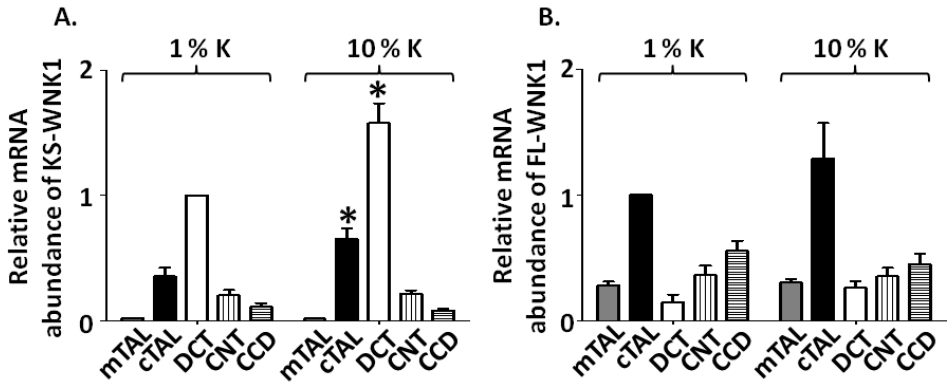

Figure 4-4. High K^+ diet upregulates KS-WNK1 mRNA expression in cortical thick ascending limb of Henle's loop and distal convoluted tubule.
(A, B) The effect of dietary K^+ on the mRNA levels of KS-WNK1 (A) and FL-WNK1 (B). The standardized mRNA expression levels of KS-WNK1 or FL-WNK1 in each individual tubular segment under control (1%) K^+ diet were compared to those under high (10%) K^+ diet. WNK1 isoforms in each sample were standardized to the mRNA level of GAPDH gene (n=10). For comparison, the standardized mRNA level of KS-WNK1 in DCT and FL-WNK1 in cTAL under control (1%) K^+ diet were set as 1 respectively. Data are presented as means ± S.E.M. * $p < 0.05$ when compare to the same segment in 1% K diet.

4.3.2 KS-WNK1 mediates high potassium diet induced suppression of sodium reabsorption in the cTAL

It has been reported that overexpression of KS-WNK1 decreases protein abundance of total and phosphorylated NKCC2 in the TAL and knockout of KS-WNK1 has opposite effects.[95] Here I studied the physiological relevance of these findings by measuring Na^+ reabsorption in isolated cTAL using in vitro

microperfusion. In cTALs isolated from wild type mice, Na^+ reabsorption occurred at a rate 175 ± 12 $pmol.min^{-1}.mm^{-1}$ (Figure 4-5A). This reabsorbed flux agrees with previous reports in cTAL.[155] Addition of furosemide (100 μM) to perfusate caused ~90% reduction of Na^+ reabsorption in cTAL (Figure 4-5C), indicating that it is mediated by NKCC2. A high K^+ diet suppressed Na^+ reabsorption in cTAL by ~24% (Figure 4-5A, left panel). In KS-WNK1 KO mice, the baseline Na^+ reabsorption in the cTAL under control K^+ diet was ~20% higher than control (Figure 4-5A). High K^+ diet didn't significantly suppress Na^+ reabsorption in the cTAL of KS-WNK1 KO mice (Fig 4-5A, right panel). Na^+ reabsorption in TAL via NKCC2 generates a lumen-positive transepithelial potential difference (PD_{TE}). A similar pattern was observed in measurements of PD_{TE} (Figure 4-5B).

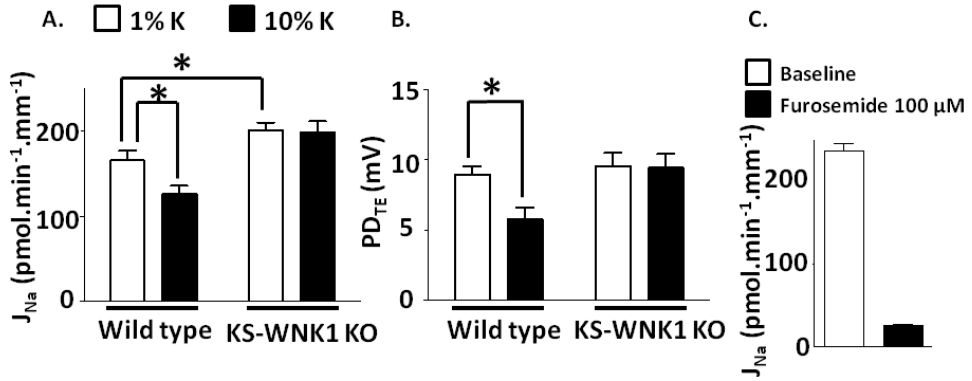

Figure 4-5. KS-WNK1 mediates chronic K^+ load-induced natriuresis in cortical thick ascending limb of Henle's loop.
(A) Na^+ reabsorption (J_{Na}) and (B) lumen positive PD_{TE} in the cTAL isolated from wild type (129/sv) or KS-WNK1 KO mice fed with control (1% K, white bars) or high (10% K, hatched bars) K^+ diet for 2 weeks. (n = 10 for 1% K, n = 8 for 10% K). (C) Effect of furosemide on Na^+ reabsorption in cTAL of wild type mouse (C57BL/6, n = 8) fed with control K^+ diet. Data are presented as means ± S.E.M. * $p < 0.05$ between designated groups.

To further support the functional role of KS-WNK1 in cTAL, I measured Na^+ flux in cTAL of transgenic (Tg) mice that overexpress KS-WNK1 in the kidney. Na^+

reabsorption in cTAL was ~33% lower in KS-WNK1 Tg mice than in control littermates under control K^+ diets (Figure 4-6A). High K^+ diet did not cause further reduction of Na^+ reabsorption in cTAL from KS-WNK1 Tg mice (Figure 4-6A, right panel). Similar changes were observed in PD_{TE} measurements (Figure 4-6B).

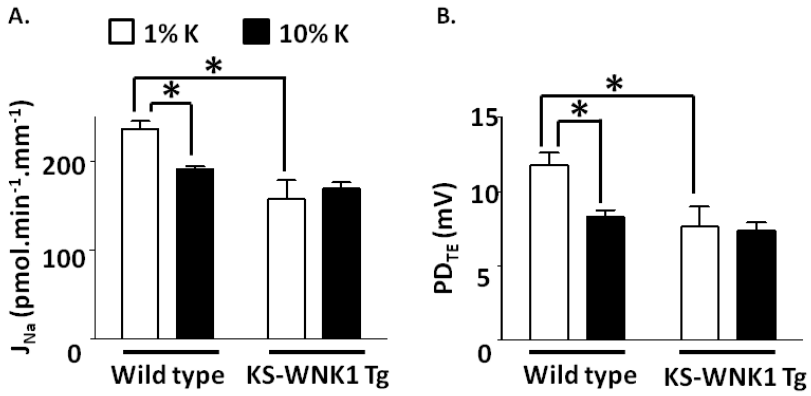

Figure 4-6. Overexpressed KS-WNK1 inhibits Na^+ reabsorption in cortical thick ascending limb of Henle's loop.
(A) Na^+ reabsorption and (*B*) lumen positive PD_{TE} in the cTAL isolated from wild type (C57BL/6) or KS-WNK1 Tg mice fed with control (1% K, white bars) or high (10% K, hatched bars) K^+ diet for 2 weeks. (n = 8 for each group). Data are presented as means ± S.E.M. * $p < 0.05$ between designated groups.

These functional results, together with previous biochemical and immunological analysis of NKCC2 in KS-WNK1 KO and KS-WNK1 Tg mice,[95] indicate that KS-WNK1 inhibits NKCC2 in cTAL, and that KS-WNK1 mediates the inhibition of Na^+ reabsorption in cTAL by a high K^+ diet.

4.3.3 KS-WNK1 Knockout Blunts the High Potassium Diet-induced Natriuresis

A high K^+ diet causes natriuresis by affecting Na^+ reabsorption at multiple nephron segments.[69, 70] To understand the contribution of KS-WNK1-mediated inhibition of NKCC2 to the overall natriuretic response in renal K^+ adaptation, I

performed whole-animal clearance studies. Mice were fed a control K^+ diet for 4 days and then switched to a high K^+ diet for 7 days. Daily urine volume and urinary Na^+ and K^+ excretion during control K^+ diet were not different between KS-WNK1 KO and wild-type mice (Table 4). A change to a high K^+ diet resulted in an increase in urine volume in both wild type and KS-WNK1 KO mice starting from the first day of high K^+ diet (Figure 4-7A). The high K^+-induced diuretic response, however, was blunted in KS-WNK1 KO mice relative to wild type littermates. Unexpectedly, urinary Na^+ excretion in both wild type and KS-WNK1 KO mice decreased on the first day of high K^+ diet (Figure 4-7B). This initial drop was likely due to palatability of the high K^+ diet causing decreased intake (see below for K^+ excretion). A similar observation has been made in mice by others.[63, 150] After the first day, urinary Na^+ excretion increased in both wild-type and KS-WNK1-KO mice reflecting natriuretic response to a high K^+ diet. Compared to wild-type, the natriuretic response in KS-WNK1 mice was somewhat blunted on the 2nd and 3rd day of a high K^+ diet (Figure 4-7C).

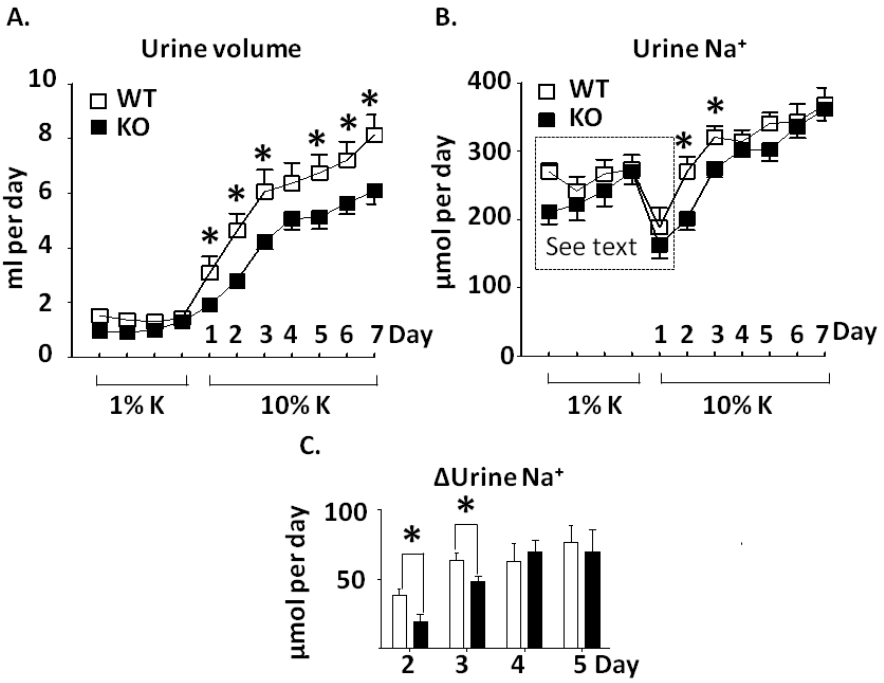

Figure 4-7. KS-WNK1 knockout mice have blunted diuretic and natriuretic responses to high K^+ diet.

(A) Urine volume (B) Urine Na^+ excretion in response to high K^+ diet. Wild type (129/sv) or KS-WNK1 KO mice (n = 10 for each group) were fed a control (1%) K^+ diet for 4 days and then a high (10%) K^+ diet for 7 days. The daily urine samples were collected. (C) The magnitude of increased urine Na^+ excretion (ΔUrine Na^+ = Urine Na^+ on Day 2-5 minus Urine Na^+ on Day 1) from Day 1 of high K^+ diet was shown. The drop of urine Na^+ from control 1% K^+ diet to first day of high 10% K^+ diet (dotted box) is explained in text. Data are presented as means ± S.E.M. * $p < 0.05$ in the comparison between wild type (WT) and KS-WNK KO (KO) mice.

As expected, urinary K^+ excretion increased on a high K^+ diet (Figure 4-8). Likely because of the decrease in intake of the high K^+ diet, daily urinary K^+ excretion increased only by ~7-fold rather than the expected 10-fold increase. Importantly, the increase in K^+ excretion was also decreased in KS-WNK1-KO mice relative to wild type mice on the 2nd and 3rd day.

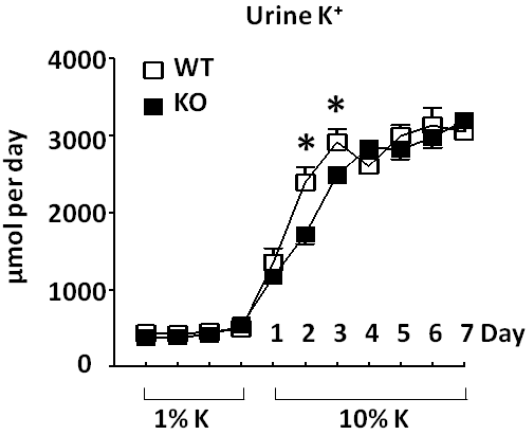

Figure 4-8. KS-WNK1 knockout mice have blunted kaliuretic responses to high K^+ diet.
Urine K^+ excretion in response to high K^+ diet. Wild type (129/sv) or KS-WNK1 KO mice (n = 10 for each group) were fed a control (1%) K^+ diet for 4 days and then a high (10%) K^+ diet for 7 days. The daily urine samples were collected. Data are presented as means ± S.E.M. * $p < 0.05$ in the comparison between wild type (WT) and KS-WNK KO (KO) mice.

The above results support the hypothesis that KS-WNK1 contributes to high K^+ diet-mediated diuresis and natriuresis. Serum K^+ levels, however, were not different between KS-WNK1-KO and wild-type mice, even on a high K^+ diet (Table 4). Thus, other mechanisms must fully compensate for the transient K^+ excretion impairment caused by loss of KS-WNK1. Interestingly, urine osmolality is significantly higher in KS-WNK1-KO than in wild-type in control K^+ as well as high K^+ diets (Table 4). Moreover, the increase of urine volume on the 7th day of a high K^+ diet was much higher than the increase of urine osmole excretion (Table 4; ~6-fold vs.

~3-fold). As the total daily urine osmole excretion was not different between the two groups on either a control or high K^+ diet, these results suggest that potassium-induced diuresis has more than an effect on osmotic diuresis, and may be in part be due to a decrease in free water reabsorption ($-C_{H2O}$) (-5.9 ± 0.4 l/min [control K^+] *vs* -4.7 ± 0.7 l/min [high K^+], p <0.05; Table 4). Interestingly, free water reabsorption was higher in KS-WNK1-KO mice than in wild-type mice. These results are consistent with the idea that KS-WNK1 inhibits NKCC2, and increased NKCC2 activity in KO-WNK1-KO mice enhances urinary concentration ability.

Table 4. Steady-state data for plasma & urine biochemistries and urine Na^+, K^+ & water excretion in control and high K^+ diets

	Control (1%) K^+ diet		High (10%) K^+ diet	
	WT (n=10)	KO (n=10)	WT (n=10)	KO (n=10)
Body weight (g)	22.5±3.0	25.1±3.9	21.5±2.7	24.0±2.9
Water intake (g)	3.9±1.0	3.1±0.7	10.6±2.9†	8.7±1.7†
Plasma				
Na^+ (mmol/l)	144.5±2.6	145.5±2.2	147.7±1.7^{ø}	146.1±1.7
K^+ (mmol/l)	5.0±0.3	4.5±0.2	5.0±0.5	4.5±0.2
Cl^- (mmol/l)	116.4±2.8	115.9±1.9	117.4±2.0	116.1±2.9
Osmolality (mOsmo/kg)	290.9±3.0	290.7±5.5	297.3±7.6^{ø}	297.1±3.8^{ø}
Creatinine (mg/dl)	0.06±0.01	0.06±0.01		
Urine				
Na^+ (μmol/day)	261±29	243±43	368±71†	362±48†
K^+ (μmol/day)	451±52	428±78	3048±571†	3197±396†
Osmolality (mOsm/kg)	2207±522	2895±431*	1199±186†	1606±138$^{\#\dagger}$
Total osmoles (mOsm/day)	2.8±0.3	2.7±0.5	8.7±1.1†	8.5±1.0†
Volume (ml/day)	1.4±0.5	1.0±0.3	8.1±2.2†	6.1±1.5$^{\#\dagger}$
CH_2O (μl/min)	-5.9±0.4	-6.7±0.6*	-4.7±0.7^{ø}	-6.2±0.9$^{\#}$

Values in mean ± S.D. * $P < 0.05$ KO versus WT in control K^+ diet, $^{\#}P < 0.05$ KO versus WT in high K^+ diet. $^{ø}P< 0.05$ High K^+ versus control K^+, $^{\dagger}P< 0.001$ High K^+ versus control K^+. CH_2O, osmole-free water clearance.

4.4 Discussion

Using quantitative measurement of mRNA and in vitro microperfusion, I show in this study that KS-WNK1 is expressed in cTAL and plays an important role in inhibition of NKCC2-mediated Na^+ reabsorption in the segment. Moreover, KS-WNK1 mediates the high K^+ diet-induced inhibition of Na^+ reabsorption in cTAL.

Since the first discovery of KS-WNK1 in 2002,[137] two studies using in situ hybridization of KS-WNK1 mRNA have shown that the expression of KS-WNK1 is exclusively in the renal cortex[99, 150] and that the DCT has strikingly high KS-WNK1 expression. Using a more quantitative and sensitive method, qRT-PCR, I show that while KS-WNK1 transcript is most abundant in DCT, but it is also present in cTAL, CNT, and CCD; the abundance in these segments relative to DCT are 30%, 17% and 8%, respectively. I confirm that KS-WNK1 is barely detected in mTAL and the proximal tubule. The physiological importance of KS-WNK1 in cTAL is demonstrated by microperfusion studies.

Transepithelial Na^+ reabsorption in cTAL is mediated in large part by the transcellular route, which requires Na^+ entry across the apical membrane predominantly through NKCC2 and exit via the basolateral Na^+-K^+-ATPase. NKCC2-mediated Na^+ reabsorption generates a lumen-positive PD, partly due to apical recycling of K^+. The Na^+-H^+ exchanger also contributes to the apical Na^+ entry, but the role is relatively minor and it does not generate lumen-positive PD.[156] Several pieces of evidence indicate that effect of KS-WNK1 on Na^+ reabsorption in cTAL is in large part through inhibition of NKCC2. First, it is inhibited by NKCC2 inhibitor, furosemide. Second, the effect on Na^+ flux parallels that on lumen-positive PD. Third, and perhaps more importantly, previous study has shown that KS-WNK1 negatively regulates NKCC2 abundance by western blot analysis and immunofluorescent

staining.[95] The additional effects of KS-WNK1 on other transporters in cTAL, nonetheless, is possible.

The other significant finding of this study is that KS-WNK1 appears to mediate high K^+-induced inhibition of Na^+ reabsorption in cTAL. It is known that a high K^+ diet inhibits Na^+ reabsorption in the proximal tubule and TAL.[69, 70, 71] Previous study also showed that a high K^+ diet upregulate KS-WNK1 mRNA in the whole kidney lysate.[100] Here, I further show that high K^+ diets upregulate KS-WNK1 mRNA in cTAL as well as DCT, but not in other segments. In microperfused cTAL, a high K^+ diet inhibits Na^+ reabsorption, and the inhibition is obliterated in KS-WNK1-KO mice. Thus, KS-WNK1 is important for inhibition of Na^+ reabsorption in cTAL by a high K^+ diet. One important physiological role of a high K^+-diet induced natriuresis and diuresis is to maximize renal K^+ excretion during high K^+ intake. The renal K^+ excretion occurs predominantly by secretion via K^+ secretory channels in CNT and early CCD that requires lumen-negative PD generated by ENaC-mediated Na^+ reabsorption. Several factors limit K^+ secretion via this mechanism. First, continuing K^+ secretion on top of water reabsorption accompanying Na^+ reabsorption in the CNT and CCD raises the luminal K^+ concentration to an extent that it favors reabsorption rather secretion in late CCD and the downstream outer medullary collecting duct (OMCD). Second, Na^+ reabsorption in the more proximal segments reduces delivery to distal segments. Inhibition of Na^+ reabsorption in the proximal tubule and TAL by high a K^+ diet would increase Na^+ and fluid delivery to the CNT and CCD to overcome the above limiting factors. Moreover, increased flow to distal nephron segments also stimulate flow-activated maxi-K channels adding to K^+ secretion. Surprisingly, I found that urinary K^+ excretion was only transiently decreased in KS-WNK1-KO mice in the second and third days of a high K^+ diet.

Serum K^+ levels and urinary K^+ excretion at day 4 of a high K^+ diet and onward were not different between KO and wild type mice. Apparently, other factors, such as inhibition of Na^+ reabsorption in the proximal tubule by high K^+ diets, compensate for the deficiency of loss of KS-WNK1.

It is well known that Na^+ reabsorption by medullary TAL is critical for establishment of hypertonic medulla essential for the urinary concentration mechanism.[157] Water restriction increases NKCC2 abundance in TAL and vasopressin stimulates trafficking and insertion of NKCC2 to the apical membrane.[158, 159] Bartter's mutations in NKCC2 and pharmacological inhibition of NKCC2 impair the urinary concentration mechanism.[160, 161] The role of cortical TAL in the urinary concentration is less clear. The results in this study demonstrate that KS-WNK1 plays a role in the urinary concentration mechanism. KS-WNK1-KO mice have a higher baseline urinary osmolality and free water reabsorption. I speculate that this is due to increased NKCC2 activity in the cortical TAL of KS-WNK1 KO mice. The role of NKCC2 in medullary TAL is unlikely because KS-WNK1 is not expressed there. The possibilities that KS-WNK1 regulates aquaporin2 and urea transporters also exit and require further investigation.

CHAPTER 5

CONCLUSION AND FUTURE DIRECTIONS

5.1 Regulations on Inward-rectifying Potassium Channels in Skeletal Muscle

The reduced Kir outward current has been demonstrated to be critical in the pathogenesis of non-familial hypoPP. However, there are still many questions remained unanswered. The first, and most obvious, is how to explain the majority of non-familial hypoPP patients do not have mutations on Kir2.6 channel. I have discussed this issue in chapter 2 (see page 55). One explanation is the inhibition of Kir channel from endogenous factors, including insulin, catecholamine and hypokalemia itself.[111, 123, 162] Many precipitating events of hypoPP, such as large amount of carbohydrate meal and strenuous exercise, increase the circulating level of insulin and catecholamine, which also stimulate Na^+, K^+ ATPase activity. Together, insulin and catecholamine are strong enhancers of net K^+ influx into muscles. However, the effects of insulin and catecholamine on Kir channel were only tested in myofibrils that contain four Kir2.x members, and expressed Kir2.1 channel in cultured cells. Their effect on Kir2.6 channel alone has never been tested. Previous studies have shown that IGF can phosphorylate tyrosine 242 in the C-terminal cytoplasmic domain of Kir2.1 and inhibit Kir2.1 activity.[163] In addition, the small GTPase Ras-mitogen-activated protein kinase (MAPK) pathway was also reported to regulate the intracellular trafficking of Kir2.1.[164] Sharing the high homology of amino acid sequence between Kir2.1 and Kir2.6, I will like to test the effect of insulin on Kir2.6 and explore the downstream signaling pathways in cultured cells.

Since skeletal muscle contains four Kir2.x channels and Kir2.x channel can form heterotetramer with other Kir2.x members,[165] it will be interesting to characterize the activity of Kir2.x heterotetramers, such as Kir2.1/2.6, in different ratios of combination. In my previous study, the Kir2.1/2.6 heterotetramer behaves in between Kir2.1 and Kir2.6 homotetramer (see page 46, Figure 2-13). With increased expression of Kir2.6, the heterotetramer becomes more like a Kir2.6 homotetramer. Using plasmid containing Kir2.1/2.6 concatemer, the activity of heterotetramers can be measured more accurately than co-expression of Kir2.1 and Kir2.6.

Other than these pioneering in vitro studies, my ultimate goal is to delineate the characters of Kir2.x channels in skeletal muscle. If the specific human Kir2.6 antibody can be created, the subcellular localization of Kir2.1 and Kir2.6 can be examined by immunohistochemical staining. Previous study found that different subcellular localization and function of Kir2.x channels in atrium and pulmonary veins.[166] The subcellular localization (T-tubule or sarcolemma) of Kir2.x channel may also result in different functions in skeletal muscle. A recent genome-wide association study of TPP patients identified a genetic variant rs623011 located at 75 kb downstream of *KCNJ2* (Kir2.1) gene, which could potentially reduce the transcription of Kir2.1 and total Kir current.[167] Unlike the loss-of-function mutations in Andersen-Tawil syndrome, the genetic variant rs623011 may slightly reduce the transcription and total amount of Kir2.1 and cause only muscular symptoms but not cardiac or skeletal symptoms. Alternatively, the rs623011 may be regulated by the precipitating factors of TPP/SPP, such as insulin and catecholamine, and affects the Kir2.1 abundance in a short-term manner. Examination of Kir2.1 transcript abundance in leucocytes or biopsied muscle samples from patients carrying disease rs623011 may be helpful to confirm the importance of this genetic variant.

5.2 Functions and Distributions of WNK Kinases and Related Proteins in Renal Tubules

It is widely accepted that WNK kinases and their related proteins, including OSR, SPAK, and SGK, play important roles in renal Na^+ and K^+ handling. However, their relative distribution and function in individual tubular segments are still controversial. For example, people used to believe that KS-WNK1 is only expressed and functions in DCT. In this thesis, I demonstrated that KS-WNK1 is also present and functions in cTAL, mostly benefited from microdissection of specific tubular segment and functional data from in vitro microperfusion. Using the same technique, I will be able to characterize the localization and function of WNK kinases and related proteins in renal tubules. In addition, additional manipulations, such as adding vasopressin or insulin into basolateral bath, can also be tested in specific tubular segment and/or genetic mouse model to answer more questions.

I will continue to exam the function of KS-WNK1 in CCD. Although the expression level of KS-WNK1 is relatively low in CCD (see page 98, Figure 4-3), the physiological function of KS-WNK1 in CCD cannot be excluded. Previous studies showed KS-WNK1 antagonize the effect of WNK1-induced ROMK endocytosis in vitro, and KS-WNK knockout mice had lower protein abundance of ENaC. The functional results in vivo have not been provided. Second, it is still unclear whether WNK1 stimulate Na^+ reabsorption in renal tubules other than DCT although in vitro studies suggested WNK1 can stimulate ENaC activity. When the conditional (kidney-specific) WNK1 knockout mouse model is available (undergoing project in Dr. Chou-Long Huang's lab), the effects of full-length WNK1 in TAL and CCD can be specifically addressed.

Studies in heterologous cell lines have shown that SPAK and OSR phosphorylate and activate NCC, and two NKCC isoforms (NKCC1, NKCC2). To study the function of SPAK in kidney, two SPAK mouse models, $SPAK^{T243A/T243A}$ and SPAK knockout mice, were created.[97, 168] Both of them exhibited renal salt wasting and decreased NCC abundance in DCT. However, the findings on NKCC2 were opposite with decrease of phosphorylated NKCC2 in $SPAK^{T243A/T243A}$ mice but increase in SPAK knockout mice. None of them showed functional evidence of SPAK in TAL, where NKCC2 is mainly expressed. Recently, a kinase-deficient isoform of SPAK (KS-SPAK) was reported being mostly expressed in renal medulla and may function as an antagonist of full-length SPAK.[169] All of these issues can be reevaluated in the future experiments using microdissected tubular segments.

BIBLIOGRAPHY

1. Youn JH, McDonough AA. Recent advances in understanding integrative control of potassium homeostasis. *Annu Rev Physiol* 2009; 71: 381-401.
2. Brown RS. Extrarenal potassium homeostasis. *Kidney Int* 1986; 30: 116-127.
3. Kristensen M, Hansen T, Juel C. Membrane proteins involved in potassium shifts during muscle activity and fatigue. *Am J Physiol Regul Integr Comp Physiol* 2006; 290: R766-772.
4. Wang WH, Giebisch G. Regulation of potassium (K) handling in the renal collecting duct. *Pflugers Arch* 2009 ; 458: 157-168.
5. Sejersted OM, Sjøgaard G. Dynamics and consequences of potassium shifts in skeletal muscle and heart during exercise. *Physiol Rev* 2000; 80: 1411-1481.
6. Sjøgaard G, Adams RP, Saltin B. Water and ion shifts in skeletal muscle of humans with intense dynamic knee extension. *Am J Physiol* 1985; 248: R190-196.
7. Rabinowitz L, Green DM, Sarason RL, Yamauchi H. Homeostatic potassium excretion in fed and fasted sheep. *Am J Physiol Regul Integr Comp Physiol* 1988; 254: R357–380.
8. DeFronzo RA, Felig P, Ferrannini E, Wahren J. Effect of graded doses of insulin on splanchnic and peripheral potassium metabolism in man. *Am J Physiol* 1980; 238: E421-427.
9. Bia MJ, DeFronzo RA. Extrarenal potassium homeostasis. *Am J Physiol* 1981; 240: F257-268.
10. Sugden AL, Bean BL, Straw JA. Effects of high potassium or low sodium diet on vascular Na^+,K^+-ATPase activity and blood pressure in young spontaneously hypertensive rats. *Hypertension* 1987; 9: 571-575.
11. Juel C. Na^+-K^+-ATPase in rat skeletal muscle: muscle fiber-specific differences in exercise-induced changes in ion affinity and maximal activity. *Am J Physiol Regul Integr Comp Physiol* 2009; 296: R125-132.
12. Hopkins PM. Skeletal muscle physiology. *Contin Educ Anaesth Crit Care Pain* 2006; 6: 1-6.
13. Clausen T. Na^+-K^+ pump regulation and skeletal muscle contractility. *Physiol Rev* 2003; 83: 1269-1324.
14. Lindinger MI. Potassium regulation during exercise and recovery in humans: implications for skeletal and cardiac muscle. *J Mol Cell Cardiol* 1995; 27: 1011-1022.
15. Shorten PR, Soboleva TK. Anomalous ion diffusion within skeletal muscle transverse tubule networks. *Theor Biol Med Model* 2007; 4: 18.
16. Clausen T, Nielsen OB, Clausen JD, Pedersen TH, Hayward LJ. Na^+,K^+-pump stimulation improves contractility in isolated muscles of mice with hyperkalemic periodic paralysis. *J Gen Physiol* 2011; 138: 117-130.
17. Galuska D, Kotova O, Barrès R, Chibalina D, Benziane B, Chibalin AV. Altered expression and insulin-induced trafficking of Na^+-K^+-ATPase in rat skeletal muscle: effects of high-fat diet and exercise. *Am J Physiol Endocrinol Metab* 2009; 297: E38-E49.
18. Knochel JP, Blachley JD, Johnson JH, Carter NW. Muscle cell electrical hyperpolarization and reduced exercise hyperkalemia in physically conditioned dogs. *J Clin Invest* 1985; 75: 740-745.
19. Kjeldsen K, Nørgaard A, Hau C. Exercise-induced hyperkalaemia can be reduced in human subjects by moderate training without change in skeletal muscle Na,K-ATPase concentration. *Eur J Clin Invest* 1990; 20: 642-647.
20. Skou JC. The influence of some cations on an adenosine triphosphatase from peripheral nerves. *Biochim Biophys Acta* 1957; 23: 394-401.
21. Skou JC. Enzymatic basis for active transport of Na^+ and K^+ across cell membrane. *Physiol Rev* 1965; 45: 596-617.

22. McDonough AA, Youn JH. Role of muscle in regulating extracellular K^+. *Semin Nephrol* 2005; 25: 335-342.
23. Clausen T. Role of Na^+,K^+-pumps and transmembrane Na^+,K^+-distribution in muscle function. The FEPS lecture - Bratislava 2007. *Acta Physiol (Oxf)* 2008; 192: 339-349.
24. Jorgensen PL, Hakansson KO, Karlish SJ. Structure and mechanism of Na,K-ATPase: functional sites and their interactions. *Annu Rev Physiol* 2003; 65: 817-849.
25. Clausen T. Clinical and therapeutic significance of the Na^+,K^+ pump. *Clin Sci (Lond)* 1998; 95: 3-17.
26. Clausen T, Everts ME, Kjeldsen K. Quantification of the maximum capacity for active sodium-potassium transport in rat skeletal muscle. *J Physiol* 1988; 388: 163-181.
27. Clausen T. Hormonal and pharmacological modification of plasma potassium homeostasis. *Fundam Clin Pharmacol* 2010; 24: 595-605.
28. Hibino H, Inanobe A, Furutani K, Murakami S, Findlay I, Kurachi Y. Inwardly rectifying potassium channels: their structure, function, and physiological roles. *Physiol Rev* 2010; 90: 291-366.
29. Lu Z. Mechanism of rectification in inward-rectifier K^+ channels. *Annu Rev Physiol* 2004; 66: 103-129.
30. Plaster NM, Tawil R, Tristani-Firouzi M, Canún S, Bendahhou S, Tsunoda A, Donaldson MR, Iannaccone ST, Brunt E, Barohn R, Clark J, Deymeer F, George AL Jr, Fish FA, Hahn A, Nitu A, Ozdemir C, Serdaroglu P, Subramony SH, Wolfe G, Fu YH, Ptácek LJ. Mutations in Kir2.1 cause the developmental and episodic electrical phenotypes of Andersen's syndrome. *Cell* 2001; 105: 511-519.
31. Ryan DP, da Silva MR, Soong TW, Fontaine B, Donaldson MR, Kung AW, Jongjaroenprasert W, Liang MC, Khoo DH, Cheah JS, Ho SC, Bernstein HS, Maciel RM, Brown RH Jr, Ptácek LJ. Mutations in potassium channel Kir2.6 cause susceptibility to thyrotoxic hypokalemic periodic paralysis. *Cell* 2010; 140: 88-98.
32. Lin SH, Lin YF, Chen DT, Chu P, Hsu CW, Halperin ML. Laboratory tests to determine the cause of hypokalemia and paralysis. *Arch Intern Med* 2004; 164: 1561-1566.
33. Ptácek LJ, Tawil R, Griggs RC, Engel AG, Layzer RB, Kwieciński H, McManis PG, Santiago L, Moore M, Fouad G, et al. Dihydropyridine receptor mutations cause hypokalemic periodic paralysis. *Cell* 1994; 77: 863-868.
34. Bulman DE, Scoggan KA, van Oene MD, Nicolle MW, Hahn AF, Tollar LL, Ebers GC. A novel sodium channel mutation in a family with hypokalemic periodic paralysis. *Neurology* 1999; 53: 1932-1936.
35. Lin SH. Thyrotoxic periodic paralysis. *Mayo Clin Proc* 2005; 80: 99-105.
36. Liu TA, Chang HK, Shieh RC. Extracellular K^+ elevates outward currents through Kir2.1 channels by increasing single-channel conductance. *Biochim Biophys Acta* 2011; 1808: 1772-1778.
37. Jurkat-Rott K, Holzherr B, Fauler M, Lehmann-Horn F. Sodium channelopathies of skeletal muscle result from gain or loss of function. *Pflugers Arch* 2010; 460: 239-248.
38. Cannon SC. Voltage-sensor mutations in channelopathies of skeletal muscle. *J Physiol* 2010; 588: 1887-1895.
39. Sokolov S, Scheuer T, Catterall WA. Gating pore current in an inherited ion channelopathy. *Nature* 2007; 446: 76-78.
40. Matthews E, Labrum R, Sweeney MG, Sud R, Haworth A, Chinnery PF, Meola G, Schorge S, Kullmann DM, Davis MB, Hanna MG. Voltage sensor charge loss accounts for most cases of hypokalemic periodic paralysis. *Neurology* 2009; 72: 1544-1547.
41. Allen AS. Pa Ping, or Kiating paralysis. *Chinese Medical Journal* 1943; 61: 296-301.

42. Alagem N, Dvir M, Reuveny E. Mechanism of Ba^{2+} block of a mouse inwardly rectifying K^+ channel: differential contribution by two discrete residues. *J Physiol* 2001; 534: 381–393.
43. Struyk AF, Cannon SC. Paradoxical depolarization of BA^{2+}- treated muscle exposed to low extracellular K^+: insights into resting potential abnormalities in hypokalemic paralysis. *Muscle Nerve* 2008; 37: 326-337.
44. Seebohm G, Strutz-Seebohm N, Ursu ON, Preisig-Müller R, Zuzarte M, Hill EV, Kienitz MC, Bendahhou S, Fauler M, Tapken D, Decher N, Collins A, Jurkat-Rott K, Steinmeyer K, Lehmann-Horn F, Daut J, Tavaré JM, Pott L, Bloch W, Lang F. Altered stress stimulation of inward rectifier potassium channels in Andersen-Tawil syndrome. *FASEB J* 2012; 26: 513-522.
45. Johnson CH, VanTassell VJ. Acute barium poisoning with respiratory failure and rhabdomyolysis. *Ann Emerg Med* 1991; 20: 1138-1142.
46. Sigue G, Gamble L, Pelitere M, Venugopal S, Arcement L, Rab ST, Thakur V. From profound hypokalemia to life-threatening hyperkalemia: a case of barium sulfide poisoning. *Arch Intern Med* 2000; 160: 548-551.
47. Dalal AK, Harding JD, Verdino RJ. Acquired long QT syndrome and monomorphic ventricular tachycardia after alternative treatment with cesium chloride for brain cancer. *Mayo Clin Proc* 2004; 79: 1065-1069.
48. Clemessy JL, Favier C, Borron SW, Hantson PE, Vicaut E, Baud FJ. Hypokalaemia related to acute chloroquine ingestion. *Lancet* 1995; 346: 877-880.
49. Neil MJ, Dale MC. Hypokalaemia with severe rebound hyperkalaemia after therapeutic barbiturate coma. *Anesth Analg* 2009; 108: 1867-1868.
50. Martin RS, Panese S, Virginillo M, Gimenez M, Litardo M, Arrizurieta E, Hayslett JP. Increased secretion of potassium in the rectum of humans with chronic renal failure. *Am J Kidney Dis* 1986; 8: 105-110.
51. Wang WH, Yue P, Sun P, Lin DH. Regulation and function of potassium channels in aldosterone-sensitive distal nephron. *Curr Opin Nephrol Hypertens* 2010; 19: 463-470.
52. Rodan AR, Cheng CJ, Huang CL. Recent advances in distal tubular potassium handling. *Am J Physiol Renal Physiol* 2011; 300: F821-827.
53. Cao XR, Shi PP, Sigmund RD, Husted RF, Sigmund CD, Williamson RA, Stokes JB, Yang B. Mice heterozygous for beta-ENaC deletion have defective potassium excretion. *Am J Physiol Renal Physiol* 2006; 291: F107-115.
54. Frindt G, Palmer LG. Apical potassium channels in the rat connecting tubule. *Am J Physiol Renal Physiol* 2004; 287: F1030-1037.
55. Silver RB, Breton S, Brown D. Potassium depletion increases proton pump (H(+)-ATPase) activity in intercalated cells of corticalcollecting duct. *Am J Physiol Renal Physiol* 2000; 279: F195-202.
56. Gumz ML, Lynch IJ, Greenlee MM, Cain BD, Wingo CS. The renal H^+-K^+-ATPases: physiology, regulation, and structure. *Am J Physiol Renal Physiol* 2010; 298: F12-21.
57. Doucet A, Katz AI. Renal potassium adaptation: Na-K-ATPase activity along the nephron after chronic potassium loading. *Am J Physiol* 1980; 238: F380-386.
58. Stanton BA. Renal potassium transport: morphological and functional adaptations. *Am J Physiol* 1989; 257: R989-R997.
59. Hayslett JP, Binder HJ. Mechanism of potassium adaptation. *Am J Physiol* 1982; 243: F103-112.
60. Frindt G, Shah A, Edvinsson J, Palmer LG. Dietary K regulates ROMK channels in connecting tubule and cortical collecting duct of rat kidney. *Am J Physiol Renal Physiol* 2009; 296: F347-354.
61. Najjar F, Zhou H, Morimoto T, Bruns JB, Li HS, Liu W, Kleyman TR, Satlin LM. Dietary K^+ regulates apical membrane expression of maxi-K channels in rabbit cortical collecting duct. *Am J Physiol Renal Physiol* 2005; 289: F922-932.

62. Huang DY, Wulff P, Völkl H, Loffing J, Richter K, Kuhl D, Lang F, Vallon V. Impaired regulation of renal K+ elimination in the sgk1-knockout mouse. *J Am Soc Nephrol* 2004; 15: 885-891.
63. Dekel B, Nakhoul F, Abassi Z, Aviv R, Winaver J, Szylman P. Complete adaptation to chronic potassium loading after adrenalectomy: possible humoral mechanisms. *J Lab Clin Med* 1997; 129: 453-461.
64. Garg LC, Narang N. Renal adaptation to potassium in the adrenalectomized rabbit. Role of distal tubular sodium-potassium adenosine triphosphatase. *J Clin Invest* 1985; 76: 1065-1070.
65. Keith NM, Binger MW. Diuretic action of potassium salts. *J Am Med Assoc* 1935; 105: 1584-1591.
66. Miller PD, Waterhouse C, Owens R, Cohen E. The effect of potassium loading on sodium excretion and plasma renin activity in Addisonian man. *J Clin Invest* 1975; 56: 346-353.
67. Rabelink TJ, Koomans HA, Hené RJ, Dorhout Mees EJ. Early and late adjustment to potassium loading in humans. *Kidney Int* 1990; 38: 942-947.
68. Wright FS, Strieder N. Fowler NB. Geibisch G. Potassium secretion by the distal tubule after potassium adaptation. *Am J Physiol* 1971; 221: 437-448.
69. Brandis M. Keyes J. Windhager EE. Potassium induced inhibition of proximal tubular fluid reabsorption in rats. *Am J Physiol* 1972; 222: 421-427.
70. Unwin R, Capasso G, Giebisch G. Potassium and sodium transport along the loop of Henle: effects of altered dietary potassium intake. *Kidney Int* 1994; 46: 1092-1099.
71. Stokes JB. Consequences of potassium recycling in the renal medulla. Effects of ion transport by the medullary thick ascending limb of Henle's loop. *J Clin Invest* 1982; 70: 219-229.
72. Jung JY, Kim S, Lee JW, Jung ES, Heo NJ, Son MJ, Oh YK, Na KY, Han JS, Joo KW. Effects of potassium on expression of renal sodium transporters in salt-sensitive hypertensive rats induced by uninephrectomy. *Am J Physiol Renal Physiol* 2011; 300: F1422-1430.
73. Vallon V, Schroth J, Lang F, Kuhl D, Uchida S. Expression and phosphorylation of the Na+-Cl- cotransporter NCC in vivo is regulated by dietary salt, potassium, and SGK1. *Am J Physiol Renal Physiol* 2009; 297: F704-712.
74. Frindt G, Palmer LG. Effects of dietary K on cell-surface expression of renal ion channels and transporters. *Am J Physiol Renal Physiol* 2010; 299: F890-897.
75. Morimoto T, Liu W, Woda C, Carattino MD, Wei Y, Hughey RP, Apodaca G, Satlin LM, Kleyman TR. Mechanism underlying flow stimulation of sodium absorption in the mammalian collecting duct. *Am J Physiol Renal Physiol* 2006; 291: F663-669.
76. Woda CB, Bragin A, Kleyman TR, Satlin LM. Flow-dependent K^+ secretion in the cortical collecting duct is mediated by a maxi-K channel. *Am J Physiol Renal Physiol* 2001; 280: F786-793.
77. Huang CL, Cha SK, Wang HR, Xie J, Cobb MH. WNKs: protein kinases with a unique kinase domain. *Exp Mol Med* 2007; 39: 565-573.
78. Xu B, English JM, Wilsbacher JL, Stippec S, Goldsmith EJ, Cobb MH: WNK1, a novel mammalian serine/threonine protein kinase lacking the catalytic lysine in subdomain II. *J Biol Chem* 2000; 275: 16795-16801.
79. Wilson FH, Disse-Nicode`me S, Choate KA, Ishikawa K, Nelson-Williams C, Desitter I, Gunel M, Milford DV, Lipkin GW, Achard JM, Feely MP, Dussol B, Berland Y, Unwin RJ, Mayan H, Simon DB, Farfel Z, Jeunemaitre X, Lifton RP: Human hypertension caused by mutations in WNK kinases. *Science* 2001; 293: 1107–1112.
80. Huang CL, Yang SS, Lin SH. Mechanism of regulation of renal ion transport by WNK kinases. *Curr Opin Nephrol Hypertens* 2008; 17: 519-525.

81 Xu BE, Stippec S, Lazrak A, Huang CL, Cobb MH: WNK1 activates SGK1 by a phosphatidylinositol 3-kinase-dependent and non-catalytic mechanism. *J Biol Chem* 2005; 280: 34218-34223.

82 Yang CL, Angell J, Mitchell R, Ellison DH: WNK kinases regulate thiazide-sensitive Na-Cl cotransport. *J Clin Invest* 2003; 111: 1039-1045.

83. Xu BE, Stippec S, Chu PY, Lazrak A, Li XJ, Lee BH, English JM, Ortega B, Huang CL, Cobb MH: WNK1 activates SGK1 to regulate the epithelial sodium channel. *Proc Natl Acad Sci U S A* 2005; 102: 10315-10320.

84. Ring AM, Cheng SX, Leng Q, Kahle KT, Rinehart J, Lalioti MD, Volkman HM, Wilson FH, Hebert SC, Lifton RP. WNK4 regulates activity of the epithelial Na+ channel in vitro and in vivo. *Proc Natl Acad Sci U S A* 2007; 104: 4020-4024.

85. Ho K, Nichols CG, Lederer WJ, Lytton J, Vassilev PM, Kanazirska MV, Hebert SC. Cloning and expression of an inwardly rectifying ATP-regulated potassium channel. *Nature* 1993; 362: 31-38.

86. Wang WH. Regulation of ROMK (Kir1.1) channels: new mechanisms and aspects. *Am J Physiol Renal Physiol* 2006; 290: F14-19.

87. Boim MA, Ho K, Shuck ME, Bienkowski MJ, Block JH, Slightom JL, Yang Y, Brenner BM, Hebert SC. ROMK inwardly rectifying ATP-sensitive K^+ channel. II. Cloning and distribution of alternative forms. *Am J Physiol* 1995; 268: F1132-1140.

88. Lorenz JN, Baird NR, Judd LM, Noonan WT, Andringa A, Doetschman T, Manning PA, Liu LH, Miller ML, Shull GE. Impaired renal NaCl absorption in mice lacking the ROMK potassium channel, a model for type IIBartter's syndrome. *J Biol Chem* 2002; 277: 37871-37880.

89. He G, Wang HR, Huang SK, Huang CL: Intersectin links WNK kinases to endocytosis of ROMK1. *J Clin Invest* 2007; 117: 1078-1087.

90. Zambrowicz BP, Abuin A, Ramirez-Solis R, Richter LJ, Piggott J, BeltrandelRio H, Buxton EC, Edwards J, Finch RA, Friddle CJ, Gupta A, Hansen G, Hu Y, Huang W, Jaing C, Key BW Jr, Kipp P, Kohlhauff B, Ma ZQ, Markesich D, Payne R, Potter DG, Qian N, Shaw J, Schrick J, Shi ZZ, Sparks MJ, Van Sligtenhorst I, Vogel P, Walke W, Xu N, Zhu Q, Person C, Sands AT. Wnk1 kinase deficiency lowers blood pressure in mice: a gene-trap screen to identify potential targets for therapeutic intervention. *Proc Natl Acad Sci U S A* 2003; 100: 14109-14114.

91. Lalioti MD, Zhang J, Volkman HM, Kahle KT, Hoffmann KE, Toka HR, Nelson-Williams C, Ellison DH, Flavell R, Booth CJ, Lu Y, Geller DS, Lifton RP. Wnk4 controls blood pressure and potassium homeostasis via regulation of mass and activity of the distal convoluted tubule. *Nat Genet* 2006; 38: 1124-1132.

92. Yang SS, Morimoto T, Rai T, Chiga M, Sohara E, Ohno M, Uchida K, Lin SH, Moriguchi T, Shibuya H, Kondo Y, Sasaki S, Uchida S. Molecular pathogenesis of pseudohypoaldosteronism type II: generation and analysis of aWnk4(D561A/+) knockin mouse model. *Cell Metab* 2007; 5: 331-344.

93. Ohta A, Rai T, Yui N, Chiga M, Yang SS, Lin SH, Sohara E, Sasaki S, Uchida S. Targeted disruption of the Wnk4 gene decreases phosphorylation of Na-Cl cotransporter, increases Na excretion and lowers blood pressure. *Hum Mol Genet* 2009; 18: 3978-3986.

94. Hadchouel J, Soukaseum C, Büsst C, Zhou XO, Baudrie V, Zürrer T, Cambillau M, Elghozi JL, Lifton RP, Loffing J, Jeunemaitre X. Decreased ENaC expression compensates the increased NCC activity following inactivation of the kidney-specific isoform of WNK1 and prevents hypertension. *Proc Natl Acad Sci U S A* 2010; 107: 18109-18114.

95. Liu Z, Xie J, Wu T, Truong T, Auchus RJ, Huang CL. Downregulation of NCC and NKCC2 cotransporters by kidney-specific WNK1 revealed by gene disruption and transgenic mouse models. *Hum Mol Genet* 2011; 20: 855-866.

96. Liu Z, Wang HR, Huang CL. Regulation of ROMK channel and K+ homeostasis by kidney-specific WNK1 kinase. *J Biol Chem* 2009; 284: 12198-12206.

97. Yang SS, Lo YF, Wu CC, Lin SW, Yeh CJ, Chu P, Sytwu HK, Uchida S, Sasaki S, Lin SH. SPAK-knockout mice manifest Gitelman syndrome and impaired vasoconstriction. *J Am Soc Nephrol* 2010; 21: 1868-1877.
98. Lin SH, Yu IS, Jiang ST, Lin SW, Chu P, Chen A, Sytwu HK, Sohara E, Uchida S, Sasaki S, Yang SS. Impaired phosphorylation of Na(+)-K(+)-2Cl(-) cotransporter by oxidative stress-responsive kinase-1 deficiency manifests hypotension and Bartter-like syndrome. *Proc Natl Acad Sci U S A* 2011; 108: 17538-17543.
99. Delaloy C, Lu J, Houot AM, Disse-Nicodeme S, Gasc JM, Corvol P, Jeunemaitre X. Multiple promoters in the WNK1 gene: one controls expression of a kidney-specific kinase-defective isoform. *Mol Cell Biol* 2003; 23: 9208-9221.
100. Lazrak A, Liu Z, Huang CL. Antagonistic regulation of ROMK by long and kidney-specific WNK1 isoforms. *Proc Natl Acad Sci U S A* 2006; 103: 1615-1620.
101. Susa K, Kita S, Iwamoto T, Yang SS, Lin SH, Ohta A, Sohara E, Rai T, Sasaki S, Alessi DR, UchidaS. Effect of heterozygous deletion of WNK1 on the WNK-OSR1/SPAK-NCC/NKCC1/NKCC2 signal cascade in the kidney and blood vessels. *Clin Exp Nephrol* 2012 Feb 1. [Epub ahead of print]
102. Lin SH, Lin YF, Halperin ML. Hypokalaemia and paralysis. *QJM* 2001; 94, 133-139.
103. Ober KP. Thyrotoxic periodic paralysis in the United States. Report of 7 cases and review of the literature. *Medicine* 1992; 71: 109-120.
104. Okinaka S, Shizume K, Iino S, Watanabe A, Irie M, Noguchi A, Kuma S, Ito T. The association of periodic paralysis and hyperthyroidism in Japan. *J Clin Endocrinol Metab* 1957; 17: 1454-1459.
105. Kelley DE, Gharib H, Kennedy FP, Duda RJ Jr, McManis PG. Thyrotoxic periodic paralysis. Report of 10 cases and review of electromyographic findings. *Arch Intern Med* 1989; 149: 2597-2600.
106. Shiang JC, Cheng CJ, Tsai MK, Hung YJ, Hsu YJ, Yang SS, Chu SJ, Lin SH. Therapeutic analysis in Chinese patients with thyrotoxic periodic paralysis over 6 years. *Eur J Endocrinol* 2009 ; 161: 911-916.
107. Kung AW. Clinical review: Thyrotoxic periodic paralysis: a diagnostic challenge. *J Clin Endocrinol Metab* 2006; 91: 2490-2495.
108. Sung CC, Cheng CJ, Lo YF, Lin MS, Yang SS, Hsu YC, Lin SH. Genotype and phenotype analysis of patients with sporadic periodic paralysis. *Am J Med Sci* 2012; 343: 281-285.
109. Dassau L, Conti LR, Radeke CM, Ptáček LJ, Vandenberg CA. Kir2.6 regulates the surface expression of Kir2.x inward rectifier potassium channels. *J Biol Chem* 2011; 286: 9526-9541.
110. Struyk AF, Cannon SC. A Na^+ channel mutation linked to hypokalemic periodic paralysis exposes a proton-selective gating pore. *J Gen Physiol* 2007; 130: 11-20.
111. Chang HK, Lee JR, Liu TA, Suen CS, Arreola J, Shieh RC. The extracellular K^+ concentration dependence of outward currents through Kir2.1 channels is regulated by extracellular Na^+ and Ca^{2+}. *J Biol Chem* 2010; 285: 23115-23125.
112. Gruener R, Stern LZ, Payne C, Hannapel L. Hyperthyroid myopathy. Intracellular electrophysiological measurements in biopsied human intercostal muscle. *J Neurol Sci* 1975; 24: 339-349.
113. Puwanant A, Ruff RL. INa and IKir are reduced in Type 1 hypokalemic and thyrotoxic periodic paralysis. *Muscle Nerve* 2010; 42: 315-327.
114. Hofmann WW, Denys EH. Effects of thyroid hormone at the neuromuscular junction. *Am J Physiol* 1972; 223: 283-287.
115. Jurkat-Rott K, Weber MA, Fauler M, Guo XH, Holzherr BD, Paczulla A, Nordsborg N, Joechle W, Lehmann-Horn F. K^+-dependent paradoxical membrane depolarization and Na^+ overload, major and reversible contributors to weakness by ion channel leaks. *Proc Natl Acad Sci U S A* 2009; 106: 4036-4041.
116. Bowen LN, Subramony SH, Cheng J, Wu SS, Okun MS. Elementary, my dear Dr. Allen: the case of barium toxicity and Pa Ping. *Neurology* 2010 ; 74: 1546-1549.

117. Zaritsky JJ, Eckman DM, Wellman GC, Nelson MT, Schwarz TL. Targeted disruption of Kir2.1 and Kir2.2 genes reveals the essential role of the inwardly rectifying K(+) current in K(+)-mediated vasodilation. *Circ Res* 2000; 87: 160-166.
118. Chen L, Lang D, Ran XW, Joncourt F, Gallati S, Burgunder JM. Clinical and molecular analysis of Chinese patients with thyrotoxic periodic paralysis. *Eur Neurol* 2003; 49: 227-230.
119. Ng WY, Lui KF, Thai AC, Cheah JS. Absence of ion channels CACN1AS and SCN4A mutations in thyrotoxic hypokalemic periodic paralysis. *Thyroid* 2004; 14: 187-190.
120. Schalin-Jantti C, Laine T, Valli-Jaakola K, Lonnqvist T, Kontula K, Valimaki MJ. Manifestation, management and molecular analysis of candidate genes in two rare cases of thyrotoxic hypokalemic periodic paralysis. *Horm Res* 2005; 63: 139-144.
121. Wang W, Jiang L, Ye L, Zhu N, Su T, Guan L, Li X, Ning G. Mutation screening in Chinese hypokalemic periodic paralysis patients. *Mol Genet Metab* 2006 ; 87: 359-363.
122. Lin SH, Hsu YD, Cheng NL, Kao MC. Skeletal muscle dihydropyridine-sensitive calcium channel (CACNA1S) gene mutations in chinese patients with hypokalemic periodic paralysis. *Am J Med Sci* 2005; 329: 66-70.
123. Ruff RL. Insulin acts in hypokalemic periodic paralysis by reducing inward rectifier K^+ current. *Neurology* 1999; 53: 1556-1563.
124. Rodan AR, Huang CL. Distal potassium handling based on flow modulation of maxi-K channel activity. *Curr Opin Nephrol Hypertens* 2009; 18: 350-355.
125. Zeng WZ, Babich V, Ortega B, Quigley R, White SJ, Welling PA, Huang CL. Evidence for endocytosis of ROMK potassium channel via clathrin-coated vesicles. *Am J Physiol Renal Physiol* 2002; 283: F630-639.
126. Veríssimo F, Jordan P. WNK kinases, a novel protein kinase subfamily in multi-cellular organisms. *Oncogene* 2001; 20: 5562-5569.
127. Vitari AC, Deak M, Morrice NA, Alessi DR. The WNK1 and WNK4 protein kinases that are mutated in Gordon's hypertension syndrome phosphorylate and activate SPAK and OSR1 protein kinases. *Biochem J* 2005; 391: 17-24.
128. Moriguchi T, Urushiyama S, Hisamoto N, Iemura S, Uchida S, Natsume T, Matsumoto K, Shibuya H. WNK1 regulates phosphorylation of cation-chloride-coupled cotransporters via the STE20-related kinases, SPAK and OSR1. *J Biol Chem* 2005; 280: 42685-42693.
129. Vitari AC, Deak M, Collins BJ, Morrice N, Prescott AR, Phelan A, Humphreys S, Alessi DR. WNK1, the kinase mutated in an inherited high-blood-pressure syndrome, is a novel PKB (protein kinase B)/Akt substrate. *Biochem J* 2004; 378: 257-268.
130. Jiang ZY, Zhou QL, Holik J, Patel S, Leszyk J, Coleman K, Chouinard M, Czech MP. Identification of WNK1 as a substrate of Akt/protein kinase B and a negative regulator of insulin-stimulated mitogenesis in 3T3-L1 cells. *J Biol Chem* 2005; 280: 21622-21628.
131. Lee IH, Dinudom A, Sanchez-Perez A, Kumar S, Cook DI. Akt mediates the effect of insulin on epithelial sodium channels by inhibiting Nedd4-2. *J Biol Chem* 2007; 282: 29866-29873.
132. Ahmed M, Gannon MC, Nuttall FQ. Postprandial plasma glucose, insulin, glucagon and triglyceride responses to a standard diet in normal subjects. *Diabetologia* 1976;12: 61-67.
133. Rechler MM, Nissley SP. The nature and regulation of the receptors for insulin-like growth factors. *Annu Rev Physiol* 1985; 47: 425-442.
134. Zapf J, Walter H, Froesch ER. Radioimmunological determination of insulinlike growth factors I and II in normal subjects and in patients with growth disorders and extrapancreatic tumor hypoglycemia. *J Clin Invest* 1981; 68: 1321-1330.
135. Kobayashi T, Cohen P. Activation of serum- and glucocorticoid-regulated protein kinase by agonists that activate phosphatidylinositide 3-kinase is mediated by 3-

phosphoinositide-dependent protein kinase-1 (PDK1) and PDK2. *Biochem J* 1999; 339: 319-328.

136. Yoo D, Kim BY, Campo C, Nance L, King A, Maouyo D, Welling PA. Cell surface expression of the ROMK (Kir 1.1) channel is regulated by the aldosterone-induced kinase, SGK-1, and protein kinase A. *J Biol Chem* 2003; 278: 23066-23075.
137. Xu Q, Modrek B, Lee C. Genome-wide detection of tissue-specific alternative splicing in the human transcriptome. *Nucleic Acids Res*2002; 30: 3754-3766.
138. Flyvbjerg A, Marshall SM, Frystyk J, Rasch R, Bornfeldt KE, Arnqvist H, Jensen PK, Pallesen G, Orskov H. Insulin-like growth factor I in initial renal hypertrophy in potassium-depleted rats. *Am J Physiol* 1992; 262: F1023-1031.
139. Giordano M, DeFronzo RA. Acute effect of human recombinant insulin-like growth factor I on renal function in humans. *Nephron* 1995; 71: 10-15.
140. Svensson J, Tivesten A, Sjögren K, Isaksson O, Bergström G, Mohan S, Mölne J, Isgaard J, Ohlsson C. Liver-derived IGF-I regulates kidney size, sodium reabsorption, and renal IGF-II expression. *J Endocrinol* 2007; 193: 359-366.
141. Li D, Wei Y, Babilonia E, Wang Z, Wang WH. Inhibition of phosphatidylinositol 3-kinase stimulates activity of the small-conductance K channel in the CCD. *Am J Physiol Renal Physiol* 2006; 290: F806-812.
142. Chen P, Guzman JP, Leong PK, Yang LE, Perianayagam A, Babilonia E, Ho JS, Youn JH, Wang WH, McDonough AA. Modest dietary K^+ restriction provokes insulin resistance of cellular K^+ uptake and phosphorylation of renal outer medulla K^+ channel without fall in plasma K^+ concentration. *Am J Physiol Cell Physiol* 2006; 290: C1355-1363.
143. DeFronzo RA, Cooke CR, Andres R, Faloona GR, Davis PJ. The effect of insulin on renal handling of sodium, potassium, calcium, and phosphate in man. *J Clin Invest* 1975; 55: 845-855.
144. DeFronzo RA, Goldberg M, Agus ZS. The effects of glucose and insulin on renal electrolyte transport. *J Clin Invest* 1976; 58: 83-90.
145. Furuya H, Tabei K, Muto S, Asano Y. Effect of insulin on potassium secretion in rabbit cortical collecting ducts. *Am J Physiol* 1992; 262: F30-35.
146. Ring AM, Leng Q, Rinehart J, Wilson FH, Kahle KT, Hebert SC, Lifton RP. An SGK1 site in WNK4 regulates Na^+ channel and K^+ channel activity and has implications for aldosterone signaling and K+ homeostasis. *Proc Natl Acad Sci U S A* 2007; 104: 4025-4029.
147. Grahammer F, Artunc F, Sandulache D, Rexhepaj R, Friedrich B, Risler T, McCormick JA, Dawson K, Wang J, Pearce D, Wulff P, Kuhl D, Lang F. Renal function of gene-targeted mice lacking both SGK1 and SGK3. *Am J Physiol Regul Integr Comp Physiol* 2006; 290: R945-950.
148. Náray-Fejes-Tóth A, Snyder PM, Fejes-Tóth G. The kidney-specific WNK1 isoform is induced by aldosterone and stimulates epithelial sodium channel-mediated Na^+ transport. *Proc Natl Acad Sci U S A* 2004; 101: 17434-17439.
149. Subramanya AR, Yang CL, Zhu X, Ellison DH. Dominant-negative regulation of WNK1 by its kidney-specific kinase-defective isoform. *Am J Physiol Renal Physiol* 2006; 290: F619-624.
150. O'Reilly M, Marshall E, Speirs HJ, Brown RW. WNK1, a gene within a novel blood pressure control pathway, tissue-specifically generates radically different isoforms with and without a kinase domain. *J Am Soc Nephrol* 2003; 14: 2447-2456.
151. Quigley R, Chakravarty S, Baum M. Antidiuretic hormone resistance in the neonatal cortical collecting tubule is mediated in part by elevated phosphodiesterase activity. *Am J Physiol Renal Physiol* 2004; 286: F317-322.
152. Cheng CJ, Lozano G, Baum M. Prenatal Programming of Rat Cortical Collecting Tubule Sodium Transport. *Am J Physiol Renal Physiol* 2012; 302: F674-678.

153. Maddrell SH, O'Donnell MJ, Caffrey R. The regulation of haemolymph potassium activity during initiation and maintenance of diuresis in fed Rhodnius prolixus. *J Exp Biol* 1993; 177: 273-285.
154. Pfaffl MW. A new mathematical model for relative quantification in real-time RT-PCR. *Nucleic Acids Research* 2001; 29: 2002-2007.
155. Mandon B, Siga E, Chabardes D, Firsov D, Roinel N, De Rouffignac C. Insulin stimulates Na^+, Cl^-, Ca^{2+}, and Mg^{2+} transports in TAL of mouse nephron: cross-potentiation with AVP. *Am J Physiol* 1993; 265: F361-369.
156. Shirley DG, Walter SJ, Unwin RJ, Giebisch G. Contribution of Na^+-H^+ exchange to sodium reabsorption in the loop of henle: a microperfusion study in rats. *J Physiol* 1998; 513: 243-249.
157. Fenton RA, Knepper MA. Mouse models and the urinary concentrating mechanism in the new millennium. *Physiol Rev* 2007; 87: 1083-1112.
158. Ecelbarger CA, Kim GH, Wade JB, Knepper MA. Regulation of the abundance of renal sodium transporters and channels by vasopressin. *Exp Neurol* 2001; 171: 227-234.
159. Gimenez I, Forbush B. Short-term stimulation of the renal Na-K-Cl cotransporter (NKCC2) by vasopressin involves phosphorylation and membrane translocation of the protein. *J Biol Chem* 2003; 278: 26946–26951.
160. Kemter E, Rathkolb B, Bankir L, Schrewe A, Hans W, Landbrecht C, Klaften M, Ivandic B, Fuchs H, Gailus-Durner V, Hrabé de Angelis M, Wolf E, Wanke R, Aigner B. Mutation of the Na(+)-K(+)-2Cl(-) cotransporter NKCC2 in mice is associated with severe polyuria and a urea-selective concentrating defect without hyperreninemia. *Am J Physiol Renal Physiol* 2010; 298: F1405-1415.
161. Kim GH, Choi NW, Jung JY, Song JH, Lee CH, Kang CM, Knepper MA. Treating lithium-induced nephrogenic diabetes insipidus with a COX-2 inhibitor improves polyuria via upregulation of AQP2 and NKCC2. *Am J Physiol Renal Physiol* 2008; 294: F702-709.
162. Koumi S, Backer CL, Arentzen CE, Sato R. beta-Adrenergic modulation of the inwardly rectifying potassium channel in isolated human ventricular myocytes. Alteration in channel response to beta-adrenergic stimulation in failing human hearts. *J Clin Invest* 1995; 96: 2870-2881.
163. Wischmeyer E, Döring F, Karschin A. Acute suppression of inwardly rectifying Kir2.1 channels by direct tyrosine kinase phosphorylation. *J Biol Chem* 1998; 273: 34063-34068.
164. Giovannardi S, Forlani G, Balestrini M, Bossi E, Tonini R, Sturani E, Peres A, Zippel R. Modulation of the inward rectifier potassium channel IRK1 by the Ras signaling pathway. *J Biol Chem* 2002; 277: 12158-12163.
165. Preisig-Müller R, Schlichthörl G, Goerge T, Heinen S, Brüggemann A, Rajan S, Derst C, Veh RW, Daut J. Heteromerization of Kir2.x potassium channels contributes to the phenotype of Andersen's syndrome. *Proc Natl Acad Sci U S A* 2002; 99: 7774-7779.
166. Melnyk P, Ehrlich JR, Pourrier M, Villeneuve L, Cha TJ, Nattel S. Comparison of ion channel distribution and expression in cardiomyocytes of canine pulmonary veins versus left atrium. *Cardiovasc Res* 2005; 65: 104-116.
167. Jongjaroenprasert W, Phusantisampan T, Mahasirimongkol S, Mushiroda T, Hirankarn N, Snabboon T, Chanprasertyotin S, Tantiwong P, Soonthornpun S, Rattanapichart P, Mamanasiri S, Himathongkam T, Ongphiphadhanakul B, Takahashi A, Kamatani N, Kubo M, Nakamura Y. A genome-wide association study identifies novel susceptibility genetic variation for thyrotoxic hypokalemic periodic paralysis. *J Hum Genet* 2012; 57: 301-304.
168. Rafiqi FH, Zuber AM, Glover M, Richardson C, Fleming S, Jovanović S, Jovanović A, O'Shaughnessy KM, Alessi DR. Role of the WNK-activated SPAK kinase in regulating blood pressure. *EMBO Mol Med* 2010; 2: 63-75.

169. McCormick JA, Mutig K, Nelson JH, Saritas T, Hoorn EJ, Yang CL, Rogers S, Curry J, Delpire E, Bachmann S, Ellison DH. A SPAK isoform switch modulates renal salt transport and blood pressure. *Cell Metab* 2011; 14: 352-364.